

ulm university universität ulm

Institute of Physiological Chemistry
Head of Institute: Prof. Dr. Thomas Wirth

Importance of SOD2 in neuronal homeostasis: Study of a novel mouse model

DISSERTATION

in partial fulfillment of the requirements for the degree of PhD
(Dr. rer. nat)

Faculty of Natural Sciences
University of Ulm

Submitted by

Gandhari Maity (Kumar)
from
Midnapore (West), India
2014

Dean	:	Prof. Dr. Joachim Ankerhold
First Reviewer	:	Prof. Dr. Thomas Wirth Institute of Physiological Chemistry University of Ulm
Second Reviewer	:	Prof. Dr. Karin Scharffetter-Kochanek Department of Dermatology and Allergic Diseases University of Ulm

Day doctorate awarded: **23.07.2014**

Die Arbeiten im Rahmen der vorliegenden Dissertation wurden am Institut für Physiologische Chemie der Universität Ulm durchgeführt und von Herrn Prof. Dr. Thomas Wirth betreut.

TABLE OF CONTENTS

Table of Contents ……... 3

Summary …… 6

1. INTRODUCTION ……. 8

1.1 Neuronal development and degeneration …….. 8

1.1.1 Apoptosis and necrosis as a cause of Neurodegenerative diseases ….. 9

1.1.2 Oxidative stress acts as an inducer of neurodegenerative diseases ….. 11

1.2 Oxidative stress …….. 12

1.3 Superoxide dismutase ……. 16

1.4 Cre LoxP System …… 17

1.5 Importance of Superoxide dismutase 2 …… 19

1.6 Aims of the study …….. 21

2. MATERIALS AND METHODS …….. 22

2.1 Generation of $SOD2^{nko}$ Mice …… 22

2.2 Genomic DNA Analysis …… 22

2.3 Primary Neuron Culture …… 23

2.4 Intracellular ROS measurement (In vitro) …… 24

2.5 Western Immunoblot Analysis …… 24

2.6 Histology and Immunostaining …… 25

2.7 Cytochrome C Oxidase and Succinate Dehydrogenase (COX-SDH) Histochemistry ……... 26

2.8 Terminal deoxynucleotidyl transferase dUTP nick end labeling (TUNEL) staining ……..... 27

2.9 Image Acquisition ……. 27

2.10 Enzyme-Linked Immunosorbent Assay (ELISA) …… 28

2.11 Blood Sugar Test ……. 28

2.12 ATP Production Assay …… 28

2.13 NAD and NADH Quantification …… 28

2.14 Quantitative Real-Time PCR (qRT-PCR) …… 29

2.15 Statistical Analysis …… 29

2.16 General Chemicals …… 31

2.17 Software Used ……... 32

3. RESULTS ……..... 33

3.1 Generation of a novel conditonal knockout mouse …… 33

3.2 Neuron specific deletion of SOD2 in SOD2n^{ko} mice …… 37

3.3 Redox imbalance associated oxidative damage in forebrain ……. 42

3.4 Oxidative stress induced endogenous antioxidant response ……. 47

3.5 Toxic neurofilamentopathy in neuronal SOD2 deficiency …… 47

3.6 Reactive astrogliosis coupled with inflammatory response …….. 49

3.7 Enhanced neuronal apoptosis and cell cycle inhibition ……. 51

3.8 Severe hypoglycemia and energy deprivation in absence of neuronal SOD2 ……..... 55

3.9 Hypoglycemia induced necrotic brain lesion in SOD2^{nko} mice …… 58

3.10 Hypothalamic neuropathology associated impaired counterregulation to hypoglycemia ……..... 61

4. DISCUSSION ……..... 65

4.1 Crucial role of neuronal SOD2 in overall survival ……..... 65

4.2 Consequences of SOD2 deficiency in neuronal homeostasis …… 68

4.3 Neuronal redox imbalance mediated energetic dysfunction ……. 69

4.4 Involvement of neuronal SOD2 in CNS-regulated energy homeostasis ….. 71

4.5 Potential mechanism of redox imbalance induced impairment of neuronal and metabolic homeostasis ……..... 75

4.6 Conclusion ……. 77

5. List of Abbreviations …… 78

6. REFERENCES ……. 82

Declaration ……. 95

Acknowledgements …… 96

Curriculum vitae ……. 97

SUMMARY

Redox imbalance is believed to contribute to the development and progression of several neurodegenerative disorders. Our aim was to develop an animal model that exhibits neuron-specific redox imbalance in the central nervous system (CNS) to study the consequences and eventually get clues regarding the pathomechanisms of oxidative insults in neurodegenerative disorders. We, therefore, generated a neuron-specific SOD2 deficient mouse by deleting exon 3 of the SOD2 gene using CamKIIα- promoter driven Cre expression. The neuron-specific SOD2 knock out ($SOD2^{nko}$) mice born at normal Mendelian frequencies. After birth, $SOD2^{nko}$ mice were distinguishable from their littermates by significantly reduced body size, body weight and presence of fewer hairs when compared with control mice within few days of life. Phenotypically $SOD2^{nko}$ mice suffered from severe growth retardation, ataxic movements, stiff tail, multiple seizures and other neurological abnormalities. All mutant mice died at the age of around 4 weeks, independent of the weaning period. Consistent with the important role in scavenging superoxide radicals, the SOD2-deficient neurons showed significant accumulation of reactive oxygen species (ROS) followed by enhanced oxidative damages, such as protein oxidation, lipid peroxidation and DNA damages in the forebrain regions where SOD2 was inactivated. In addition, $SOD2^{nko}$ mice exhibited severe neuronal alterations, such as abnormal distribution and aggregation of neurofilament proteins, reactive astrogliosis, infiltration of blood-borne immune cells and activation of microglia. Moreover, neuronal SOD2-deficiency resulted in upregulation of p21, neuronal cell cycle arrest and induction of Caspase-mediated apoptotic cascade. JNK activation and stabilization of p53, as a result of ROS accumulation are most likely the inducers of neuronal apoptosis in $SOD2^{nko}$ mice. In addition, induction of PUMA and Bax contributed to the neuronal apoptotic phenomena. Interestingly, the $SOD2^{nko}$ mice suffered from profound hypoglycemia along with critical energy failure. Prolonged energy deprivation resulted in hypoglycemia-induced necrotic lesions in different regions of $SOD2^{nko}$ mice brain. Remarkably, hypothalamus-mediated counterregulatory pathways to hypoglycemia were significantly altered. Downregulation of important hypothalamic neuropeptides such as CRH, GHRH and POMC revealed an abnormal hypothalamic function in $SOD2^{nko}$ mice. Furthermore, significant reduction of hypothalamus-regulated essential pituitary hormones,

such as ACTH and GH suggested alterations in hypothalamic-pituitary axis and thus resulting in a perturbed central regulation of metabolic homeostasis.

Taken together, the findings of present study suggest that deficiency of SOD2 in forebrain neurons results in induction of neuronal apoptosis, an impaired central regulation of glucose metabolism as well as energy homeostasis that leads to persistant hypoglycemia, hypoglycemia-related neurodegeneration and an early postnatal lethality of the mutant mice.

1. INTRODUCTION

1.1 Neuronal development and degeneration

Mammalian nervous system is a highly advanced and complex organ, where neurons act as information processing centres [Stiles and Jernigan, 2010]. Embryonic neuronal development involves three stages, proliferation, migration and differentiation, where multipotent neural progenitors are converted into neurons and glial cells [Iwai et al., 2003; Hartl et al., 2008]. In mammals, during early brain development stage, which is known as expansion phase, neuroepithelial cells which form the neural plate and neural tubes start dividing within the ventricular zone to increase the pool of stem cell [Gotz and Huttner, 2005; Merkle and Alvarez-Buylla, 2006]. The newly formed daughter cells, which are called neuroblasts start migrating along the processes of radial glial cells, a special types glial like cells bearing many features of neuroepithelial cells. Since, radial glial cells also share features of neuroepithelial cells, it is most likely that neuroepithelial cells transform directly into radical glial cells, although it needs experimental proof [Gotz and Huttner, 2005; Merkle and Alvarez-Buylla, 2006]. In mice, around embryonic day 11.5 (E11.5) there is a switch from division to differentiation, when committed subset of a neural progenitors differentiate into neurons. Around E17, glial cells start appearing, although gliaogenesis continued even after birth [Hartl et al., 2008]. Several proneural genes [Demir et al., 2009] essentially regulate the whole neurogenesis process [Gotz and Huttner, 2005]. In human the development of CNS begins with the formation of neural plate, 19 days post fertilization (E19) [Levene and Chervenak, 2009]. The neural tube closes around embryonic day 30 (E30). Around E33, in the later part of cortical wall, the neuroepithelial cells switch from symmetrical to asymmetrical mode of cell division, which in mouse is around E10. Asymmetrical cell division keeps one daughter cell as progenitor and the other postmitotic daughter cell is destined to become either neuron or glial cell [Bystron et al., 2008]. Although neuronal development is largely completed by midgestation, brain development continues for an extended period of time postnatally [Stiles and Jernigan, 2010].

Neurodegenerative diseases, where neurons degenerate and ultimately die refer to the pathology associated the disorders such as Alzheimer's disease, Parkinson's disease, Huntington's

disease, multiple sclerosis and amyotrophic lateral sclerosis etc [Maragakis and Rothstein, 2006]. Although, pathophysiologically neurodegenerative diseases are all characterized by progressive dysfunction and death of the cells that affect specific neural systems, the pathogenesis of these diseases are however multifactorial and can be influenced by genetic, environmental and endogenous factors [Qureshi and Parvez, 2007]. Several lines of evidences suggest that the common pathogenic mechanisms underlying neurodegenerative diseases include but not limited to abnormal protein dynamics with protein misfolding, defective protein degradation and aggregation, mitochondrial dysfunction and impaired bioenergetics, disruption of axonal and cellular transport, neuroinflammation and oxidative stress. All these events are interrelated and can lead to cell death [Qureshi and Parvez, 2007]. In spite of available knowledge, still neurodegenerative diseases affect millions of people worldwide and lack effective treatment options.

1.1.1 Apoptosis and necrosis as a cause of Neurodegenerative diseases

Apoptosis occurs in all cells of the nervous system, such as neuron, glial, and neural progenitor cells. About half of the original cell population is eliminated as a result of apoptosis in the developing nervous system [Nijhawan et al., 2000]. The apoptotic process during neural development is essential for the optimization of synaptic connections, removal of unnecessary neurons, and pattern formation. The chance for survival of a particular neuron during development is believed to directly depend on the extent of its connections to a postsynaptic target. This explains why neurons are initially overproduced and then compete for target-derived neurotrophic factors, provided by glial cells and presynaptic cells [Nijhawan et al., 2000]. Mice deficient in intrinsic apoptotic pathway genes, such as caspase-9, caspase-3 and apaf-1, show severe developmental and structural defects in brain [Nonomura et al., 2013]. Neuronal apoptosis also shares the features of typical apoptotic cell death, such as decreased cell volume, chromatin condensation (pyknosis), nuclear fragmentation (karyorrhexis) along with membrane blebbing. Proteolytic enzymes such as caspases are also found to be activated during neuronal apoptosis [Ghavami et al., 2014]. The process of apoptosis that shape the nervous system during development can be overactivated and results in several neurodegenerative diseases. During the past several years, the understanding of the mechanisms mediating cell death in neurologic diseases has improved considerably. Cell death through apoptosis and necrosis is found to take place both in acute and chronic neu-

rological diseases [Friedlander, 2003]. In chronic neurodegenerative diseases, cell death through apoptosis is the predominant form of cell death [Friedlander, 2003; Okouchi et al., 2007]. The primary difference between acute and chronic neurologic disorders is the magnitude of the stimulus that causes cell death. The greater the stimulus strength in acute diseases, the more induction of both necrotic and apoptotic cell death, whereas the milder insults in chronic diseases initiate apoptotic cell death [Friedlander, 2003]. There is an emerging concept that although apoptosis and necrosis are considered to be distinct forms of cell death, there is apoptosis-necrosis continuum. In this continuum, neuronal death results from varying contributions of coexisting apoptotic and necrotic mechanisms. Therefore, the differences between apoptosis and necrosis during neurodegenerative changes are becoming unclear [Martin, 2001]. An emerging concept suggests that apoptotic activation can be localized to synapses and distal neurites without causing immediate neuronal death or neuronal cell body. This may lead to localized breakdown of nerve terminal and its synapse. This type of synaptic deficit may contribute to cognitive decline in several neurodegenerative diseases [Glantz et al., 2006].

The principal molecular components of neuronal apoptotic pathway include Bcl-2 family of proteins and caspases. Inhibition of caspases in acute neurological diseases condition reduces neural damage and shows neurological improvement [Friedlander, 2003]. Proapoptotic Bcl-2 family members, such as Bax, Bak and Bid are found to be activated by several neurological insults, such as oxidative stress, DNA damage, decline of trophic supports as well as during inhibition of antiapototic Bcl-2 and Bcl-xl proteins. DNA damage through activation of p53 pathway activates the proapoptotic proteins in the neurons, leading to cytochrome c release and caspase-3 activation [Ghavami et al., 2014] (Figure 1.1). Overactivation of glutamate receptor is also known to induce apoptosis through calcium signaling. This type of excitotoxicity is common in both acute and chronic neurodegenerative diseases [Mattson, 2000]. Neuronal apoptosis can be triggered by a wide number of factors including ROS, products of oxidation, such as lipid peroxide, DNA damage, loss of trophic factors etc. Among all the inducers, redox imbalance or oxidative stress is the most important for the activation of neuronal cell death in a variety of neurological diseases. The extent of neuronal cell death correlates with markers of oxidative injury to lipids, proteins and nucleic acids in both animal models as well in patients. Moreover the oxidative damage is also ob-

served at the level of mitochondria [Soane et al., 2007]. Mitochondrially targeted antioxidants can cause neuroprotection in several animals and in vitro models [Soane et al., 2007].

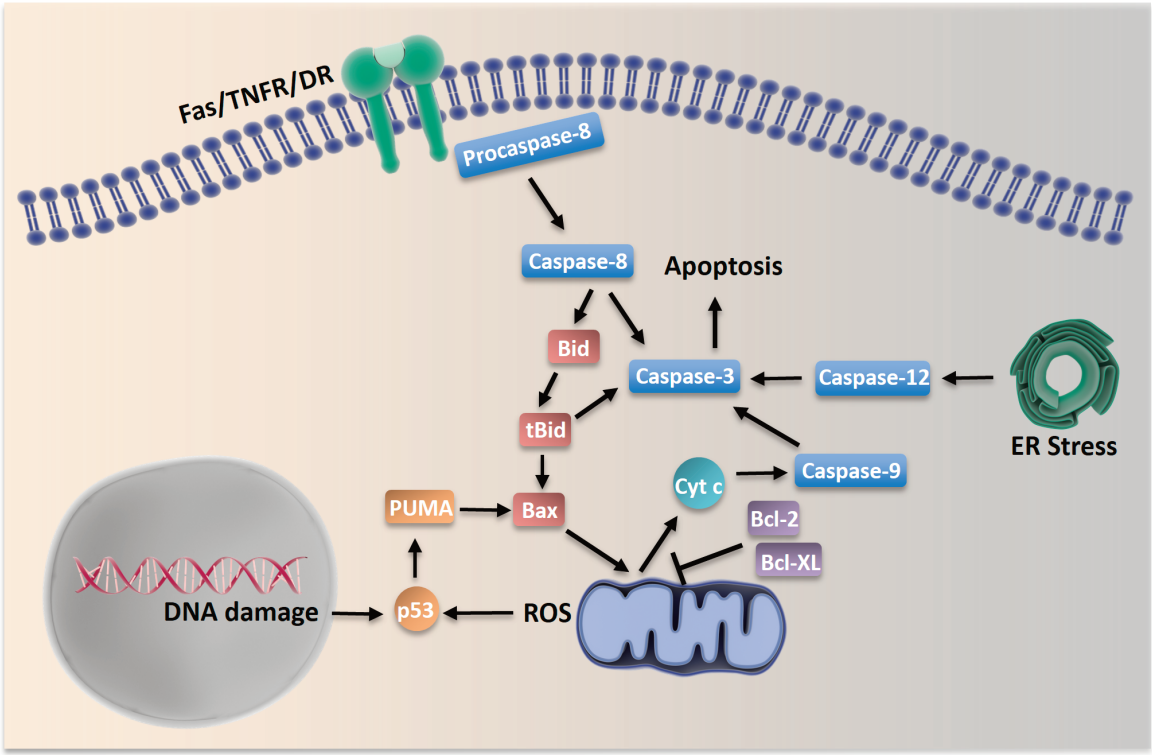

Figure 1.1 Caspase dependent neuronal apoptotic pathway

Neuronal apoptosis can be triggered by ligand mediated activation of death receptors, such as Fas, TNF- receptor, TRAIL-receptor. Activation of death receptor leads to activation of caspase-8 that can directly activate caspase-3 or through cleavage and activation of Bid can initiate mitochondrial pathway of apoptosis. DNA damage and/or generation of reactive oxygen species (ROS) activate p53, which through induction of PUMA activate Bax. PUMA by binding with Bcl-2, frees the Bax molecules. Bax can also be activated by caspase-8 cleaved Bid (truncated Bid, tBid). Free Bax in the cytosol then oligomerizes and initiates the formation of mitochondrial permeability transition pore through which cytochrome c escapes to the cytosol and participate in the activation of caspase-9, which in turn activate caspase-3. Endoplasmic reticular stress (ER stress) through activation of caspase-12 can also activate caspase-3. Activation of caspase-3 finally leads to execution of apoptosis.

1.1.2 Oxidative stress acts as an inducer of neurodegenerative diseases

A growing body of evidence links mitochondria mediated redox imbalance as a key step in the pathogenesis of several neurodegenerative diseases, with the promise that mitochondrial processes may represent potential therapeutic targets [Simonian and Coyle, 1996; Wallace,

1999; Gadoth and Göbel, 2011; Duchen, 2012]. Markers of oxidative stress are indeed elevated in postmortem examination of brains from patients with neurodegenerative disorders [Sayre et al., 2001]. However, there is still a controversy whether increased oxidative burdens is causative for neurodegeneration or rather the consequence. The brain and nervous system are highly vulnerable to ROS mediated injury because of several reasons, such as (i) high oxygen consumption may result in higher ROS production, (ii) neuronal membranes, which are made of polyunsaturated fatty acids (PUFA) susceptible to ROS induced damage, (iii) the antioxidant defence mechanism in neurons is not powerful due to low levels of several antioxidants in comparison with other organs, (iv) neuronal cells are nonreplicative and therefore more sensitive to damage [Gadoth and Göbel, 2011]. The brain although accounts 2% of body weight, consumes about 20% of total oxygen inspired. This high amount of oxygen is required because of high ATP requirement of the brain and upto 5% of oxygen consumed by the cells in brain can de diverted to ROS production [Mariani et al., 2005; Migliore et al., 2005; Gadoth and Göbel, 2011].

1.2 Oxidative stress

Reactive oxygen species (ROS) are chemically reactive products that are generated during both normal as well as abnormal cellular metabolism. Several convincing reports suggest that ROS also act as important cellular signaling mediators [Murphy et al., 2011]. Oxidative stress or redox imbalance is defined as a disturbance in the delicate balance between production of ROS and their efficient elimination by antioxidant systems. This can result either from enhanced production of reactive oxidants or impairment of their elimination due to defective antioxidant system [Betteridge, 2000]. A moderate increase in ROS production can promote cell proliferation and differentiation, while excessive production of ROS cause oxidative damage to cellular macromolecules, such as lipids, proteins, and DNA [Trachootham et al., 2008] (Figure 1.2). Increased production of ROS or defective antioxidant systems that induce redox imbalance has been shown to be involved in the pathogenesis of several diseases, such as atherosclerosis, cardiovascular diseases, cancer, diabetes, renal diseases and neurodegeneration [Finkel and Holbrook, 2000; Wallace, 2005].

In mammalian cell, mitochondria are one of the main sites for ROS production. Mitochondrial electron transport chain transfers electrons from one sub-unit (complex I and Complex

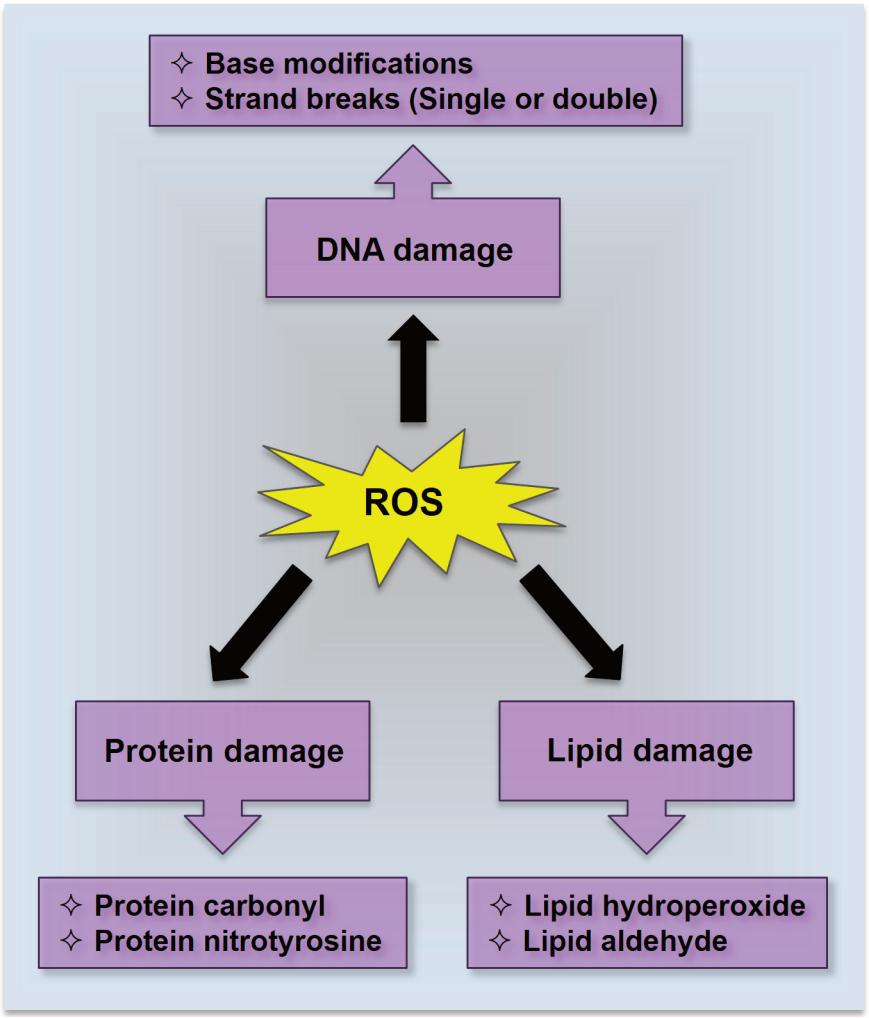

Figure 1.2 Oxidative damage

Reactive oxygen species (ROS) leads to damage of cellular macromolecules, such as lipid damage through formation of lipid hydroperoxide and lipid aldehyde, protein damage through protein carbonyl formation and nitration in the tyrisone residues as well as DNA damage through oxidative base modification that can also lead to strand breakage.

II) to another and finally to molecular oxygen (complex IV) to form water. During this process, electrons can exit the transport chain. It was shown that electrons mainly can escape the transport chain through complex I and complex III [Jastroch et al., 2010]. Single electron that escapes the transport chain can be transferred to dioxygen and forms superoxide anion ($O_2^{\bullet -}$). Complex I generates $O_2^{\bullet -}$ only within the mitochondrial matrix, whereas complex III generates $O_2^{\bullet -}$ both in the matrix as well as in the intermembrane space [Bell et al., 2007]. In addition to complex I and complex III, other enzyme systems present in mitochondrial matrix, such as 2-oxoglutarate dehydrogenase (OGDH) and pyruvate dehydroge-

nase (PDH), and the mitochondrial membrane forms of glycerol 3-phosphate dehydrogenase (GPDH; also known as GPDM) and the FQR (electron transfer flavoprotein-ubiquinone oxidoreductase, mitochondrial) are also known to produce $O_2^{\bullet -}$ [Murphy, 2009; Brand, 2010; Holmstrom and Finkel, 2014]. $O_2^{\bullet -}$ however can initiate and propagate free radical oxidation and leads to oxidative damage to DNA, lipids and proteins [Fridovich, 1997] (Figure 1.3). $O_2^{\bullet -}$ can react with nitric oxide (NO) synthesized by mitochondrial nitric oxide synthatase (NOS) to form peroxynitrite ($ONOO^-$) [Jourd'heuil et al., 2001]. At low concentration $ONOO^-$ is essential for triggering neuroprotective signaling, however, when generated at high concentration can act as neurotoxins [Soane et al., 2007]. $ONOO^-$ can also irreversibly inhibit several components of mitochondrial electron transport chain. This results in impairment of energy production and mitochondrial dysfunction [Stewart and Heales, 2003]. $ONOO^-$ can also inhibit many functional and structural proteins essential for cellular functions [Soane et al., 2007]. Moreover, $O_2^{\bullet -}$ can react with iron-sulfer cluster $[4Fe\text{-}4S]^{2+}$ of mitochondrial aconitase and generates highly reactive hydrogen peroxide ($^{\bullet}OH$) [Vasquez-Vivar et al., 2000]. Other than mitochondrial electron transport chain, important sources of ROS in mammalian cell include NADPH oxidase, nitric oxide synthease (NOS), xanthine oxidase, cyclooxygenase, cytochrome P450 systems [Halliwell and Gutteridge, 2007; Holmstrom and Finkel, 2014]. In addition to mitochondria, there are several other organelles that also generate considerable amount of ROS. A recent report shows that endoplasmic reticulum and peroxidsomes have great capacity to generate ROS at least in some tissues [Brown and Borutaite, 2012].

Eukaryotic cells express a variety of protective antioxidative enzymes with a certain functional overlap [Halliwell and Gutteridge, 2007]. The superoxide dismutase (SOD, EC 1.15.1.1) is one of the important antioxidant enzymes instantly and efficiently dismutates $O_2^{\bullet -}$ into hydrogen peroxide (H_2O_2), which is later scavenged by glutathione, peroxiredoxin, thioredoxin systems [Miranda-Vizuete et al., 2000; Cao et al., 2007; Halliwell and Gutteridge, 2007] (Figure 1.3). In the peroxisome, H_2O_2 is mainly scavenged by catalase. The cytotoxic effect of H_2O_2 is also mediated through hydroxyl radicals, which can be generated from metal catalyzed reactions and subsequently damage DNA, proteins, and lipids [Halliwell and Gutteridge, 2007]. Therefore, rapid removal of H_2O_2 is essential for the protection of cellular macromolecules. There are several controversies regarding the H_2O_2 de-

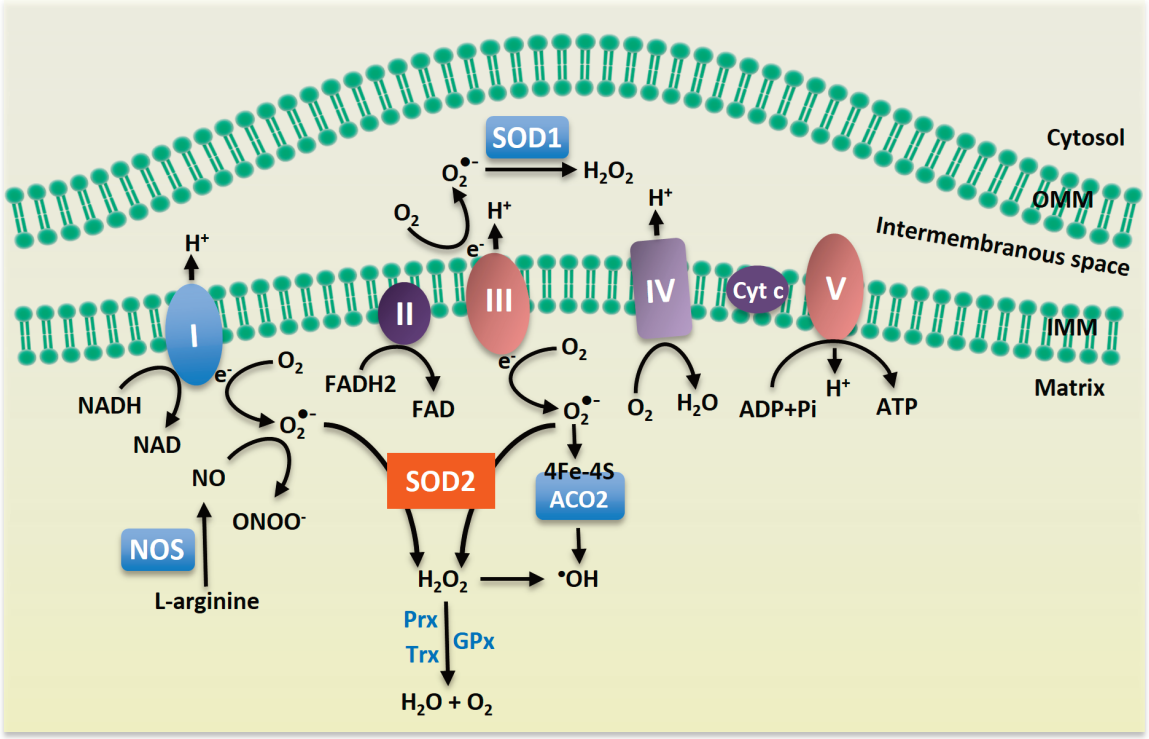

Figure 1.3 Generation of reactive oxygen species through mitochondrial electron transport chain
Electron leakage from mitochondrial electron transport chain complex I and III leads to partial reduction of molecular oxygen (O_2) to form superoxide anion ($O_2^{\bullet-}$). From complex I, electrons leak to the matrix side, whereas from complex III, electron can leak to the matrix as well as to the intermembranous space. The intermembranous space is the space between inner mitochondrial membrane (IMM) and outer mitochondrial membrane (OMM). In the matrix, $O_2^{\bullet-}$ is dismutated by superoxide dismutase (SOD2) to hydrogen peroxide (H_2O_2), which is then degraded to water (H_2O) and O_2 by several systems, such as peroxiredoxin (Prx), thioredoxin (Trx) and glutathione system, including glutathione peroxidase (Gpx). $O_2^{\bullet-}$ if not scavenged can react with nitric oxide (NO) synthesized by mitochondrial nitric oxide synthase (NOS) to generate peroxiynitrite ($ONOO^-$). $O_2^{\bullet-}$ can also react with iron sulfur cluster of mitochondrial aconitase (ACO2) to produce hydroxyl radical ($^{\bullet}OH$). $^{\bullet}OH$ can also be generated from H_2O_2 mediated Fenton reaction and Haber-Weiss reaction. $O_2^{\bullet-}$ released into the intermembranous space is dismutated by superoxide dismutase 1 (SOD1).

grading effects of catalase. Some earlier reports suggest that at low H_2O_2 concentration, catalase plays almost no role in H_2O_2 degradation. It is the glutathione-glutathione peroxidase system that acts as predominant H_2O_2 scavenging agent in that circumstance [Keilin and Hartree, 1945; Cohen and Hochstein, 1963]. However, recent reports demonstrated a clear predominance of catalase in removing H_2O_2, even in very low concentration of H_2O_2 [Mueller et al., 1997; Vetrano et al., 2005].

1.3 Superoxide dismutase

There are three different SOD isoenzymes in eukaryotic cells, SOD1 (CuZnSOD) which is primarily cytoplasmic and also presents in the mitochondrial intermembrane space, SOD2 (MnSOD) presents in mitochondrial matrix, while SOD3 (CuZnSOD) is an extracellular enzyme [Zelko et al., 2002; Halliwell and Gutteridge, 2007; Miao and St Clair, 2009; Fridovich, 2013]. The mitochondrial superoxide dismutase 2 (SOD2), also known as MnSOD (Figure 1.4), is an important mitochondrial antioxidant enzyme and considered as the first line of defence in the mitochondria. Reduced SOD2 activity has been well docu-

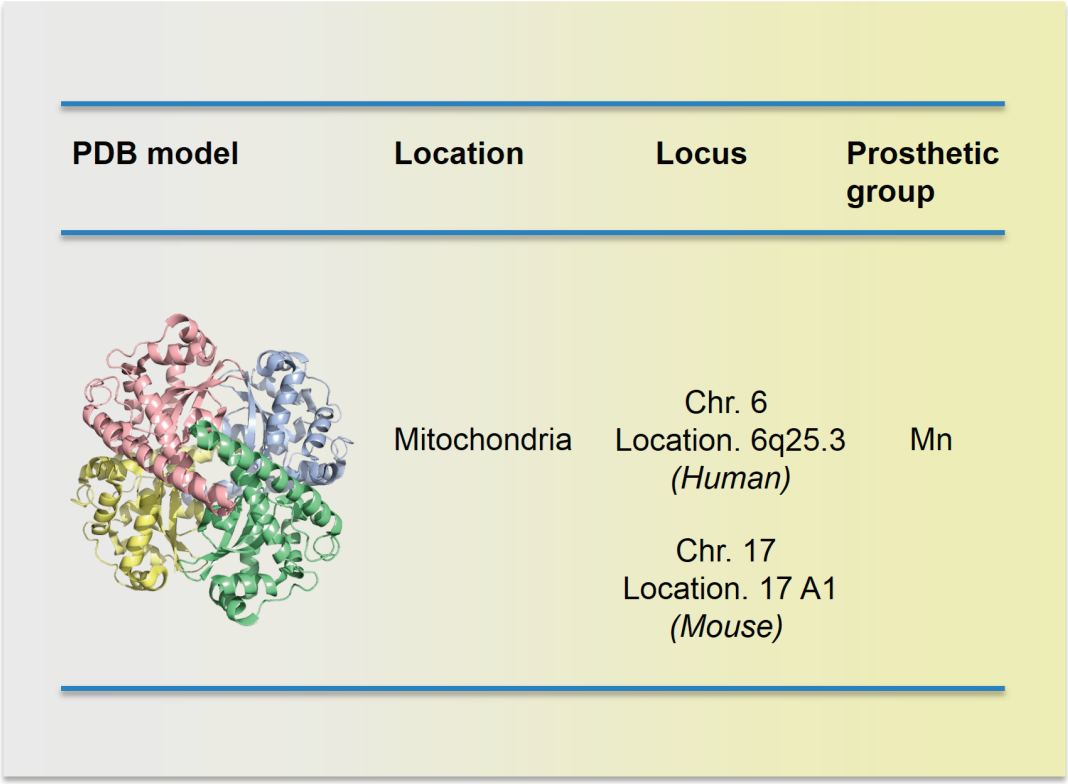

Figure 1.4 SOD2 structure and chromosomal location
SOD2 (PDB:2GDS [Ramilo et al., 1999]), a mitochondrial matrix protein uses manganese (Mn) as prosthetic group

mented in several diseases and can lead to development of oxidative stress within the mitochondria and/or the cell [Miao and St Clair, 2009; Holley et al., 2012]. SOD catalysed dismutation reaction is summarized below, where M stands for metal (Cu^{2+} or Mn^{3+}). The rate constants of SOD catalysed reaction is very high (SOD1 rate constant ~$6.4 \times 10^9\ M^{-1}\ S^{-1}$; SOD2 rate constant ~$6.8 \times 10^8\ M^{-1}\ S^{-1}$) and do not vary in the wide pH ranging from 5.5

to 9.0 [Gray and Carmichael, 1992; Miwa et al., 2008]. Although spotaneous dismutation reaction in absence of SOD is also occurring, but at a much slower rate, the rate constant of this reaction is approximately $2 \times 10^5\ M^{-1}\ S^{-1}$ [Gray and Carmichael, 1992].

$$M^{n+}.SOD + O_2^{\bullet -} \longleftrightarrow [M^{n+}.SOD\text{-}O_2^-] \longleftrightarrow M^{(n-1)+}.SOD + O_2 \quad (1)$$

$$M^{(n-1)+}.SOD + O_2^{\bullet -} + 2H^+ \longleftrightarrow [M^{n+}.SOD\text{-}O_2H_2] \longleftrightarrow M^{n+}.SOD + H_2O_2 \quad (2)$$

1.4 Cre-LoxP System

Gene targeting in mouse become a very popular strategy to study gene function in vivo. Most of this technique utilizes the advantages of bacteriophage P1 derived Cre-LoxP and to a lesser extent *Saccharomyces cerevisiae* derived Flpe-FRT systems [Kos, 2004; Maizels, 2013; Tahimic et al., 2013]. Much of the dominance of Cre-loxP system obtains from the potential to generate conditional or tissue specific mutants. Conditional deletions can overcome the barrier of embryonic lethality of essential genes as well as can study the function of a gene in a tissue specific manner [Kos, 2004; Maizels, 2013; Tahimic et al., 2013]. Cre is a member of site specific tyrosine recombinase [Branda and Dymecki, 2004] that recognizes a target site, termed as loxP and mediates the recombination between two loxP sites. LoxP site is a 34 base pair DNA sequence with 8 base pair core sequence that determines the direction and flanking this 8 base pair core are 13 base pair palindromic sequences or

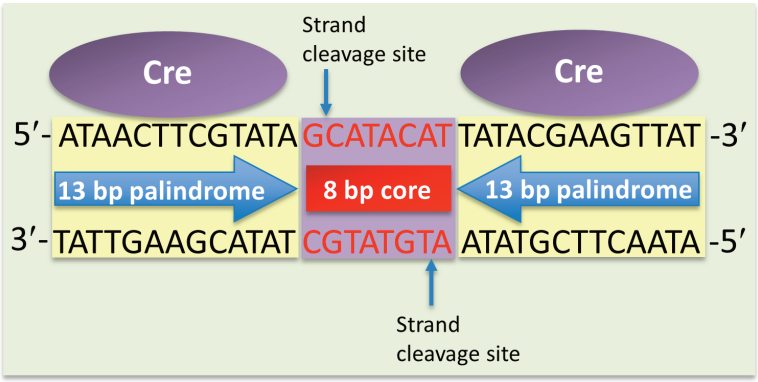

Figure 1.5 LoxP Site and Cre recombinase recognition

LoxP site constists of a 13 base pair palindromes (inverted repeats) and a 8 base pair core. Cre recombinase recognizes 13 base pair inverted repeats.

inverted repeats [Branda and Dymecki, 2004; Kos, 2004]. Cre protein binds to the 13 base pair inverted repeats and then mediates the recombination within 8 base pair core (Figure 1.5). Depending on the position and orientation of the two loxP sites relative to each other,

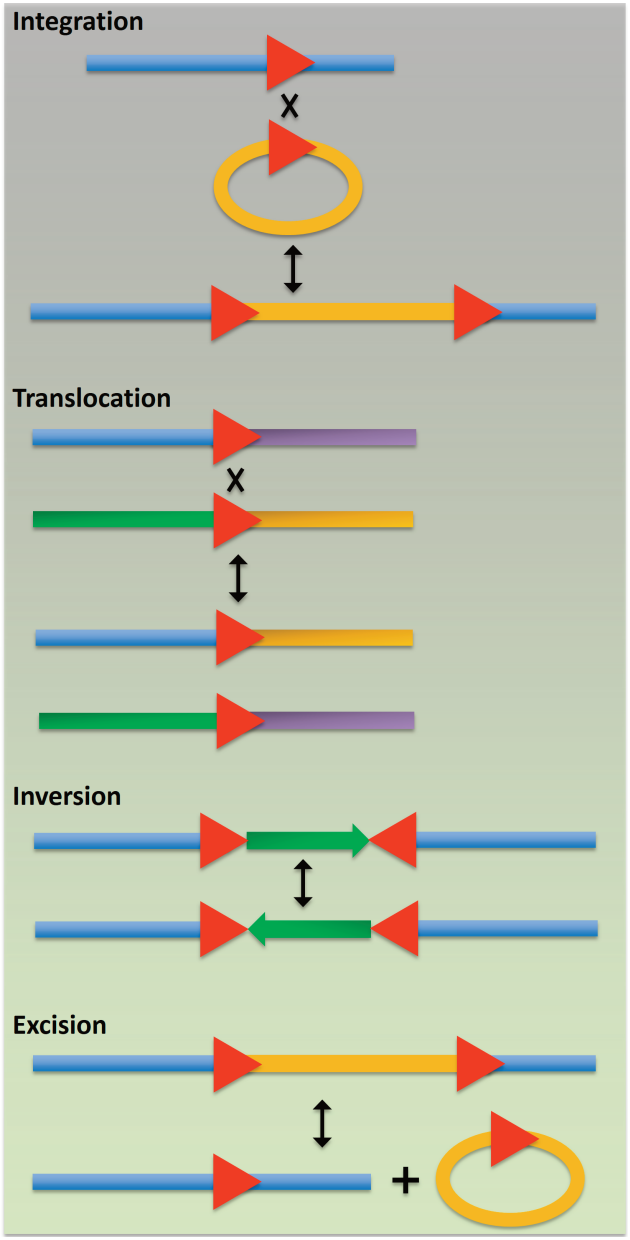

Figure 1.6 Cre recombinase mediated recombination events

Different types of Cre recombinase mediated recombination events can happen depending on the orientation (direction) and position of two loxP sites on DNA molecule. Integration occurs between two loxP sites (red triangle) when they are present on two different DNA molecules. Translocation occurs when two loxP sites are present in two different chromsomes, resulting in exchange of chromosomal segments. Inversion of the sequence between two loxP sites occurs, when these loxP sites are present in opposite direction. When two loxP sites are present in same direction in a DNA molecule, the region between the loxP sites is circularized and excised out by Cre recombinase.

different types of site specific recombination events are mediated by Cre recombinase, viz., integration, translocation, inversion and excision [Tahimic et al., 2013]. Integration occurs between two loxP sites present in two separate DNA molecules, while translocation event occurs between two chromosomal segments that each carry a loxP site. When two loxP sites are present in a DNA molecule in opposite directions, Cre recombinase inverses the sequence between the loxP sites. When two loxP sites of similar direction are located in the same DNA molecule, Cre recombinase excise the sequence between the loxP sites [Wu et al., 2007; Tahimic et al., 2013] (Figure 1.6).

In Cre-LoxP system for the generation of conditional or tissue specific knockout mice, two different mice are used. One mouse (Cre transgenic mouse) contains the Cre recombinase transgene downstream of a cell type specific promoter of interest. The second mouse contains two loxP sites in same direction around an essential part of a gene of interest (floxed mouse). When this mouse (floxed mouse) containing the floxed alleles (region of interest flanked on both sides by loxP sites) are crossed with a specific Cre-expressing mouse (Cre transgenic mouse), the resulting offspring will inherit both the floxed gene and the Cre-expressing transgene. In the tissue where the Cre recombinase is expressed, the DNA region flanked by the loxP sites will be excised, while in other tissues, which do not express Cre recombinase, the targeted gene region flanked by loxP sites remains unaltered [Nagy, 2000; Kos, 2004].

1.5 Importance of Superoxide dismutase 2

The mitochondrial superoxide dismutase 2 (SOD2) is an important mitochondrial antioxidant enzyme [Zelko et al., 2002; Halliwell and Gutteridge, 2007; Miao and St Clair, 2009; Fridovich, 2013]. To study the importance of SOD2, several models of SOD2-deletion have been developed in different organisms. In mouse a constitutive deletion of SOD2 is found to be lethal [Li et al., 1995; Lebovitz et al., 1996; Huang et al., 2006]. The time point of death depends on the mouse strain and varies from late embryogenesis to early postnatal life (up to 18 days). The reasons for the early lethality are complex. Animals suffer from metabolic changes, alterations in liver physiology, cardiac dysfunction in terms of dilated cardiomyopathy (DCM), neuronal degeneration predominantly in the brainstem and basal ganglia, and several other defects. These mice also show growth defects [Lebovitz et al.,

1996; Melov et al., 1998]. Consistent with a critical role of SOD2 in cardiomyocytes, it was also reported that the lifespan of these animals could be extended by treatment with antioxidants, which prevented DCM development in these mice [Melov et al., 1998]. Interestingly, the level of life-span extension depended on the ability of the antioxidants to cross the blood brain barrier. Nevertheless, even the treated mice died at around one month of age, most likely due to a neuronal phenotype [Melov et al., 1998]. More recently, conditional mutants of SOD2 have been developed and it was shown that specific deletion of SOD2 in the liver, kidney, and skeletal muscle is non-lethal in mice [Ikegami et al., 2002; Lustgarten et al., 2009; Kuwahara et al., 2010; Lustgarten et al., 2011; Parajuli et al., 2011]. In contrast and in line with the constitutive knockout, mice with heart/smooth muscle-specific deletion of SOD2 were found to develop congestive heart failure and the animals died at around 4 months of age [Nojiri et al., 2006]. Interestingly, connective tissue-specific deletion of SOD2 results in a premature aging phenotype and reduced survival with a median lifespan of 444 days [Treiber et al., 2011].

There were so far few attempts to study the function of SOD2 in the nervous system by generating a conditional deletion in motor neurons and in PNS neurons. Incomplete deletion of SOD2 in motor neurons by using VAChT-Cre exhibited normal lifespan of the mice, displayed no motor weakness, tremors or paralysis and maintained normal neuronal numbers [Misawa et al., 2006]. Nestin-promoter driven Cre resulted in complete loss of SOD2 in all cell types in the CNS and an incomplete deletion in the PNS, causing early postnatal mortality and morphological alterations in the brain similar to mice bearing a constitutive deletion [Oh et al., 2012].

Aims of the study

As mentioned earlier, previous studies have reported phenotypic characteristics of germline knockout of SOD2 and have explained DCM as the most probable cause for early lethality. The other studies including conditional knockout of SOD2 on contrary have not described any further involvement of SOD2 in life expectancy. Although various SOD2 knockout models mostly have reported signs of neurodegenaration, however, the specific contribution of neuronal ROS was not clearly characterized so far.

The present study, therefore, was designed to investigate the physiological role of SOD2 in neuronal homeostasis by generating a novel conditional-knockout mouse model. This mouse model was constructed with neuron-specific deletion of SOD2 using iCre under the control of CamKIIα promoter, which express in excitatory neurons of the forebrain. This work should allow to address the following questions:

I) Is there a difference between the functions of neuronal and non-neuronal SOD2, particularly in forebrain?
II) What are the consequences of neuronal redox imbalance in forebrain?
III) How does neuronal redox imbalance contribute to neurodegenerations as well as cerebral homeostasis?

2. MATERIALS AND METHODS

2.1 Generation of SOD2^{nko} Mice

Mice expressing Cre recombinase under the control of Ca2+ /calmodulin-dependent protein kinase IIα promotor (CamKIIα-iCre$^{+/-}$) [Casanova et al., 2001] were crossed with mice carrying the homozygous floxed SOD2 allele (SOD2$^{fl/fl}$) [Strassburger et al., 2005, Treiber et al., 2011] to generate CamKIIα-iCre$^{+/-}$;SOD2$^{fl/+}$ mice. In a second breeding step, CamKIIα-iCre$^{+/-}$;SOD2$^{fl/+}$ mice, which came from the first breeding were crossed with homozygous SOD2$^{fl/fl}$ mice to generate neuron-specific SOD2-deficient offsprings (CamKIIα-iCre$^{+/-}$;SOD2$^{fl/fl}$). All mice were back crossed to C57BL/6J background for at least 11 generations. Mice were maintained under specific pathogen-free conditions in the animal facility (12 hrs light-dark cycle) of University of Ulm. All experiments were performed in compliance with institutional guidelines and German animal protection law and approved by Regierungspräsidium Tübingen (Tübingen, Germany).

2.2 Genomic DNA Analysis

Genomic DNA was prepared from brain tissue (different regions) and tail tips according to the standard protocols. In brief, tissue was digested with Proteinase K overnight at 65°C and then nucleic acid fraction was precipitated with phenol-chroloroform-isoamyl alcohol, the precipitate was washed with 70% ethanol, air dried and them dissolved in TE (10 mM Tris, pH 8, 1 mM EDTA) followed by RNase treatment for 30 min at 37°C. This DNA sample was used for genotyping PCR. Recombination and deletion of SOD2 floxed site was determined by PCR using Genomic DNA purified from brain tissues. In case of SOD2, presence of 840 base pair (bp) band signifies the flox allele, while band in 800 bp denotes wild type allele and band at 200 bp represents recombined or deleted allele. For CamKIIα-iCre, 521 bp PCR product indicates the presence of Cre transgene (Cre positive). For the quantification of recombined SOD2 allels in brain tissues, quantitative realtime PCR was performed using Applied Biosystem 7300 system and SYBR Green based chemistry. The relative amount of exon 3, which would be deleted as a result of Cre mediated recombination, was quantified from the Ct values of exon 1 and exon 3 of SOD2 gene and this value was normalized with the Ct value of an unrelated gene, β-actin.

Table 2.1.1 PCR primers and PCR programs

Gene Name	Primers	Program	Product Size
SOD2 mouse	Fwd: GAAAGTCACCTCCACACACAGA Rev: GAGGGGCATCTAGTGGAGAA	94°C – 3 min 30 cycles of 94°C – 40 sec 55°C – 40 sec 72°C–1 min 10 sec Final extension 72°C–10 min	850 bp flox SOD2, 800 bp wild type SOD2, 200 bp SOD2 deleted
iCre mouse	Fwd:CTCCAACCTGCTGACTGTGCACC Rev:CAATGCGCAGCAGGGTGTTGTAGG	94°C – 3 min 30 cycles of 94°C – 40 sec 60°C – 40 sec 72°C–1 min 10 sec Final extension 72°C–10 min	521 bp
SOD2 mouse	Exon 1 Fwd:ACCGCTTCGCTGTGTCCTTGC Rev:TTTACACGACCGCTGCTCTCCTC Exon 3 Fwd:ATGTTACAACTCAGGTCGCTCTTCAG Rev: CTTAGGGCTCAGGTTTGTCCAGAA	95°C – 10 min 40 cycles of 95°C – 15 sec 60°C – 1 min	
β-Actin mouse	Fwd: ACGCGCAGCCACTGTCGAGTC Rev: CGGCGTCCCTGCTTACCTGG	95°C – 10 min 40 cycles of 95°C – 15 sec 60°C – 1 min	

2.3 Primary Neuron Culture

Hippocampal cultures obtained from P1-P2 days old pups and were incubated in neuronal minimal essential medium (NMEM)/B27 medium as described previously [Goetze et al., 2003; Knoll et al., 2006]. In brief, hippocampal neurons (5×10^3-5×10^4) were cultured on poly-l-lysine (100 µg/mL; Sigma) and laminin-coated (20 µg/mL; Gibco) coverslips (13 mm) and were incubated either in conventional culture conditions (20% O_2) or in presence of 3% O_2 , 5% CO_2 at 37°C for 3-5 days.

2.4 Intracellular ROS measurement (In vitro)

Generation of reactive oxygen species (ROS) was determined in primary hippocampal neurons using indirect fluorescence with 5-(and-6)-chloromethyl-2',7'-dichlorodihydrofluorescein diacetate (CM-H_2DCFDA, Life Technologies). In brief, 5×10^3 primary neurons were seeded into six well culture plates and stained with 5 µM CM-H_2DCFDA dissolve in DMSO for 30 minutes at 37°C. After incubation, neurons were washed with sterile HBSS, suspended in 200 µl of HBSS and were subjected to fluorescence microscopy using Zeiss Axiovert 200M microscope with FITC (green) filter.

2.5 Western Immunoblot Analysis

Tissues were washed with ice cold PBS and then homogenized in RIPA buffer (Pierce) containing protease and phosphatase inhibitors (Pierce) using TissueLyser II (Qiagen). The homogenate was then centrifuged at 14000 RPM for 20 min to collect the supernatant. The protein content in the supernatant was determined by Bradford assay (Biorad). In brief, 1 µl of supernatant was mixed with 200 µl of Bradford Reagent and 799 ml of milli-Q water. After 5 min of incubation the absorbance of the sample was measured at 595 nm. The concentration of the protein present in the sample was calculated from the BSA standard curve. 70-100 µg of protein were subjected to 10%, 12% and 4-20% Tris–Glycine SDS–PAGE gels (as applied). After the SDS-PAGE separation, the proteins were transferred onto nitrocellulose membrane (Whatman Protran, 0.45µm) overnight at 4°C using a wet transfer system. After the transfer, the blot was subsequently blocked with blocking buffer (5% nonfat dry milk or BSA for phosphorytated protein detection, 0.1% Tween-20 in 50 mM Tris, pH 7.6, 150 mM NaCl). Thereafter, the membrane was incubated with primary antibody (in blocking buffer) for overninght at 4°C. After the primary antibody incubation, the membrane was washed with TBS-T (50 mM Tris, 150 mM NaCl, 0.1% Tween-20), and then incubated with HRP conjugated appropriate secondary antibody (Jackson Immunoresearch Laboratories) for 1 hour in room temparature. After wahsing with TBS-T, the membrane was incubated with Lumiglo ECL reagent (Cell Signaling Technologies) and luminescence signals were detected in Luminescent Image Analyzer (Fujiflim). Primary and seconadry antibodies used for western blot analyses are listed in Table 2.5.1.

Table 2.5.1 List of primary antibodies used in this study for Western Immunoblotting

Name of Antigen	Company	Catalogue Nr.	Dilution
SOD2	Millipore	06-984	1:2000
Histone H2AX (phospho-Ser139)	Stressgen	KAM-CC255	1:1000
Nrf2	Santa Cruz	Sc-13032	1:1000
Phospho-JNK	Cell Signaling	9255	1:2000
JNK	Cell Signaling	9258	1:1000
p21	BD Pharmingen	556430	1:1000
MBP	Abcam	ab40390	1:1000
β-Actin	Cell Signaling	4970	1:1000
Goat anti-Mouse IgG (H+L)	Jackson Immunoresearch	115-035-146	1:12000
Goat anti-Mouse IgG (H+L)	Jackson Immunoresearch	111-035-144	1:12000

2.6 Histology and Immunostaining

Brains were perfused and fixed with 4% PFA (overnight at 4°C) and then embedded in paraffin using a Tissue Processor (Leica TP1020). 5-7 µm thick coronal sections were used for routine histology and other immunostainings. Heat-mediated antigen retieval was performed with 10 mM sodium citrate buffer (pH 6). Sections were washed in PBS (137 mM NaCl, 2.7 mM KCl, 10 mM Na_2HPO4, 1.8 mM KH_2PO4, pH 7.4), blocked with 5% BSA and 5% serum (from the same host where the secondary antibody was raised in) for 1 hour at room temparature and then incubated with primary antibodies for overnight at 4°C. The sections were washed with PBS and then incubated either with biotinylated secondary antibodies (Vector Labs) or alexa fluor dye conjugated secondary antibodies (Life Technologies) for 1 hour in room temparature. For cryosections, brains were cryofixed using standard protocol, embedded in cryoprotectants and cut into 3-5 µm coronal sections. For permeabilization, sections were incubated with 0.5% Triton X-100 or Citrate buffer (0.1% citrate, 0.1% Triton X-100 in PBS) for 15 minutes. Blocking was performed using 1:100 mouse Fc block (BD pharmingen) in PBS. Staining was performed as described above. In immuno-

fluorescence studies, DAPI was applied for nuclear counterstaining. Isotype control sections were incubated with respective IgG as primary antibodies. Primary and seconadry antibodies used for immunostainings are listed in Table 2.6.1.

Table 2.6.1. List of primary antibodies used in this study for Immunohistochemistry/ Immunofluorescence

Name of Antigen	Company	Catalogue Nr.	Dilution
NeuN	Millipore	MAB377	1:1000
SOD2	Stressgen	ADI-SOD-110	1:100
β-Tubulin (Class III)	Covance	MMS-435P	1:1000
MAP2	Abcam	ab28032	1:1000
Heme Oxygenase 1 (HO1)	Abcam	ab13248	1:500
Bax	Cell signaling	2772	1:200
Neurofilament-H	Cell signaling	2836	1:200
Cleaved Caspase-3	Cell signaling	9664	1:200
Phospho-p53	Cell Signaling	9284	1:450
PUMA	Abcam	ab54288	1:150
8-Oxoguanine	Millipore	MAB3560	1:300
GFAP	Cell Signaling	3670	1:300
Iba1	Wako	019-19741	1:250
Doublecortin	Abcam	ab18723	1:500
Insulin	Cell Signaling	3014	1:400
MDA	Abcam	ab6463	1:200
CRH-R1	Pierce	PA5-18801	1:200

2.7 Cytochrome C Oxidase and Succinate Dehydrogenase (COX-SDH) Histochemistry

10µM brain cryosections were used for COX-SDH histochemistry staining, which is a measure of mitochondrial respiratory acitvities [Seligman et al., 1968; Trifunovic et al., 2004; Nojiri et al., 2006; Ross, 2011]. For COX (Complex IV) histochemistry, the air dried

cryosections were incubated in the 3-3' Diaminobenzidine (DAB) staining solution (50 mM sodium phosphate, pH 7.4, 1 mg/ml DAB, 1 mg/ml Cytochrome C, 75 mg/ml Sucrose and 24 Units/ml Catalase) for 20 min at room temperature in the dark. For SDH (Complex II) histochemistry, the air dried cryosections were incubated in the Nitroblue tetrazolium (NBT) staining solution (50 mM sodium phosphate, pH 7.4, 84 mM Succinate, 0.2 mM Phenazine methasulphate, 2 mg/ml NBT, 4.5 mM EDTA) for 20 min at room temperature in the dark. After the staining, the slides were washed with PBS three times and then series of gradual dehydration steps cleared in xylene and finally mounted in Entellan (Millipore). Addition of 2.5 mM sodium azide in the COX staining solution and omission of sodium succinate in the SDH staining solution act as negetive control for the COX and SDH staining, respectively [Ross, 2011].

2.8 Terminal deoxynucleotidyl transferase dUTP nick end labeling (TUNEL) staining

For in situ detection of cell death, TUNEL staining was performed with cryosections (7µm) of P21-P24 days old mice brain using In Situ Cell Death Detection Kit, Fluorescein (Roche). Paraffin embedded tissue sections were deparaffinized by incubating at 60°C and then through two changes in xylene. The deparaffinized tissue sections were then rehydrated through a graded series of ethanol and finally water. The section was then permeabilized with Proteinase K for 30 min at 37°C and then rinsed twice with PBS. The section was then incubated with labeling solution (Terminal deoxynucleotidyl transferase, fluorescein labelled nucleotides) for 60 min at 37°C in dark. After labelling, the sections were wached two times with PBS and counter stained with DAPI and mounted in antifade.

2.9 Image Acquisition

Fluorescence images were acquired on a Zeiss Axiovert 200M microscope equipped with filters for DAPI, FITC, DsRed and Texas Red. The Zeiss Axiovert 200M microscope was connected with Axiocam camera and using Zeiss AxioVision software images were acquired. Zeiss objective lenses with 10X, 20X, 40X and 63X (oil) magnification were used. Caspase-3 immunofluorescence images were aquired on Olympus scan^R microscope. Bright-field images were acquired with a compound light microscope (Leica).

2.10 Enzyme-Linked Immunosorbent Assay (ELISA)

Protein carbonyl content was detected using OxiSelect™ Protein Carbonyl ELISA Kit (Cell Biolabs) and quantity of 3-nitrotyrosine was measured using OxiSelect™ Nitrotyrosine ELISA Kit (Cell Biolabs). Plasma ACTH level was measured using ACTH (Mouse/Rat) ELISA Kit (Abnova). Serum growth hormone (GH) level was determined using Rat/Mouse Growth Hormone ELISA Kit (Millipore). Serum insulin was meaured using Ultra Sensitive Mouse Insulin ELISA Kit (Crystal Chem). All of the above mentioned experiments were performed following the instructions of the respective manufacturers.

2.11 Blood Sugar Test

Blood sugar level (mg/dl) was determined in fasted as well as in fed mice. P21 days old mice were kept fasted for 12 hours. Blood samples were collected by tail vein incision. Fed and fasting blood glucose level was measured using a glucose meter (Contour, Bayer).

2.12 ATP Production Assay

ATP production in the cortical tissue was measured using a commercial kit, which utilizes the phosphorylation of glycerol to generate a product that is easily quantified by colorimetric method (OD 570 nm) (ATP Colorimetric/Fluorometric Assay Kit, Biovision). The assay was perfomred as per manufacturer instruction, in breif, tissue was homogenized in ATP assay buffer provided with the kit. The homogenate was then deproteinized and filtered through 10kDa spin column. The protein free lysate was then mixed with ATP probe and ATP converter, provided in the kit and after 30 min incubation at room temperature, the absorbance of the sample was measured (OD 570 nm) in a microplate reader. ATP concentration (nmol) was calculated by plotting the absorbance against Standard Curve.

2.13 NAD and NADH Quantification

NAD/NADH quantification was performed using a commercial kit (NAD+/NADH Quantification Colorimetric Kit, Biovision #K337-100). 20 mg of brain tissue was washed with ice cold PBS two time, afterwards the tissue was homogenized in NADH/NAD extraction buffer using TissueLyser II (Qiagen). The tissue homogenate was centrifuged at 14000 rpm

for 5 min and 4°C. The supernatant was then passed through 10kDa molecular cut off filter to remove the enzymes that may consume NADH in the sample. This filtrate was used for the measurement of total NADt (NADH and NAD) as well as NADH. For the measurement of NADt, 50 µl of filtrate was used and for the measurement of NADH, the NAD present in the filtrate was first decomposed by heating the samples in 60°C for 30 min and then 50 µl these NAD decomposed samples was used. The kit utilizes a proprietary developer system that measure NADH. Therefore, in the NADt, the NAD present in the sample was first converted into NADH using a enzyme mix and then NADH developer was added, followed by incubation at room for 1 hr. In the NAD decomposed sample, where only NADH was present, NADH developer was added and incubated at room temperature for 1 hr. After the incubation, NADH level was quantified in both the NADt (containing NADH as well as NAD converted NADH) and NAD decomposed (only NADH) samples by measuring the absorbance at 450 nm. The NAD/NADH ratio was calculated using the formula (NADt-NADH)/NADH.

2.14 Quantitative Real-Time PCR (qRT-PCR)

Total RNA was isolated from hypothalamic tissue (surgically isolated from whole brain) of P21 days old mice using RNeasy lipid tissue mini kit (Qiagen) as per recommended protocol. 2 µg of total RNA was reverse transcribed to synthesise cDNA using illustra Ready-To-Go RT-PCR beads (GE Healthcare) and oligo(dT)$_{12\text{-}18}$ with program 42°C for 30 min (reverse transcription reaction) and 95°C for 5 min (inactivation of reverse transcriptase and denaturation of total RNA). This cDNA was later used for quantitative PCR analyses using SYBR green master mix (Life Technologies) and 7300 Realtime PCR system (Applied Biosystem) with a program setting 95°C for 10 min (activation of AmpliTaq polymerase), 40 cycles of 95°C for 15 sec (denaturition) and 60°C for 1 min (annealing and extension). The relative expression of different genes was calculated based on previously described method [Pfaffl, 2001]. Primer sequences are provided in Table 2.14.1.

2.15 Statistical Analysis

The two-tailed t-test or one-way ANOVA were used to compare the independent measurements. For repeated comparison at different time points, a correction of the *P*-values ac-

cording to Bonferroni (i.e. multiplication of each *P*-value by the number of time points) was performed. For comparisons of survival times, the log-rank test was applied, optionally stratified for gender. All tests were two-sided. Error bars depict standard error of mean (SEM). Data were analyzed by GraphPad Prism and MS-Excel.

Table 2.14.1 Primer sequences used for PCR and qRT-PCR analysis.

Gene Name	Forward and Reverse Primer Sequence
CRH mouse	Fwd: TCTGCGGGAAGTCTTGGAAATGG
	Rev: CAAGCGCAACATTTCATTTCCCG
GHRH mouse	Fwd: ATGCTGCTCTGGGTGCTCTTTGTG
	Rev: CATCTACGTGTCGCTGCATCCTG
TRH mouse	Fwd: CCCTGGATGGAGTCTGATGTCACC
	Rev: ACCCTCCTCTCCCTCTGTTTCTTCC
NPY mouse	Fwd: CGCTCTATCTCTGCTCGTGTGTTTGG
	Rev: AGAGCGGAGTAGTATCTGGCCATGTC
HCRT mouse	Fwd: GCTGCGGGTATCCTGACTCTGG
	Rev: TGCGTGGTTACCGTTGGCCTG
PMCH mouse	Fwd: ACTGCAGAAAGATCCGTTGTCGCC
	Rev: AGATTCTGTTTGGAGCCTGTGTTCTTTG
AGRP mouse	Fwd: GTTCTCCGCGTCGCTGTGTAAG
	Rev: AGGCATTGAAGAAGCGGCAGTAGC
GnRH mouse	Fwd: ACATGATCCTCAAACTGATGGCCG
	Rev: GGCGCAACCCATAGGACCAGTG
POMC mouse	Fwd: CTAGAGTTCAAGAGGGAGCTGGAAGG
	Rev: GCCCGTCGTCCTTCTCCGC
GFAF mouse	Fwd: AACGTTAAGCTAGCCCTGGACATCG
	Rev: GTACAGGAATGGTGATGCGGTTTTC
18S mouse	Fwd: CACGGACAGGATTGACAGATTGATAGC
	Rev: GGAATTAACCAGACAAATCGCTCCACC

2.16 General Chemicals

General chemicals (acids, standard organic salts, solvents, anorganic chemicals, etc.) were purchased from Sigma-Aldrich, Roth (Karlsruhe), Merck (Darmstadt) and Applichem (Darmstadt).

2.16.1 Common buffers and solutions

Dignam C buffer: 20 mM Hepes (pH 7.9), 25 % glycerol, 0.42 M NaCl, 1.5 mM $MgCl_2$, 0.2 mM EDTA + (1 mM PMSF, 1 mM DTT, 1 tablet/10 ml complete mini protease inhibitor [Roche, Mannheim]).

2x Laemmli/urea buffer (loading): glycerol 15 ml, 22.5 ml SDS 20%, 9.4 ml Tris (2M, pH 6.8), 28.83 g urea (final concentration 6 M), bromphenol blue + (5 % **β**-mercaptoethanol).

4x Laemmli buffer (loading): 125 mM Tris-Hcl (pH 6.8), 20 % SDS, 25 % glycerol, bromphenol blue + (5 % β-mercaptoethanol).

PBS Buffer (10x): 87.65 g/l NaCl, 2 g/l KCl, 11.7 g/l Na_2HPO_4, 2.4 g/l NaH_2PO_4; pH 7.3.

RIPA buffer: 50 mM Tris-HCl (stock 1M pH 7.4), 150 mM NaCl, 1 % Triton X-100; 0.5 % sodium desoxycholate, 0.1 % SDS + (1 mM PMSF, 1 tablet/10 ml complete mini protease inhibitor (Roche, Mannheim)).

TBS (10x): 24.2 g/l Tris, 80g/l NaCl; pH 7.6.

TNES-buffer: 50 mM Tris-HCl (stock 1M pH 7.5), 0.1 M EDTA (stock 0.5 M, pH 8.0), 0.1 M NaCl, 1 % SDS; + (Proteinase K (Applichem, Darmstadt) 0.45 µg/µl).

2.16.2 Media and buffers for neuronal culture

NMEM medium (For 100 ml): 10 ml MEM 10X (Gibco, Life technologies), 1 ml Pyruvate solution 100X (Gibco, Life technologies), 1 ml L-glutamine 200mM (Gibco, Life technologies), 4 ml $NaHCO_3$ 5.5%, 3 ml Glucose 20%, 2 ml B27 supplement (Gibco, Life technologies); volume adjusted to 100 ml with dH_2O; stored at 4^0C.

Borate-buffer: 1.24 g Boric acid + 1.9 g Borax, 400 ml dH_2O; pH 8.5; stored at 4^0C.

HBSS buffer (PAA, Pasching, Austria): Trypsin 0.05% / EDTA (Gibco, Life Technologies).

DMEM medium (Gibco, Life Technologies).

Laminin (Sigma-Aldrich).

Poly-L-Lysin (Sigma-Aldrich).

2.16.3 Chemicals and buffers for molecular biology

TBE (10x): 121.1 g/l Tris, 61.8 g/l hydroboric acid, 7,4 g/l EDTA.

1kb plus DNA ladder (Invitrogen, Life Technologies).

Agarose Ultrapure, Electrophoresis Grade (Invitrogen, Life Technologies).

Ethidium bromide (Sigma-Aldrich).

Taq Poymerase and **5x Green GoTaq Reaction buffer** (Promega, Mannheim).

dNTPs (Genaxxon, Ulm).

*All primers were purchased from Biomers, Ulm.

2.17 Softwares Used

Microsoft Office 2011
Adobe Photoshop CS6 V13.0.0
Adobe Illustrator CS6 V16.0.4
Adobe InDesign CS6 V8.0.2.413
Graphpad Prism V6.0e
ImageJ 1.48
Zeiss Axiovision 4.8
Olympus scan^R

3. RESULTS

3.1 Generation of a novel conditonal knockout mouse

To identify the specific role of neuronal SOD2 and to investigate the impact of redox imbalance on neuronal homeostasis, a mouse model was generated where the exon 3 of SOD2 gene (Figure 3.1) was specifically deleted in forebrain excitatory neurons. This exon encodes for 39 amino acids, which are responsible for the formation of the active SOD2 tetrameric protein and deletion of exon 3 has been shown to completely abrogate SOD2 function [Li et al., 1995]. To achieve this, Cre-LoxP based strategy was used. CamKIIα promoter driven

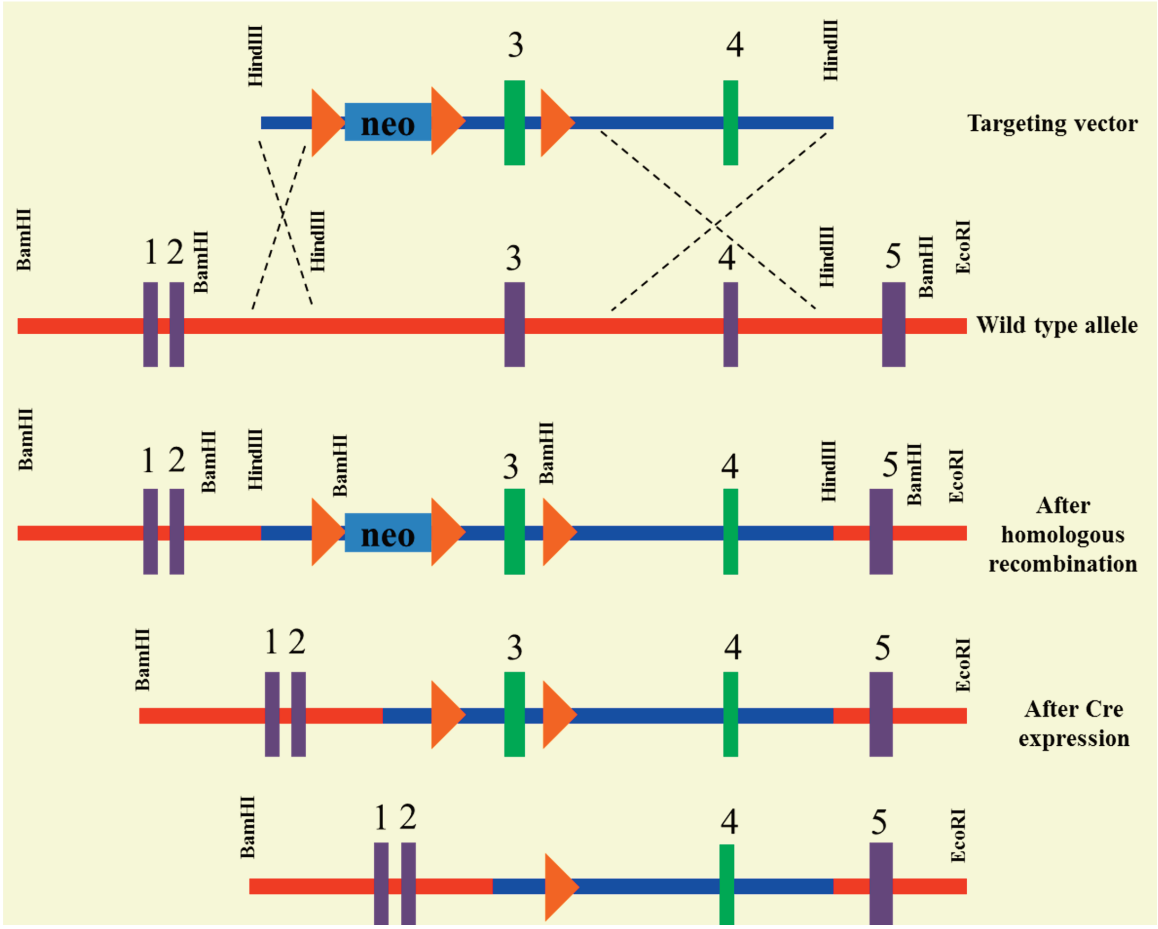

Figure 3.1. Gene targting scheme

Gene targeting vector containing 5‘ and 3‘ homology arms of SOD2 gene and LoxP sites on both 5‘ and 3‘ ends of exon 3 [Strassburger et al., 2005]. Targeting vector also contaied neomycin (neo) selection marker for the selection of targeted mouse embryonic stem cells. Homologous recommbination of targeting vector generated flox SOD2 allele. Cre recominase mediated recombination between two loxP sites led to deletion of exon 3 of SOD2 gene.

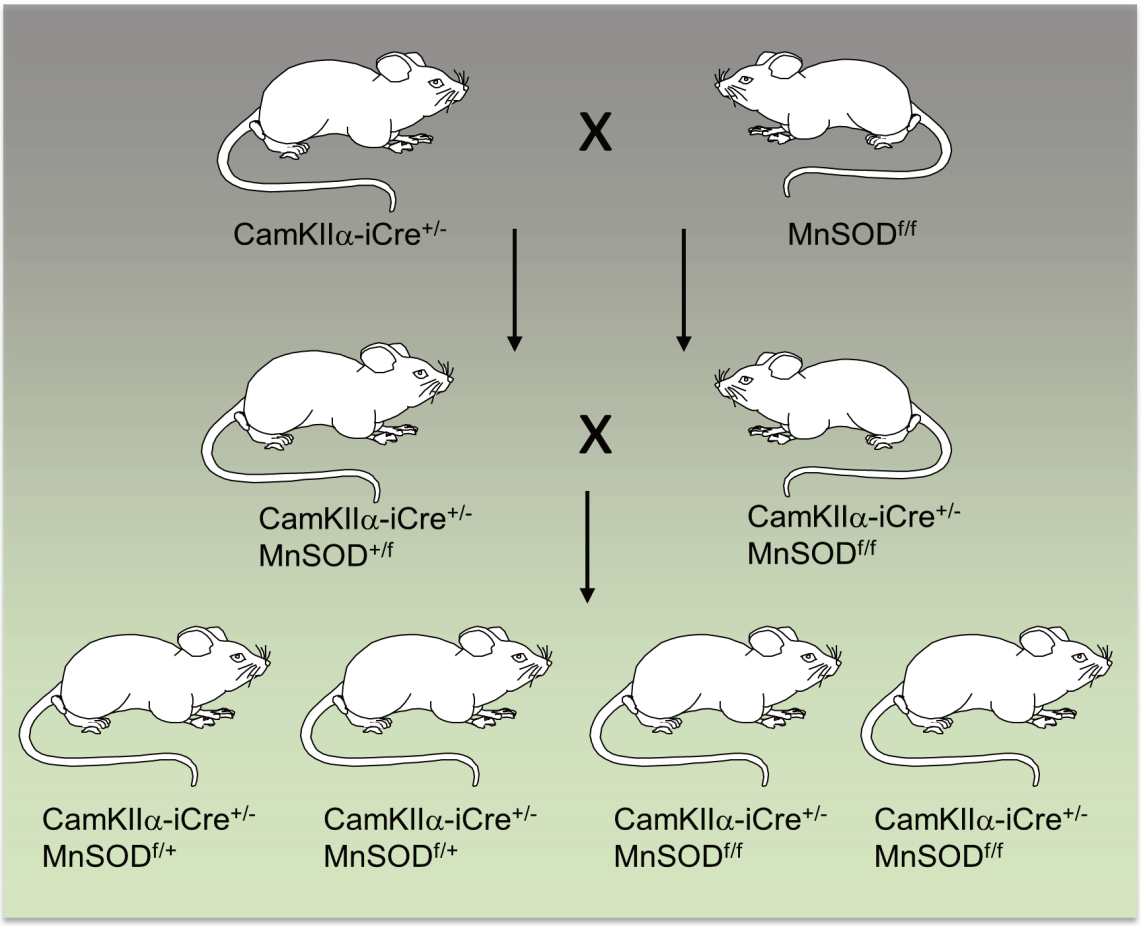

Figure 3.2. Mouse breeding scheme

In the first breeding step, CamKIIα-iCre mice (CamKIIα-iCre$^{+/-}$) were crossed with SOD2 flox mice (MnSOD$^{f/f}$). This crossing resulted in pups with two different types of genotypes (CamKIIα–iCre$^{+/-}$; MnSOD$^{+/f}$ and CamKIIα–iCre$^{-/-}$; MnSOD$^{+/f}$). CamKIIα–iCre$^{+/-}$; MnSOD$^{+/f}$ mice those came from the first breeding was then crossed with SOD2 flox mice (MnSOD$^{f/f}$) in the second breeding step. The second breeding step produces four different genotypes of mice. Mice with genotyping of CamKIIα–iCre$^{-/-}$; MnSOD$^{f/+}$ and CamKIIα–iCre$^{-/-}$; MnSOD$^{f/f}$ were considered as control (CO). Mice with genotyping of CamKIIα–iCre$^{+/-}$; MnSOD$^{f/f}$ were considered as forebrain neuron specific knockout or mutant (SOD2^{nko}) and mice with CamKIIα–iCre$^{+/-}$; MnSOD$^{f/+}$ were considered as heterozygous (HET).

iCre expressing transgenic mice (CamKIIα-iCre$^{+/-}$) [Casanova et al., 2001] were crossed with SOD2 floxed mice (SOD2$^{fl/fl}$), where exon 3 of the SOD2 gene was flanked by two loxP sites [Strassburger et al., 2005]. In this study, the resulting mice will be referred to as control (CO), heterozygous (HET) and forebrain-specific SOD2-deficient (SOD2^{nko}) mice (Figure 3.2). The detailed genotypes (with respect to CamKIIα-iCre and SOD2) of mice used in this study are represented below (Table 3.1).

Table 3.1 Genotypes of mice

CamKIIα–iCre	SOD2	Genotype
-/-	+/+	Control (CO)
-/-	fl/fl	Control (CO)
-/-	fl/+	Control (CO)
+/-	+/+	Control (CO)
+/-	fl/+	Heterozygous (HET)
+/-	fl/fl	SOD2-mutant (SOD2^{nko})

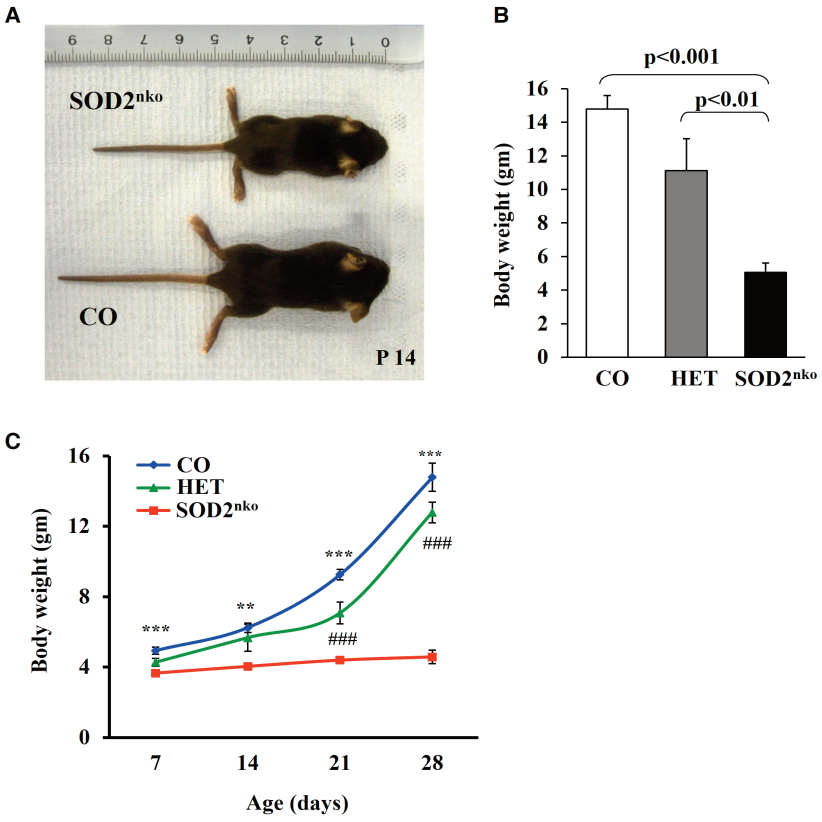

Figure 3.3. Growth retardation upon SOD2 deletion in SOD2^{nko} mice.

A. Gross appearance of the 14 days old SOD2 mutant mice (SOD2^{nko}) compared with age matched control littermates (CO) showing decreased body size.

B. Significantly reduced body weight of SOD2^{nko} mice compared with CO ($p<0.001$) and heterozygous (HET) mice ($p<0.01$) at 21 days. (CO vs SOD2^{nko} $p<0.001$, HET vs SOD2^{nko} $p<0.01$, Bonferroni Multiple comparison t-test, following One Way ANOVA).

C. Significantly reduced body weight at different time points in the life span of SOD2 mutant mice (n=15). (CO vs SOD2^{nko} ***=$p<0.001$, **=$p<0.01$; HET vs SOD2^{nko} ###=$p<0.001$, Bonferroni Multiple comparison t-test, following One Way ANOVA).

SOD2^{nko} mice were born at the expected Mendelian frequency, however 6-7 days after birth these mice could be distinguished from control (CO) and heterozygous (HET) littermates. SOD2^{nko} mice exhibited smaller body size (Figure 3.3A) and significantly decreased body weight (Figure 3.3B), which were maintained throughout the life span of SOD2^{nko} mice. In addition, these mice developed obvious motor deficits such as ataxia, imbalanced body movements, stiff tail, and half-opened eyes. These phenotypic characteristics become more obvious at later time points, often showing hyperactivity followed by spontanious multiple seizures. SOD2^{nko} mice essentially failed to thrive thus giving a static growth curve compared to the controls and heterozygous mice (CO vs KO $p<0.001$, $p<0.01$; Het vs KO $p<0.001$) (Figure 3.3C). Importantly all mutant mice died within 28-32 days (Figure 3.4) independent of the weaning timeline, whereas heterozygous mice did not display any obvious problems at least untill the time of observation (up to 6 months).

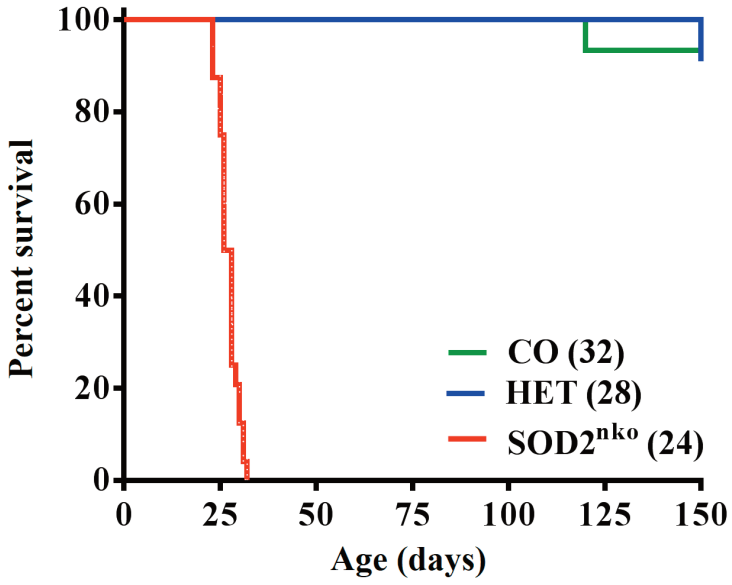

Figure 3.4. Postnatal lethality upon SOD2 deletion in SOD2^{nko} mice.
Survival curve showing early postnatal lethality (24-30 days postnataly: P24-P30) of SOD2 deficient mice (SOD2^{nko}) compared with heterogygous (HET) and control (CO) littermates.

The brains of mutant mice were analyzed at postnatal day 20 to 24. The overall appearance of the brains of mutant mice was found almost normal macroscopically and they only exhibited a smaller size compared with control. The wet brain weight of the mutant mice was

significantly lower than that of control and heterozygous mice (Figure 3.5A). However, when the brain weight is represented in relation to body weight, this ratio is higher due to the even more reduced body weight (Figure 3.5B).

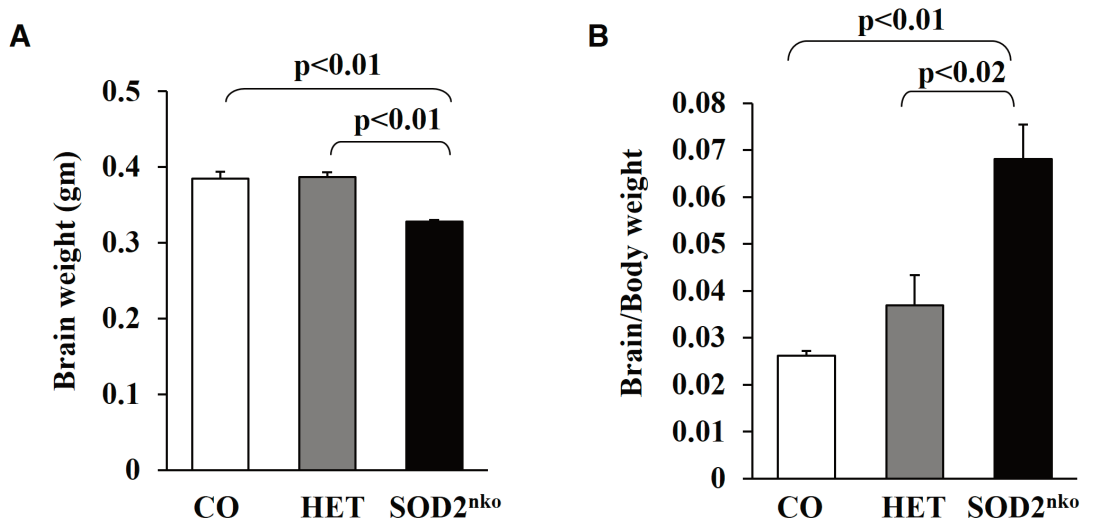

Figure 3.5. Reduced brain weight in SOD2^{nko} mice.

A. Significant reduction of wet brain weight of control (CO), heterozygous (HET) and knockout (SOD2^{nko}) mice were presented (CO vs KO $p< 0.01$, Het vs KO $p< 0.01$; Bonferroni Multiple comparison t-test, following One Way ANOVA).

B. Due to severe reduction of body weight, the brain to body weight ratio in SOD2^{nko} mice appeared higher compared with CO ($p<0.01$) and HET ($p<0.02$).

3.2 Neuron specific deletion of SOD2 in SOD2^{nko} mice

To confirm the specific and efficient deletion of SOD2, PCR analyses as well as biochemical and immunohistochemical studies were performed. Genomic DNA isolated from mouse tail was used for the routine PCR based genotyping. For iCre transgene, presence of 521 bp product reflects the presence of transgene (Figure 3.6A), while in SOD2 presence of 850 bp product reflect floxed Exon3 allele and 800 bp products denotes wild type allele. PCR analysis of cortical genomic DNA isolated from control mice showed the SOD2 floxed band of 850 base pairs, whereas in SOD2^{nko} mice this band was reduced in intensity and a novel 200 base pair fragment indicative of successful deletion was observed (Figure 3.6B).

To quantify the deletion (recombination efficiency) of Exon 3 by CamKIIα–iCre, a quantitative PCR approach was used. A portion of Exon 1 and Exon 3 of SOD2 gene and Exon 1 of β-actin gene was PCR amplified separately using SYBR green based chemistry. The

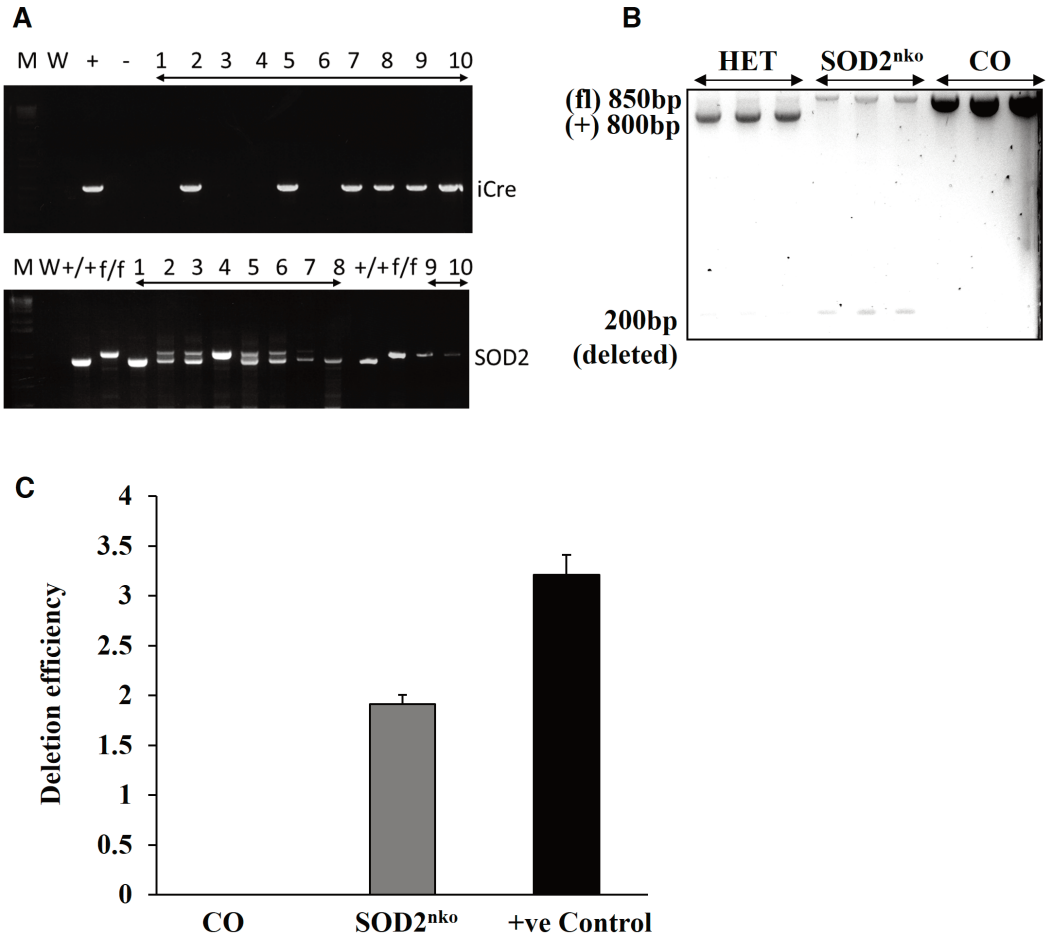

Figure 3.6. PCR based genotyping analyses

A. PCR analyses of tail genomic DNA for the detection of different genotypes of mice. The upper panel represented a typical agarose gel of iCre genotyping PCR reaction. Presence of iCre transgene was shown by a prearance of a product at 521 bp. The lower panel represened a typical 1% agarose gel of SOD2 genotyping PCR. Presence of flox SOD2 allele was reflected by apprearance of a product at 850 bp, while wild type SOD2 allele was shown by appearance of a product at 800 bp. M=DNA size ladder, W=water (negative control).

B. PCR analyses from the cortical genomic DNA suggested deletion of floxed band in knockout (200 bp product), presence of some floxed band in $SOD2^{nko}$ was indicative of nondeletion in non-neuronal cells, while in CO, only floxed band was present.

C. Deletion or recombination efficiency of SOD2 allele was quantified by real time PCR. The data shows the relative deletion of exon 3 gene in terms of Ct values ($Ct_{exon3} - Ct_{exon1}$) in the cortical genomic DNA of different genotypes (CO and $SOD2^{nko}$). The value in control is considered as no deltion (zero or near to zero). SOD2 deficient mouse dermal fibroblast, which lacked exon 3 of SOD2 gene was used as postive control for this analysis.

relative amount of product formation (Ct value) of Exon 1 and Exon 3 of SOD2 gene was normalized with actin gene (Ct value). The normalized Ct value of Exon 1 was subtracted from that of Exon 3. Value near or equal to zero considered as no deletion, which was ob-

served in cortical genomic DNA of control mice, while in SOD2^{nko} absence of Exon 3 results in less product formation (mostly coming from non-neural cells). Therefore, the subtraction value between normalized Ct values of Exon 3 and Exon 1 was always higher (Figure 3.6C). SOD2-deficient mouse fibroblast where Exon 3 was absent used as a positive control for deletion.

Western immunoblot analyses indicated a 70% -75% decrease of SOD2 protein levels in different forebrain regions (cortex, striatum, hippocampus, thalamus and hypothalamus) of SOD2^{nko} mice (Figure 3.7A-B). The residual expression of SOD2 protein seen in the Western

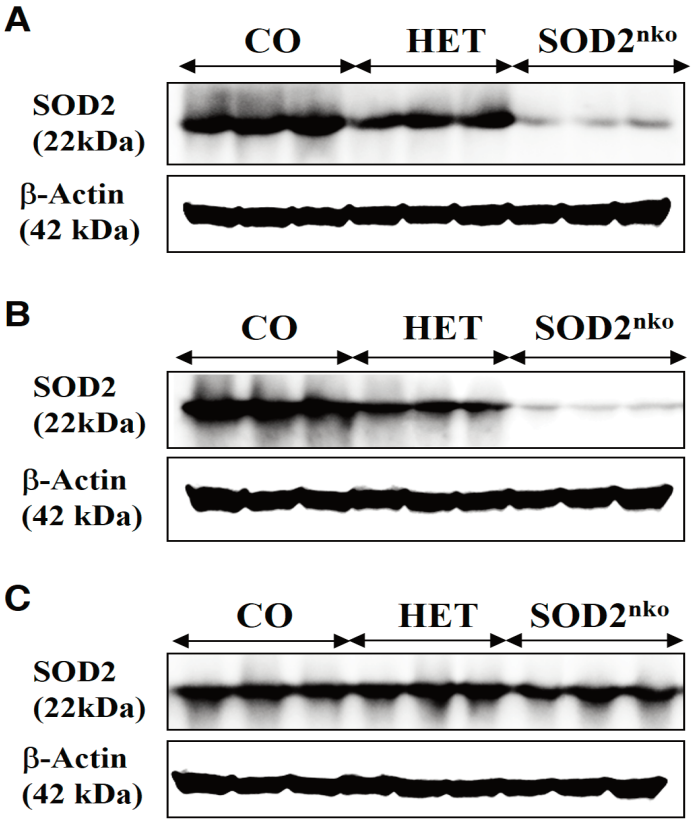

Figure 3.7. Validation of SOD2 deletion in vivo.

A-B. Representative western blot analyses of different brain regions (A) Cortex, striatum, hippocampus, and (B) thalamus, hypothalamus of SOD2 competent (CO), Heterozygous (HET) and SOD2 deficient mice (SOD2^{nko}) showed significantly lowered amount of SOD2 protein in SOD2^{nko} mice. The representative Western immunoblots presented here were one of three independent analyses.

C. In cerebellum no changes in the level of SOD2 protein was found when compared amoung control (CO), heterozygous (HET) and SOD2 deficient (SOD2^{nko}) mice. The representative Western immunoblots presented here were one of three independent analyses.

immunoblots is consistent with the fact that CaMKIIα-iCre exclusively deletes SOD2 in neurons but not in other non-neural cells of the CNS. Furthermore, as CamKIIα-iCre is not expressed in the cerebellum, the cerebellar SOD2 protein level was found to be unaltered in knockout mice and the cerebellum can be considered to function as an internal control region in the brain of knockout mice (Figure 3.7C). To reconfirm the deletion of SOD2 specifically within the brain, Western blot analyses were also performed with other organs such as heart, liver and kidney having unaltered level of SOD2 protein (Figure 3.8).

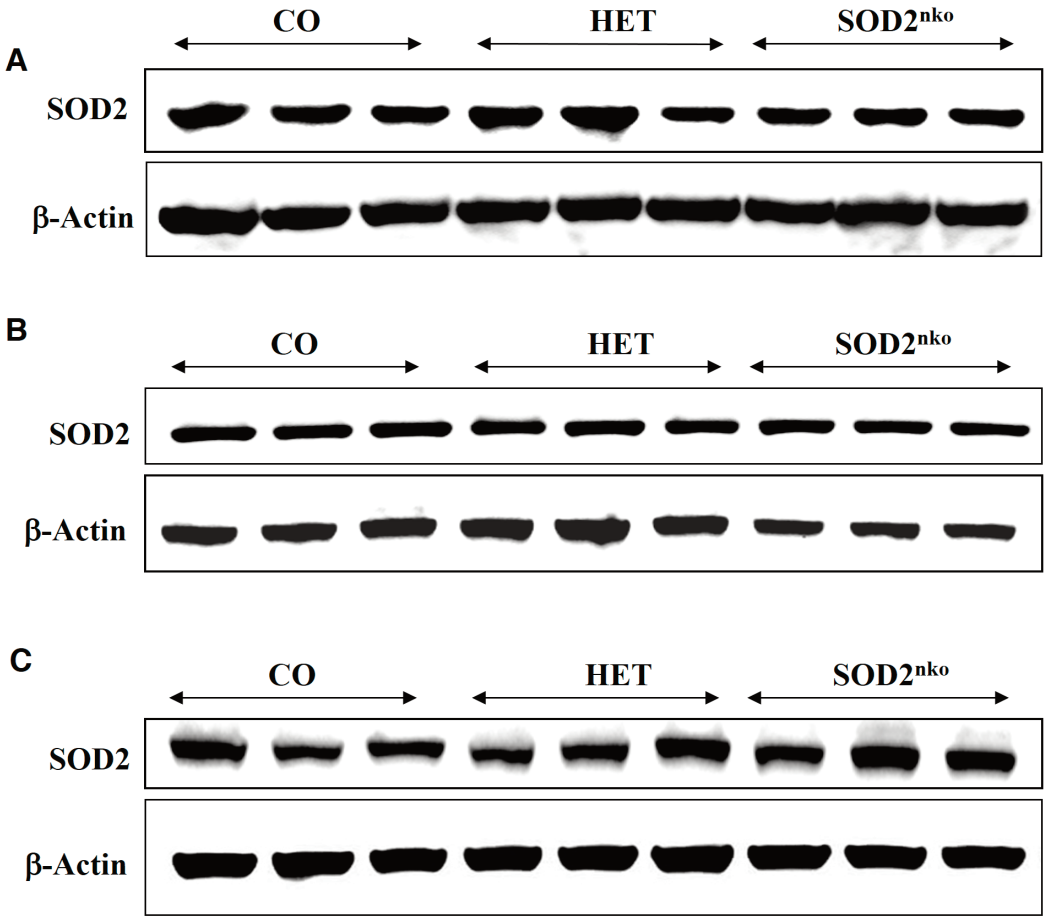

Figure 3.8. Unaltered SOD2 expression in extraneural tissue in vivo.

Western immunoblot analyses showed there were no alteration of SOD2 protein levels in several extraneural tissues such as, (A) Heart, (B) Liver and (C) Kidney. β-actin was used as a loading control. The representative Western immunoblots presented here were one of three independent analyses.

To investigate the neuron-specific deletion of SOD2, immunofluorescence studies were performed with brain cryosections using antibodies against SOD2 and a neuron-specific nuclear protein, NeuN (Figure 3.9). Only few cells stained positive for SOD2 in SOD2^{nko} mice and

they all were NeuN negative. This indicated that the presence of SOD2 was limited to non-neuronal cell types. Overall, SOD2 immunostaining was strongly reduced in brain from $SOD2^{nko}$ mice, but there was still residential expression consistant with the Western immunoblot analyses.

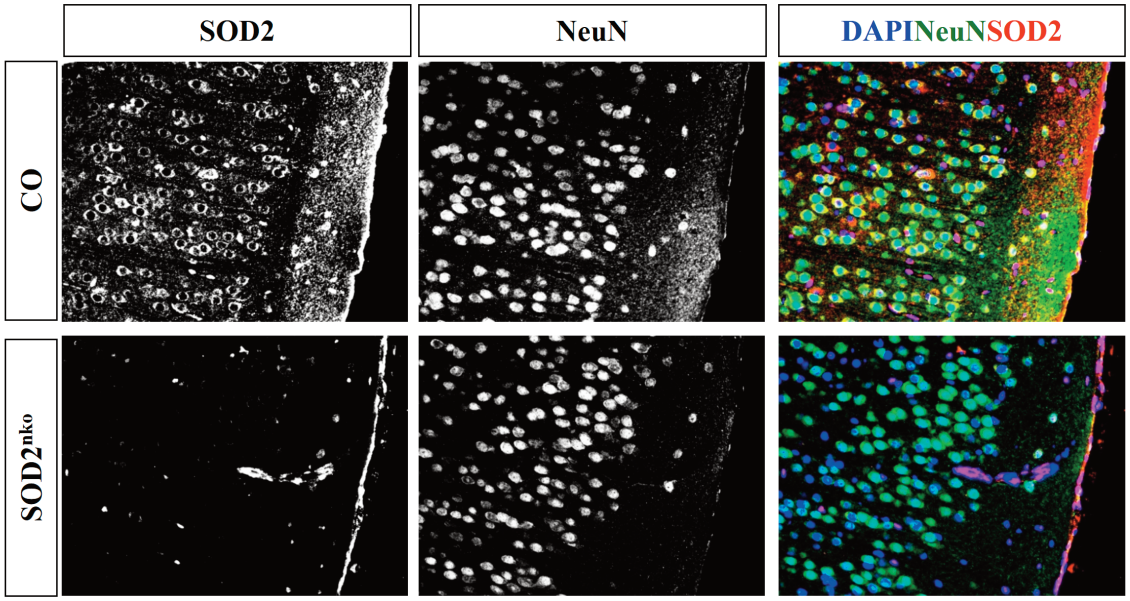

Figure 3.9. Neuron specific deletion of SOD2 in vivo
Immunofluorescence study showed residual SOD2 protein limited in non-neural cells which were identified by NeuN-negative cells (anti-SOD2: red; anti-NeuN: green, DAPI: blue, x20) in cerebral cortex.

To unequivocally demonstrate the absence of SOD2 protein in neurons, primary hippocampal neurons were isolated from $SOD2^{nko}$ mice at postnatal day 1. When such primary neuron cultures were kept in conventional culture conditions (20% O_2), the $SOD2^{nko}$ neurons did not grow efficiently and died within 24 hours of culture. However, these cultures could be established at reduced oxygen concentrations (3% O_2), where the mutant primary neurons survived for at least 5 days. Immunofluorescence studies with antibodies against the neuronal marker β-tubulin III confirmed the absence of SOD2 protein in these $SOD2^{nko}$ primary neurons (Figure 3.10A). Furthermore, neurons from $SOD2^{nko}$ mice displayed abnormal development with respect to neurite outgrowth, as predominantly uni-polar and bipolar neurites were observed, whereas neurons from control animals showed a more developed neuritic tree (Figure 3.10B).

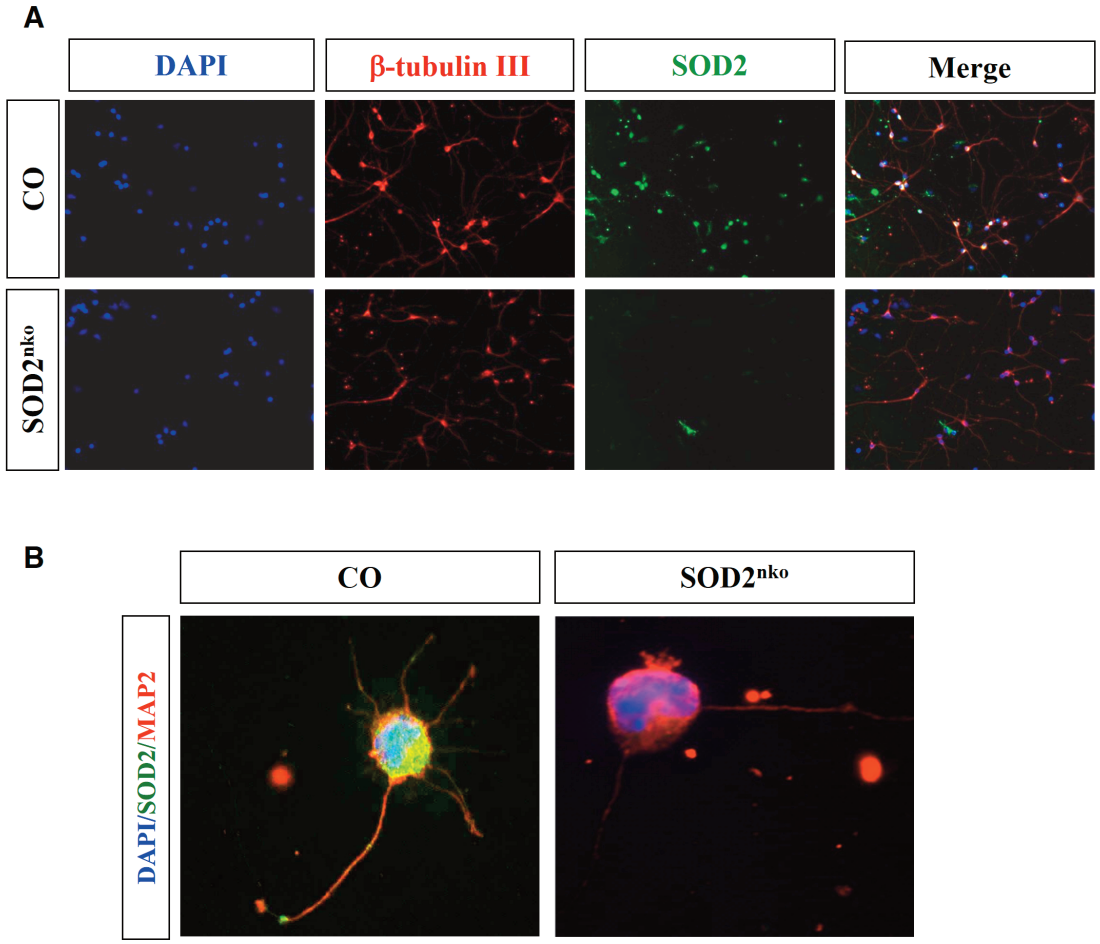

Figure 3.10. Validation of SOD2 deletion and in primary hippocampal neurons.
A. Different morphology and absence of SOD2 protein in primary hippocampal neurons (SOD2: green, β-Tubulin: red, DAPI: blue) isolated from SOD2 deficient mice at postnatal day 2.
B. SOD2 deficient neuron with abnormal neurite growth (Map2: red, SOD2: green, DAPI: blue) compared with wild-type neuron in higher magnification (63X) (n=7).

3.3 Redox imbalance associated oxidative damage in forebrain

A likely consequence of the SOD2-deficiency is the accumulation of oxidative burdens, given its role as an important antioxidant enzyme in mitochondria (Holley et al., 2011). To determine the redox state of SOD2-deficient neurons, primary neurons were stained with a cell permeable fluorescence ROS probe 2'-7'-Dichlorodihydrofluorescein diacetate (H_2DCF-DA). The reduced nonfluorescent fluorescence H_2DCF-DA after entering the cells, was first cleaved by intracellular esterases, producing a polar and cell membrane non-permeant H_2DCF, which then can be oxidized and converted into fluorescent 2',7'-dichloro-

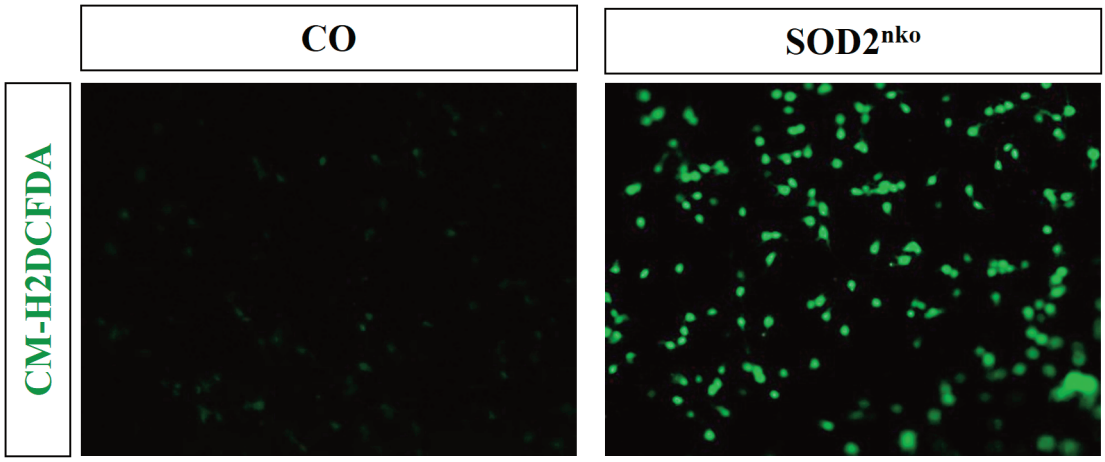

Figure 3.11. Generation of ROS in primary hippocampal neurons of SOD2^{nko} mice.
Primary hippocampal neurons (Postnatal day 1) from both control and SOD2 deleted mice brain were isolated and cultured for 5 days in vitro with 3% oxygen; then these neurons were stained with a fluorescence probe 2'-7'-Dichlorodihydrofluorescein diacetate (H_2DCF-DA) and ROS were detected by presence of green fluorescence.

fluorescein (DCF) by intracellular ROS. Indeed, a significantly increased generation of reactive oxygen species (ROS) as evidenced by higher intensity of the fluorescence was found in SOD2-deficient neurons, compared with SOD2 competent neurons (Figure 3.11).

Afterwards, experiments were performed using the brains from control, heterozygous and SOD2^{nko} mice for the detection of oxidative damage of proteins, lipids and nucleic acids using immunohistochemistry and ELISA. Metal catalyzed oxidation of protein results in protein carbonylation, which was detected by direct ELISA. There were significantly higher levels of protein carbonylation in brain lysates of SOD2^{nko} mice (Figure 3.12A-B). Interestingly, the heterozygous mice also showed an increased tendency towards protein oxidation when compared with controls (Figure 3.12A-B). As neurons express nNOS [Fuentealba et al., 2008] and NO is one of the favored reactants of $O_2^{\bullet -}$ to form peroxynitrite [Beckman and Koppenol, 1996], the level of peroxynitrite mediated nitrative damage in SOD2^{nko} mice was also examined. Competitive ELISA assays of brain lysates demonstrated significantly increased level of protein nitrotyrosine, a marker for NO dependent nitrative stress [Beckman and Koppenol, 1996], in SOD2^{nko} mice compared with control ($p<0.001$) and heterozygous ($p<0.01$) mice (Figure 3.12C-D). Due to higher lipid content in CNS, brain lipids were

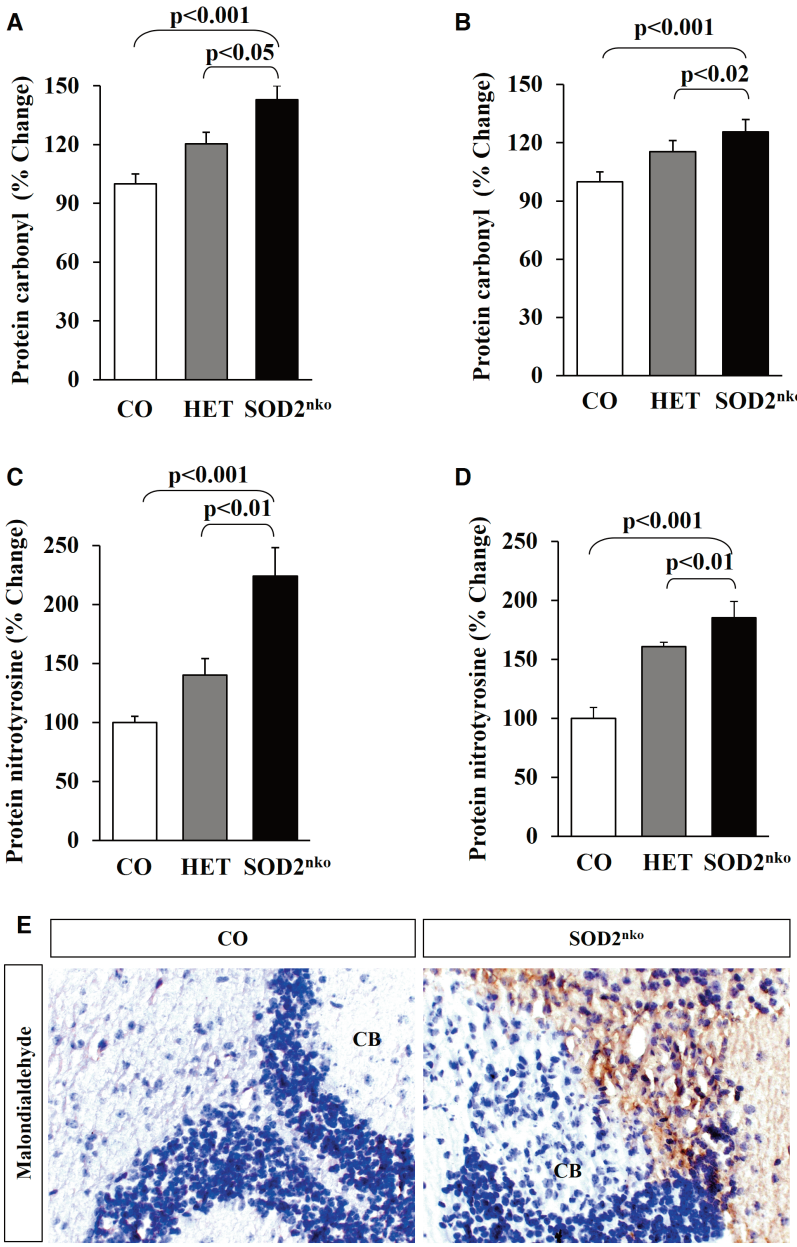

Figure 3.12. Oxidative damage in the brain of SOD2^{nko} mice.

A-B. Elevated protein carbonyl levels as measured by direct ELISA assays indicating significant increase (CO vs SOD2^{nko} $p<0.001$, HET Vs SOD2^{nko} $p<0.05$) in oxidative protein damage in different regions of brains (A) Cortex, striatum, hippocampus, and (B) thalamus, hypothalamus of SOD2^{nko} mice compared with control (CO) and heterozygous (HET) littermates (n=9).

C-D. Significantly higher protein nitration (CO vs SOD2^{nko} $p<0.001$, Het vs SOD2^{nko} $p<0.01$) was found in different regions of brains (C) Cortex, striatum, hippocampus, and (D) thalamus, hypothalamus of SOD2^{nko} mice compared with control (CO) and heterozygous (HET) littermates (n=9).

E. Immunohistochemical detection of malondialdehyde (MDA) in mice brain coronal sections. SOD2^{nko} mice brain showed accumulation of MDA, while no such accumulation was found in adjacent cerebellar regions (where CamKIIα was not expressed); cerebellum (CB) served as internal control.

reported to play a major role both in degenerative disorders and several brain injuries [Adibhatla and Hatcher, 2007]. Upon oxidative insults lipids undergo lipid peroxidation, where both primary and secondary lipid can be decomposed to several end products. Malondialdehyde is one of those endogenous genotoxic products, which is frequently considered as an indicator of lipid peroxidation. Immunohistochemical analyses revealed a marked increase in Malondialdehyde accumulation in the SOD2^{nko} mice brain (Figure 3.12E).

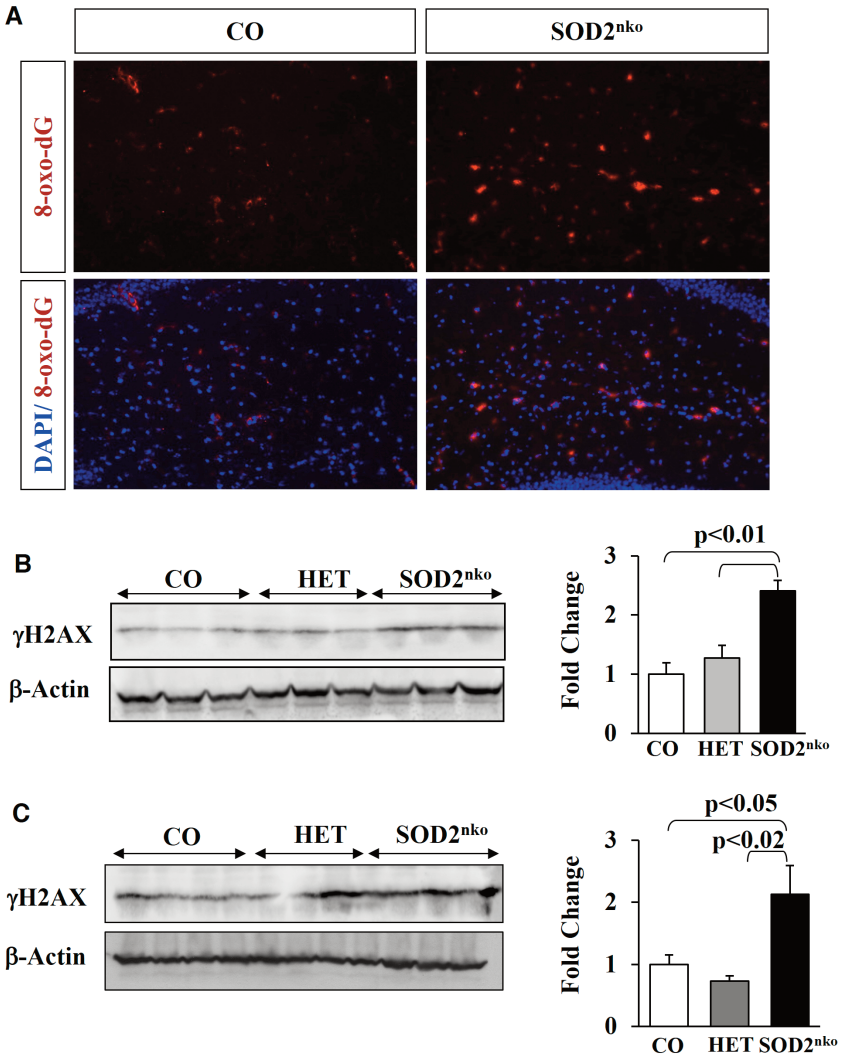

Figure 3.13. Oxidative DNA damage and DNA double stranded breaks in the brain of SOD2^{nko} mice.
A. Immunofluorescence study with antibodies against 8-Oxo-2'-deoxyguanosine (8-oxo-dG), an well-known marker of nucleotide oxidation (8-oxo-dG: red, DAPI: blue), showing increased accumulation of 8-oxo-dG in cell nuclei as well as in mitochondria (Inset pic: 20X magnification) in hippocampus of SOD2^{nko} mice (SOD2^{nko}) with compared to control mice (n=5).
B-C. Representative western blot analysis of γH2AX, a phosphorylated product of H2AX, showing significant accumulation (2.5 fold p<0.01 vs both CO and HET) in (B) Cortex, striatum, hippocampus, and (C) thalamus, hypothalamus , indicating DNA double strand breaks in mutant mice brain.

Moreover, experiments were also performed to detect the oxidative damage of DNA by determining the levels of 8-oxo-guanosine, because guanosine is most reactive with ROS and can be easily oxidized [Halliwell and Gutteridge, 2007]. Immunofluorescence studies with antibodies recognizing 8-Oxo-2'-deoxyguanosine (8-oxo-dG) in brain cryosections exhibits accumulation of 8-oxo-dG in SOD2^{nko} mice (Figure 3.13A). Redox imbalance induces DNA double strand breaks, which can be detected by the accumulation of serine 139-phosphorylated histone H2AX (γH2AX). A specific antibody was used to determine γH2AX levels in control and mutant mice. Western immunoblot analyses showed a significant increase in γH2AX levels in brains lysates from SOD2^{nko} mice compared with control (Figure 3.13B-C).

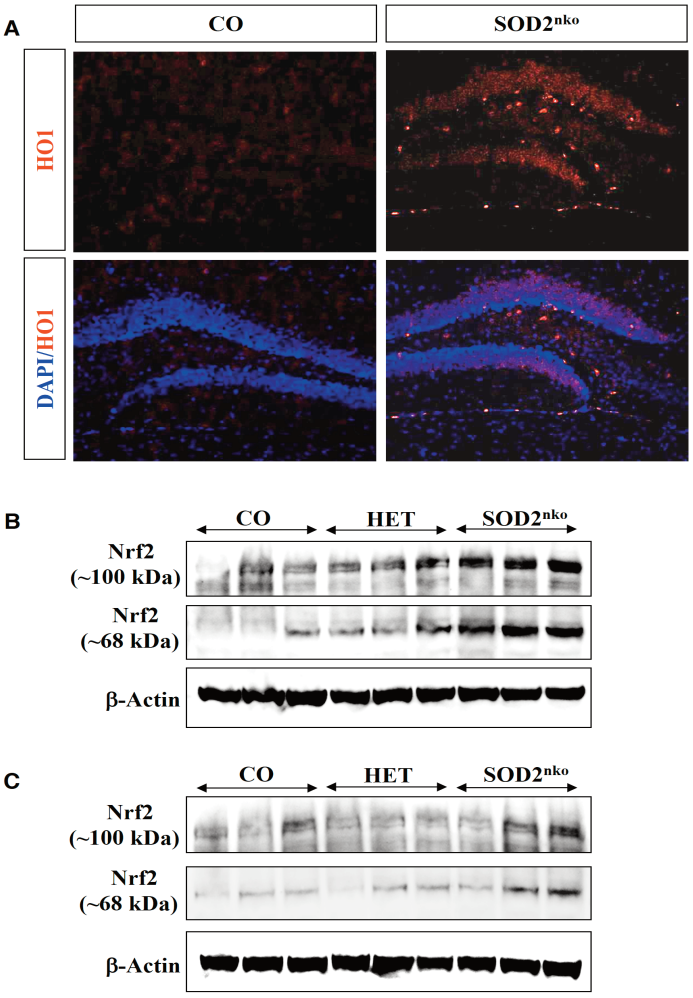

Figure 3.14. Induction of antioxidant response in the brain of SOD2^{nko} mice.

A. Heme oxygenase 1 (HO1), an important cellular antioxidant protective enzyme was upregulated (HO1: red, DAPI: blue, x20) in the SOD2 mutant brain.

B-C. Representative immunoblot analyses of Nrf2 expression revealed upregulation of Nrf2 in the lysates from (B) cortex,striatum,hippocampus and (C) thalamus, hypothalamus of SOD^{nko} mice brain (100 kD and 68 kD).

3.4 Oxidative stress induced endogenous antioxidant response

In order to determine whether oxidative stress in the brain resulted in the induction of an antioxidant response, the expression of heme oxygenase-1 (HO-1) was analyzed. HO-1 was reported to encounter the reactive oxidant burden and protect cells from more damage [Choi and Alam, 1996]. Immunostaining of brain cryosections showed significantly increased levels of HO-1 in $SOD2^{nko}$ mice (Figure 3.14A). Expression of HO-1 is under the control of stress-induced transcription factor Nrf2 (nuclear factor erythroid-derived 2, like 2), a basic leucine zipper transcription factor that can bind to the antioxidant response element (ARE) core sequence present in the promoter of HO-1 [Alam et al., 1999] and many other genes encoding antioxidant proteins. Western immunoblot analyses of brain lysates indicated a significant induction of Nrf2, (both of the 68 kDa and the ubiquitinated 100 kDa subunits, (Figure 3.14B-C) mostly in cerebral cortex, striatum and hippocampus (where CaMKIIα is mostly expressed) of $SOD2^{nko}$ mice.

3.5 Toxic neurofilamentopathy in neuronal SOD2 deficiency

Changes in neurite architecture were studied by neurofilament immunostaining. Immunohistochemical analyses with antibodies against heavy subunits of neurofilament (NF-H/200kDa) revealed alterations in the neurofilament distribution in SOD2-deficient mice in comparison to wildtype littermates. At first glance NF-H positive structures seemed to be similarly distributed both in the mutant mice (Figure 3.15A) and in SOD2-competent control mice (Figure 3.15D). But at a higher magnification, NF-H positive somata were seen in cortical layers II – VI of the secondary somatosensory (S2) cortex in mutant mouse brains (Figure 3.15B-C) whereas such neurons were concentrated to layers III and V in control animals (Figure 3.15E). At the cellular level, S2 cortical neurons exhibited cytoplasmic and neuritic NF-H-positive inclusions, which were not found in control littermates (Figure 3.15F). Furthermore, NF-H-positive aggregates were also found in the thalamus (Thal) of SOD2-deficient mice brain (Figures 3.15G-H), while no evidence for such aggregations was observed in the control brains (Figure 3.15I). Moreover, single thalamic capillaries appeared enlarged in the mutant mice (Figure 3.15G arrowhead) and such changes were not noticed in wildtype animals (Figure 3.15I). In addition, inclusion bodies were also detectable as ball-like globules within the neuropil by immunostaining with antibodies against light chain subunits

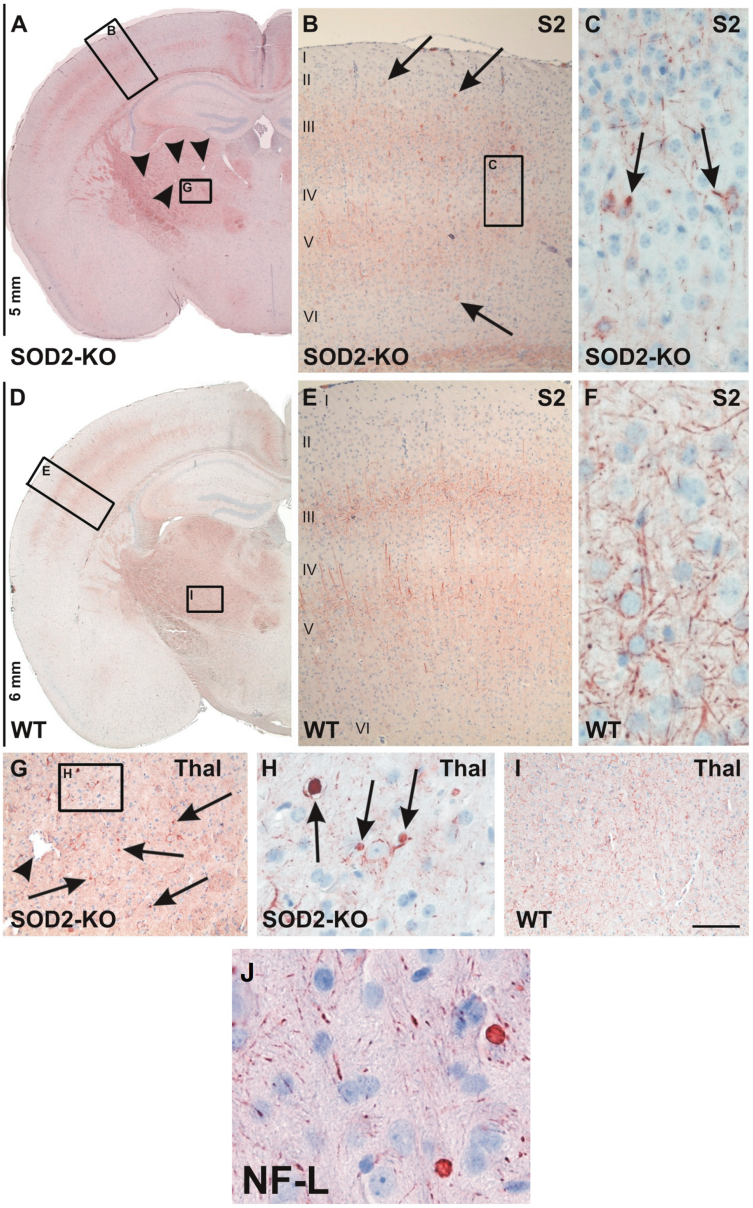

Figure 3.15. Alterations in the neurofilament distribution in SOD2-KO (SOD2^{nko}) mice.

A, D. On the first glance neurofilament (NF-H/ 200 kDa subunit) positive structures are similarly distributed as in SOD2-KO and wildtype mice.

B, E. At higher magnification level of the S2 cortex NF-H positive somata were seen in layers II – VI in SOD2-KO mice, whereas such neurons were concentrated to layers III and V in wildtype animals. NF-H positive neurons in layers II and VI are indicated by arrows.

C, F. At the cellular level S2 cortex neurons exhibited cytoplasmic and dendritic NF-H-positive inclusions (arrows) not seen in wildtype mice.

G-I. NF-H-positive aggregates were also found in the thalamus (Thal) of SOD2-KO mice (arrows) but not in wildtype controls. Moreover single thalamic capillary appeared enlarged in SOD2-KO mice (arrowheads in A and G). Such changes were not observed in wildtype animals.

Calibration bar in I: valid for: B, E: 220 µm, C, F, H: 25 µm, G, I: 60 µm.

J. Inclusion bodies of neurofilament light (NF-L/68 kDa subunit); ball-like globular aggregates withing the neuropil.

(NF-L/68kDa) of neurofilaments in brain sections of $SOD2^{nko}$ mice (Figure 3.15J). Though we did not observe any marked alteration in other types of aggregation such as phospho-tau (τ), ubiquitin, α-synuclein etc. (Table 3.2) in $SOD2^{nko}$ mice brain.

Table 3.2. Characterization of globular neurofilament aggregates.

Antibody	Detection of globular aggragates
NF-H	+
NF-L	+
abnormal τ-protein (AT8)	-
α-synuclein	-
amyloid β-protein (4G8)	-
pTDP43	-
FUS	-
p62	-
ubiquitin	-

3.6 Reactive astrogliosis coupled with inflammatory response

Neuronal damage is often associated with an abnormal activation and proliferation of astrocytes and microglial cells collectively known as astrogliosis, which is believed to be the most obvious reaction to maintain brain homeostasis. Immunofluorescence studies showed strongly increased presence of GFAP (an astrocyte marker) positive cells in the hippocampus and subgranular zone of the dentate gyrus (Figure 3.16A), as well as in additional brain regions of $SOD2^{nko}$ mice. Oligodendrocyte is another type of neuroglial cells found in CNS and previous studies showed enhancement of oligodendrocyte generation often associated in chronic demyelinating diseases [Emery, 2010]. MBP (Myelin basic protein), a well-known marker for oligodendrocyte was upregulated in cerebral lysates of $SOD2^{nko}$ mice (Figure 3.16B).

In addition, immunostainings with antibodies against CD4 (+) and CD8 (+) T cells revealed a moderate increase in the infiltration of these immune cells, suggesting an ongoing inflammatory response in the brains of $SOD2^{nko}$ mice (Figures 3.16C). In CNS, the inflammatory response is mediated by activation of microglia, the resident immune cells also known as brain-macrophages. Microglia become activated in response to neuronal damages and in-

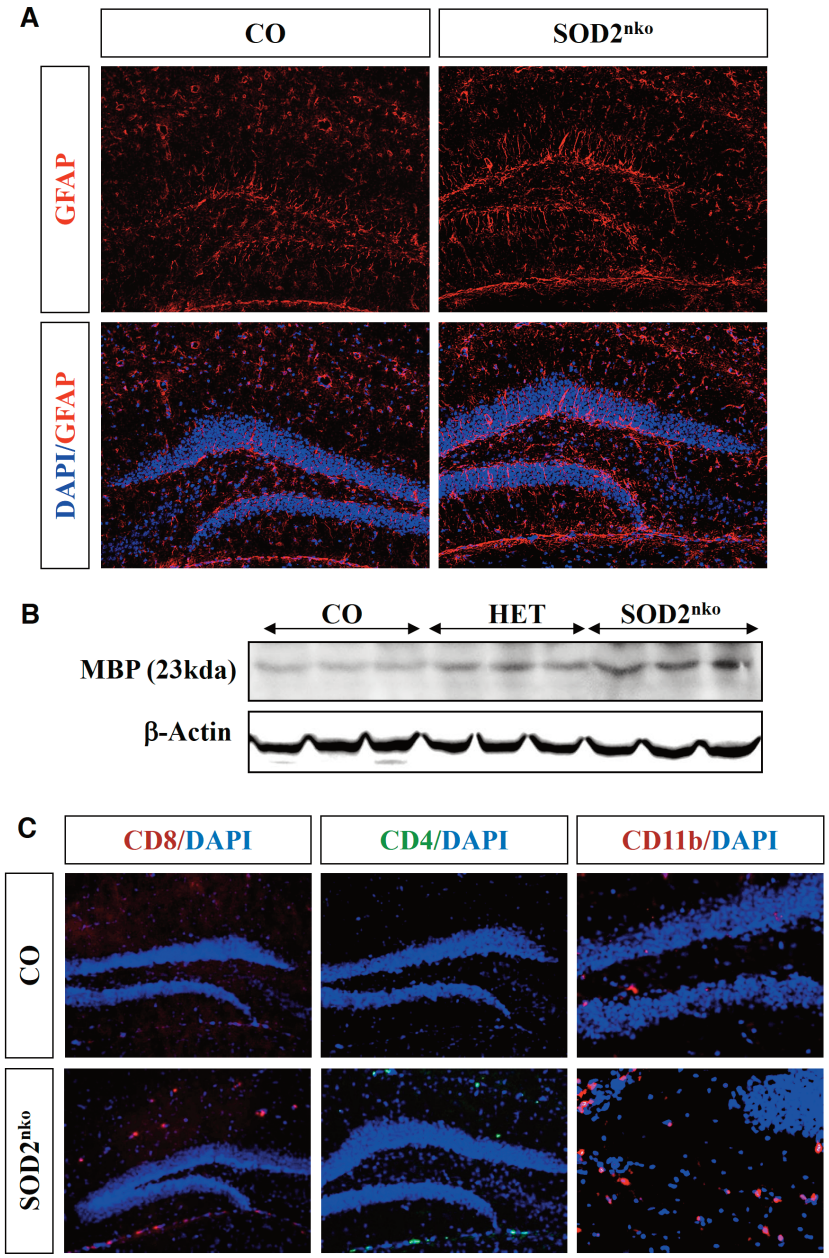

Figure 3.16.

A. Immunostaining with antibodies against glial fibrillary acidic protein, an established marker of astrocytes, showing increased amount of GFAP positive cells (GFAP: red, DAPI: blue) in dentate gyrus and in CA1 region of hippocampus of SOD2^{nko} mice, indicating activated astrocytosis and abnormal neural homeostasis.

B. Increased generation of a subtype of nonneuroal cell, oligodendrocytes; Western immunoblotting showed elevation of MBP (myelin basic protein), a well-known marker for mature oligodendrocytes, in cortical lysates of SOD2^{nko} mice (n=6).

C. Inflammatory response of microglia was detected by immunofluorescence staining of CD11b, a marker for activated microglia (CD11b: red, DAPI:blue); Immunofluorescence staining with antibodies against CD4 and CD8 T-cells showed significant increase of infiltrating immune cells (CD4: green, CD8: red, DAPI: blue) in dentate gyrus of SOD2 mutant mice brain when compared with control mice (n=5).

fections; and mediates phagocytic removal of damaged cells [Dheen et al., 2007]. Microglial activation is considered as a hallmark of brain pathology. When immunostained with antibodies against CD11b, a marker for microglial cells, increased numbers of activated CD11b positive cells were found in the dentate gyrus (Figure 3.16C) of SOD2^{nko} mice.

3.7 Enhanced neuronal apoptosis and cell cycle inhibition

Now the question arose whether this inflammatory phenotype was associated with neuronal cell death. Therefore, the levels of apoptosis were analyzed in the SOD2^{nko} mice using

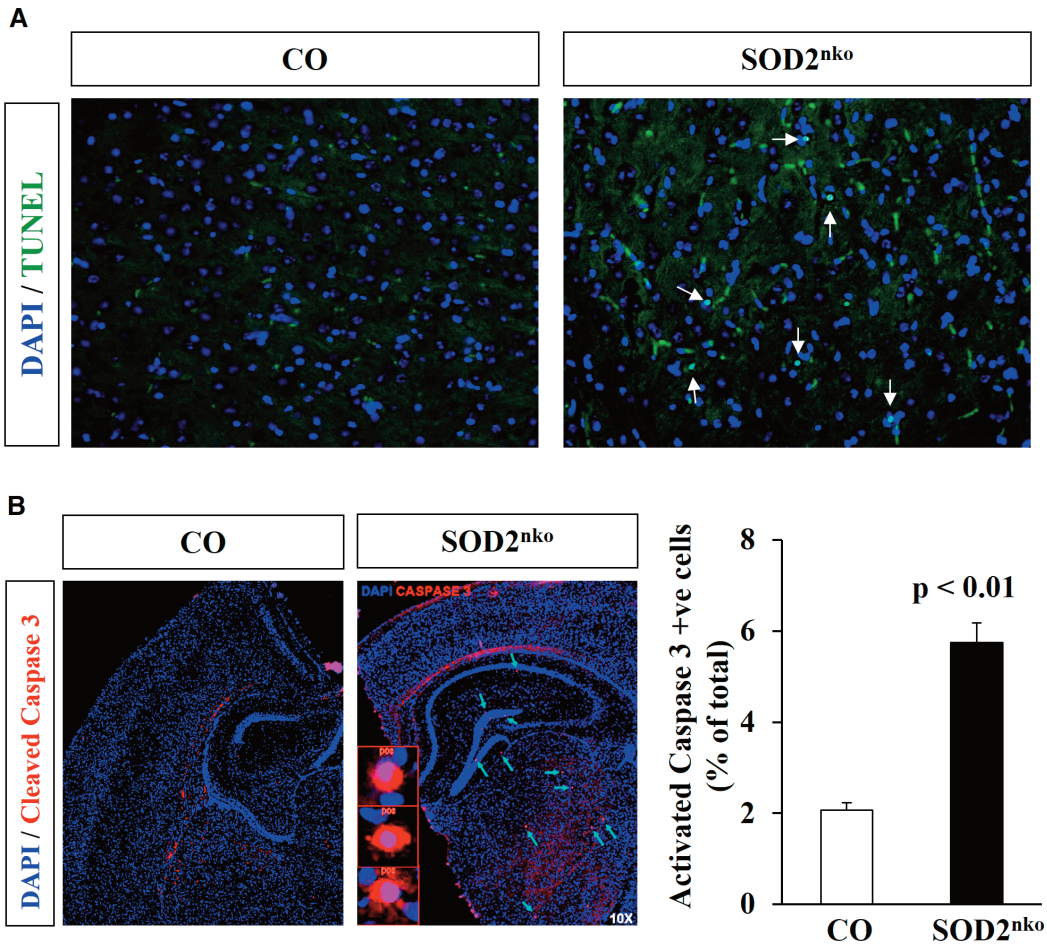

Figure 3.17. Activation of caspase-dependent neuronal apoptosis in SOD2^{nko}.

A. Significantly increased number of terminal apoptotic cells (arrows to nuclear colocalization of green TUNEL positive cells) in SOD2^{nko} mice brain sections (n=7) identified by 'Terminal deoxynucleotidyl' Transferase dUTP nick end labelling (TUNEL) assay.

B. Immunofluorescence study with antibodies against cleaved (active) caspase-3 was performed on brain sections; increased amount of active caspase-3 positive cells (Cleaved Caspase-3: red, DAPI: blue) found in mutant mice brain (inset picture focusing higher magnification) compared with controls. Quantification of cleaved caspase-3 positive cells in the forebrain areas showed significantly increased apoptosis in SOD2^{nko} mice (n=5). ($p<0.01$, two-tail t-test).

TUNEL assays. This revealed a significant increase in TUNEL-positive signals throughout the forebrain regions of mutant mice as compared with controls (Figure 3.17A). The increase in apoptosis was further confirmed by immunostaining with antibodies against cleaved caspase-3 (CO vs SOD2^{nko} $p<0.01$) (Figure 3.17B). Several pathways have been described by which oxidative stress can induce apoptosis; one prominent pathway involves the activation of c-Jun N-terminal kinase (JNK) [Aoki et al., 2002]. To investigate whether there was any activation of this pathway, we performed Western immunoblots for determining the phospho-JNK (activated) levels. Indeed, a marked increase was observed in brain lysates of SOD2^{nko} mice compared to age-matched controls (Figure 3.18A). A potential effector mech-

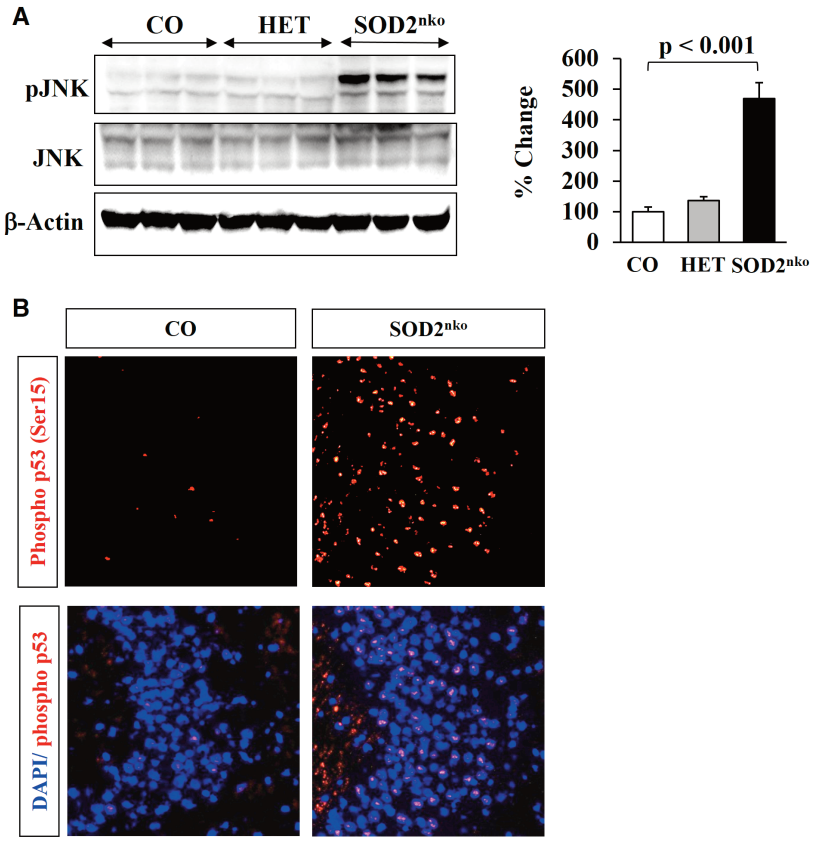

Figure 3.18. Activation of JNK and p53 in SOD2^{nko}.

A. Oxidative damage induces activation of JNK, followed by activation of p53 cascade pathway in SOD2 knock-out mice. Representative western blot analysis with antibodies against phospho-JNK and JNK (for all JNK1, JNK2 and JNK3) showing significantly higher phosphorylation and activation of c-JUN N-terminal kinases ($p<0.001$, Bonferroni Multiple comparison t-test, following One Way ANOVA) in SOD2 deficient brain-lysates compared with heterozygous and controls (n=9). The levels of phospho-JNK and total JNK were normalized with that of β-actin. The normalized values of phospho-JNK and JNKwere used to make a ratio of phosphorylated and total and was plotted.

B. Accumulation of phospho p53 (Ser15) in the cell nucleus observed by immunofluorescence study (p53: red, DAPI: blue, x20) in brain sections of SOD2 mutant mice (SOD2^{nko}) with compared to control littermates (CO) (n=5).

anism of JNK-induced apoptosis involves the stabilization of p53 [Choi et al., 2011]. Immunofluorescence staining showed increased phospho-p53 (Ser15) protein levels in the hippocampal regions of SOD2^{nko} mice brain (Figure 3.18B).

A mediator of p53-induced apoptosis is the activation of pro-apoptotic bcl2-family member PUMA [Nakano and Vousden, 2001]. Immunofluorescence analysis revealed an induction of PUMA protein in the SOD2^{nko} mouse brains (Figure 3.19). Activation of PUMA often

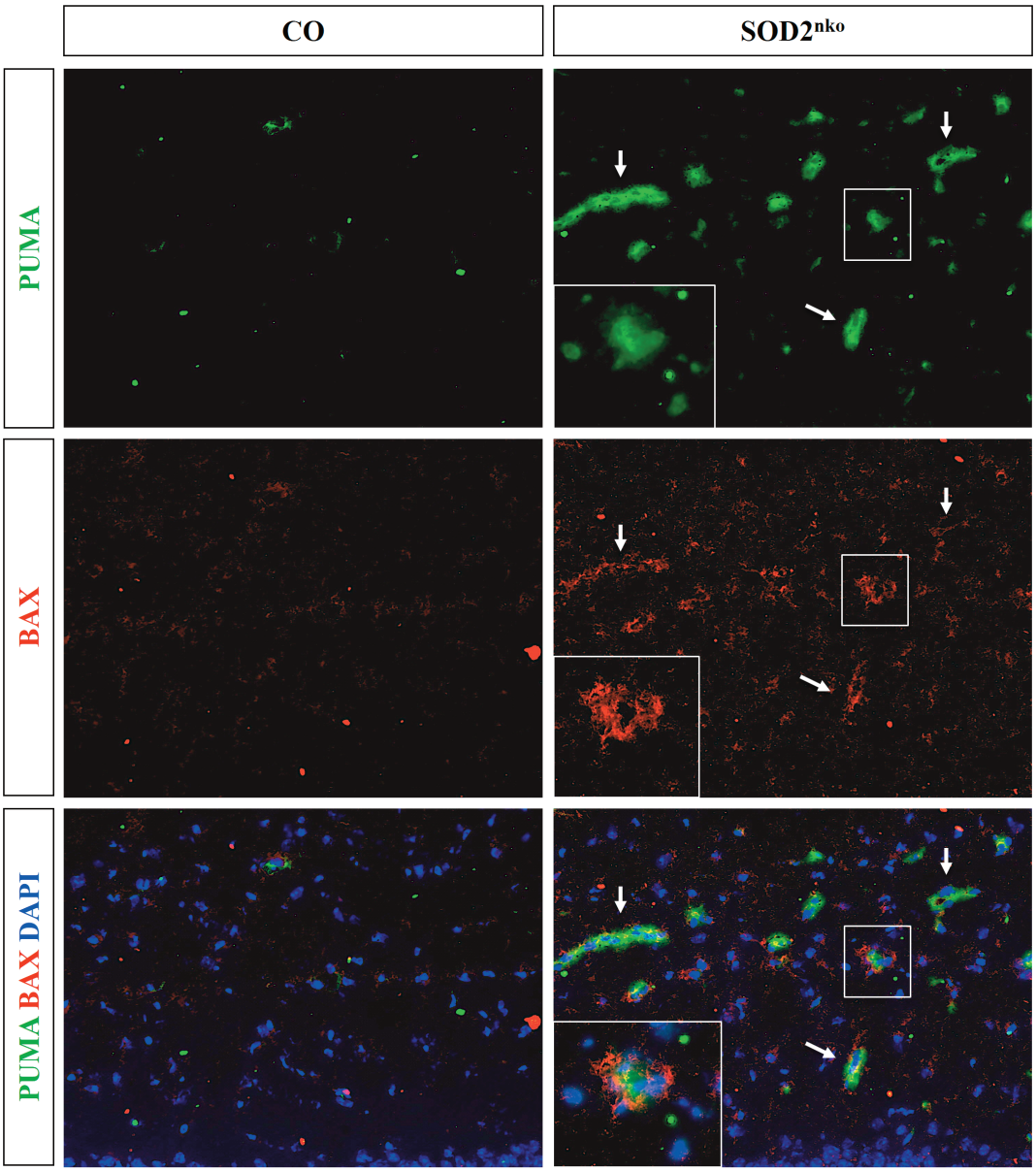

Figure 3.19. Induction of PUMA and Bax in SOD2^{nko}.
Induction of PUMA and Bax was observed by immunofluorescence study (PUMA: green; Bax: red, DAPI: blue; x20) in SOD2^{nko} mice brain coronal sections when compared with control mice (n=5). The inserts showed 40x magnification of the selected regions.

leads to the activation of Bax [Shibue et al., 2006; Yu and Zhang, 2008]. Activated Bax translocated to mitochondria, oligomerize and participate in the mitochondrial outer membrane permeabilization and cytochrome c release for the activation of caspase cascade [Shibue et al., 2006]. Immunofluorescence studies also revealed an induction of Bax protein in the SOD2^{nko} mouse brains (Figure 3.19).

Furthermore, upregulation of p53 typically results in the transcriptional induction of the cell cycle inhibitor p21 and increased p21 protein levels were detected in SOD2^{nko} brain by Western immunoblots (Figure 3.20A). Ki-67 protein has been described to be involved in all ac-

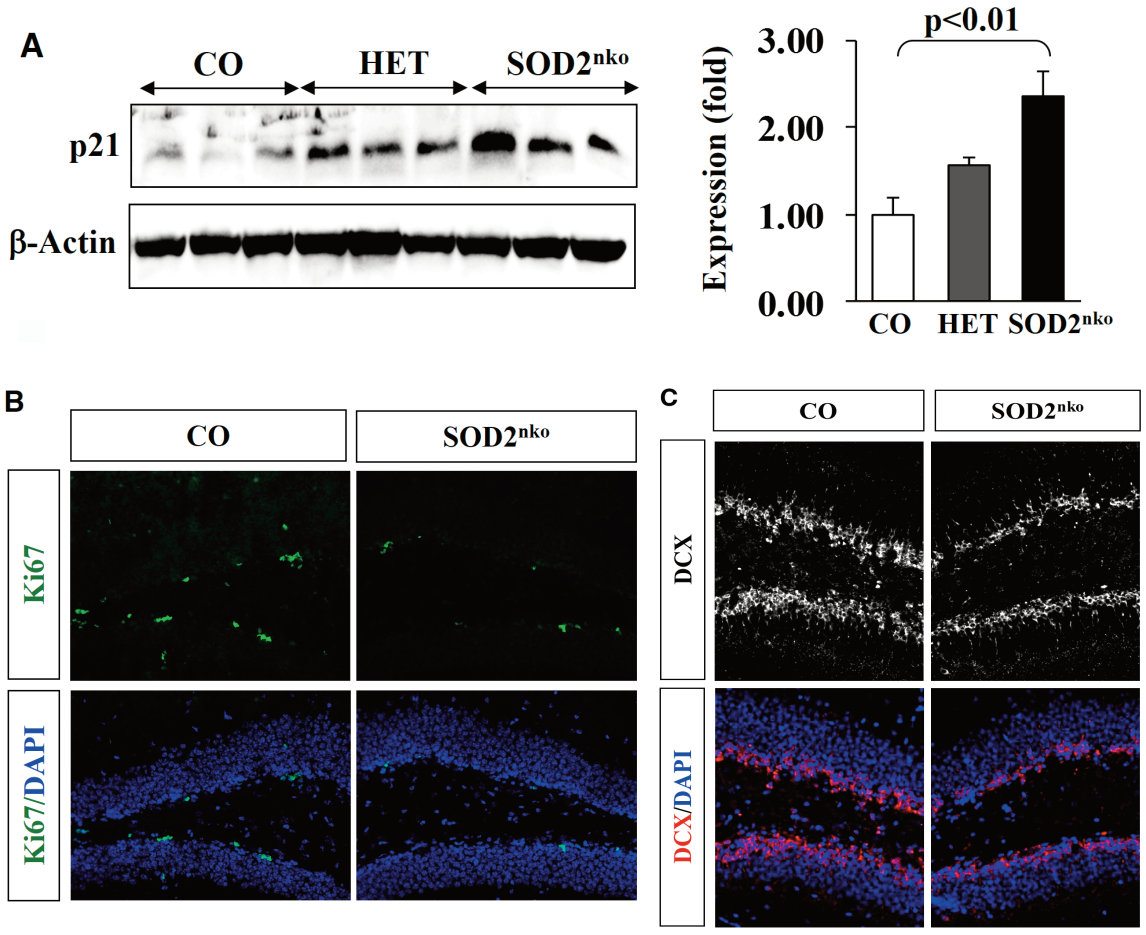

Figure 3.20. Cell cycle arrest and reduced postnatal neurogenesis in SOD2^{nko} mice.

A. Representative Western Immunoblot and respective densitometric analyses indicate significant upregulation of p21 indicating cell cycle arrest in SOD2^{nko} mice in comparison with heterozygous and control mice (n=6).

B. Immunofluorescence staining showed a significantly reduced Ki67 positive cells in sub-granular zone of dentate gyrus of SOD2^{nko} mice compared with control littermates.

C. Immunofluorescence staining with antibodies against Doublecortin (DCX) showed reduced postnatal neurogenesis (DCX: red, DAPI: blue) in subgranular zone of dentate gyrus of SOD2^{nko} mice brain (n=7).

tive phases (G_1, S, G_2) of cell cycle, although absent in resting (G_0) phase and the expression of Ki-67 is required for the progression through cell-division cycle [Scholzen and Gerdes, 2000]. Therefore, Ki-67 serves as an established marker for cycling cells (both neuronal and neuroglial) of all active phases. In mammalian brain, postnatal neurogenesis is restricted to relatively limited areas, e.g., in hippocampus neurogenesis takes place in sub-granular zone (SGZ) of the dentate gyrus [Eriksson et al., 1998]. Consequently, a significant reduction of cycling cells as marked by Ki-67 positive immunofluorescence staining observed in the sub-granular zone of dentate gyrus of $SOD2^{nko}$ mice brain. (Figure 3.20B).

As we observed the incidence of astrogliosis in the sub-granular zone of dentate gyrus, therefore, the possiblity arises whether p21 mediated cell cycle arrest is restricted to the neuronal compartment. To investigate this, immunofluorescence studies using antibodies against doublecortin (DCX), which labels late mitotic neural precursors and early postmitotic neurons were performed. Doublecortin, a protein that promotes microtubule polymerization, is present in migrating neuroblasts and young neurons. Expression of DCX can be detected from late phases of stage 2 until early phases of stage 5 [Gleeson et al., 1999]. A reduction in Doublecortin expression was observed in the sub-granular zone of dentate gyrus of $SOD2^{nko}$ mice brain (Figure 3.20C) where specific occurance of postnatal neurogenesis has been described earlier [Eriksson et al., 1998].

3.8 Severe hypoglycemia and energy deprivation in absence of neuronal SOD2

To investigate the reason behind the intense failure to thrive, the status of energy metabolism in $SOD2^{nko}$ mice was measured. Interestingly, the SOD2 mutant mice showed dramatically reduced (CO vs KO $p<0.001$) both fed and fasting blood glucose levels (Figure 3.21A-B). Immunofluorescence studies exhibited no marked changes in distribution of insulin positive β-cells between control and $SOD2^{nko}$ pancreas (Figure 3.21C). However, analysis of serum insulin level showed 2 fold higher serum insulin in the $SOD2^{nko}$ mice compared with their control littermates (Figure 3.21D).

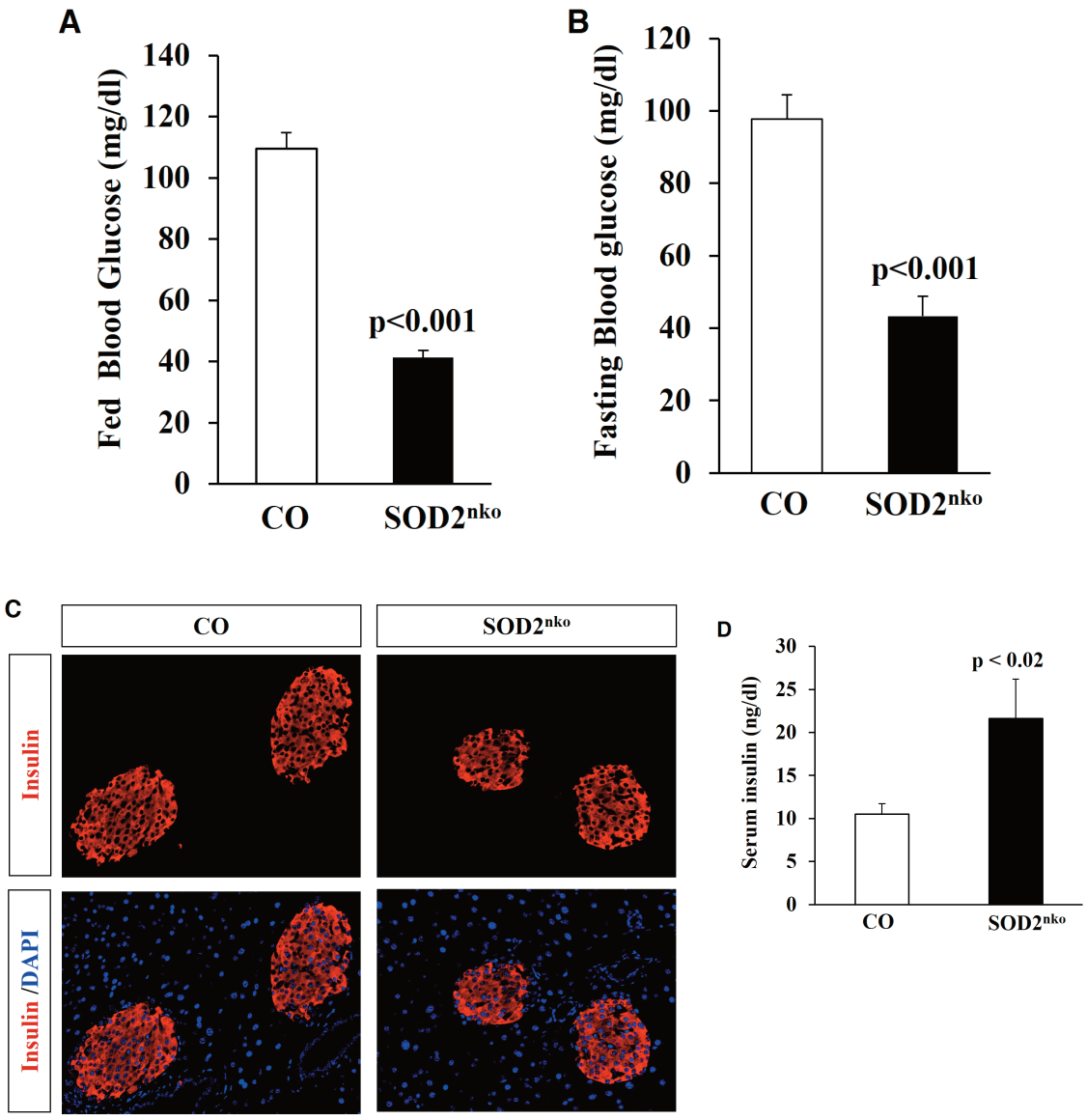

Figure 3.21. Severe hypoglycemia with insulinemia in SOD2^{nko} mice.

A-B. Determination of blood glucose levels (mg/dl); (A) fasting and (B) fed blood glucose levels indicating significant reduction ($p<0.001$) in P21 days old SOD2^{nko} mice compared with control littermates (n=15).

C. Inmmunofluorescence staining of pancreas with anti-insulin antibody showed no significant changes in the distribution as well as intensities of fluorescence between control and SOD2^{nko} mice.

D. Serum insulin measurement showed significantly higher serum insulin level in SOD2^{nko} mice ($p<0.02$, two-tailed t-test) compared with control littermates.

In addition, significantly decreased ATP levels (Figure 3.22A) and higher NAD/NADH ratio (CO vs SOD2^{nko} $p<0.01$) (3.22B) were found in cerebral lysates of SOD2^{nko} mice, reflecting abnormal cellular energy state. Lower energy status is also associated with reduced SDH (complex II) activity in SOD2^{nko} brain compared with CO, while there is no change in COX (complex IV) activity between CO and SOD2^{nko} brain (Figure 3.22C).

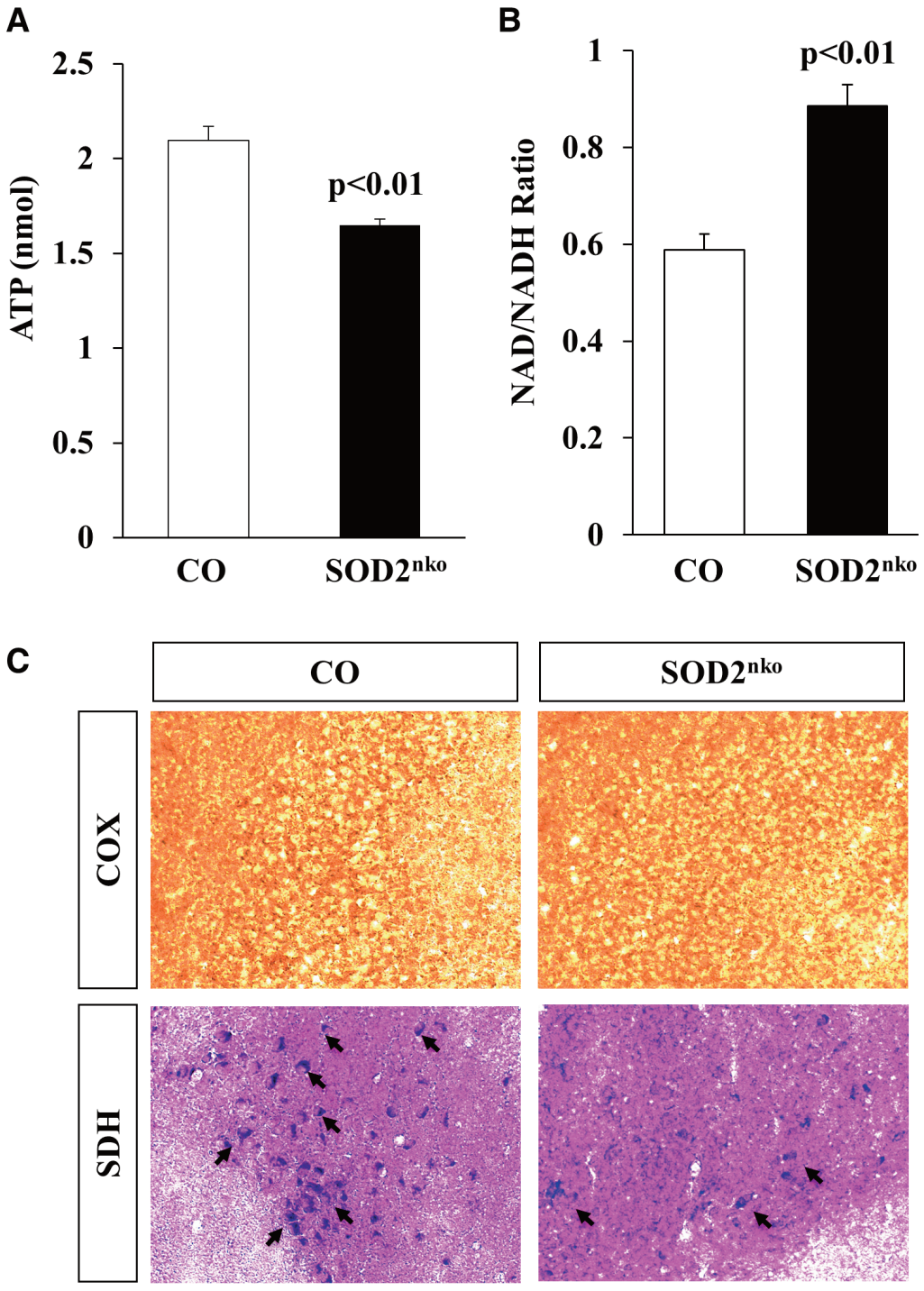

Figure 3.22. Severe energy deprivation in SOD2^{nko} mice.

A. ATP level was significantly reduced in SOD2^{nko} mice ($p<0.01$, two-tailed t-test) brain cortical lysates compared with control littermates (n=6-8). P21 days older mice were studied.

B. NAD/NADH ratio was reduced ($p<0.01$, two-tailed t-test) in the brain cortical lysate of SOD2^{nko} mice compared with control littermates (n=6).

C. There was no alteration of cytochrome c oxidase (COX) or complex IV activity between control (CO) and SOD2^{nko} mice, on the contrary, the activity of succinate dehydrogenase (SDH) or complex II was significantly reduced in SOD2^{nko} mice, compared with CO, as revealed from more intense blue staining.in CO brain cryosection. Arrows were inserted to mark some of the positive cells.

3.9 Hypoglycemia induced necrotic brain lesion in SOD2^{nko} mice

Energy deprivations along with hypoglycemic conditions may result in specific brain damages known as hypoglycemic lesions. Such hypoglycemia induced brain lesions were previously reported mostly in hippocampal regions of hypoglycemic patients and as well as in rat brain [Auer, 2004]. Upon H&E staining, significant accumulation of necrotic neurons in hippocampus ($p<0.001$) and dentate gyrus ($p<0.001$) were identified by the presence of acidophilic dying neurons (Figures 3.23A-B).

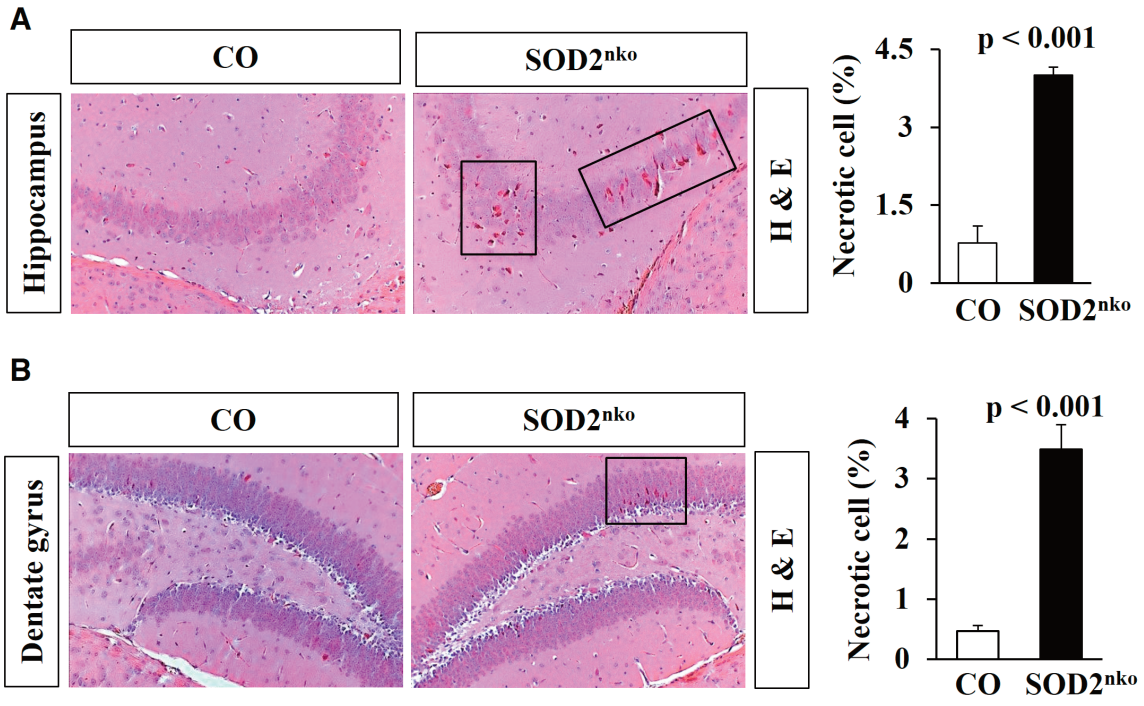

Figure 3.23. Severe pannecrosis in SOD2^{nko} mice.
Increased amount of necrotic neurons found in A. hippocampus and B. dentate gyrus of SOD2^{nko} mice compared with control mice (n=5). Bar diagrams represented quantification showing significant necrosis in SOD2^{nko} mice brain compared with control. ($p<0.001$, two-tail t-test).

The central regulation of energy metabolism is conducted through different centers of hypothalamus in CNS. We examined specific hypothalamic regions to investigate whether hypoglycemia associated energy failure influenced hypothalamic neuronal homeostasis. Severely increased lesions of hypoglycemia-induced nerve cell death without glial cell loss were noticed in different hypothalamic nuclei of SOD2^{nko} mice. Though major neuropathology was mainly observed in the magnocellular nucleus of medial basal hypothalamus, diffuse necrosis of neurons was also detected in other important hypothalamic nuclei like

paraventicular and arcuate nucleus (Figure 3.24A). Moreover, qRT-PCR analyses of total hypothalamic cDNA showed significant increase in GFAP upregulation, suggesting a compensatory generation of supporting glial cells (Figure 3.24B).

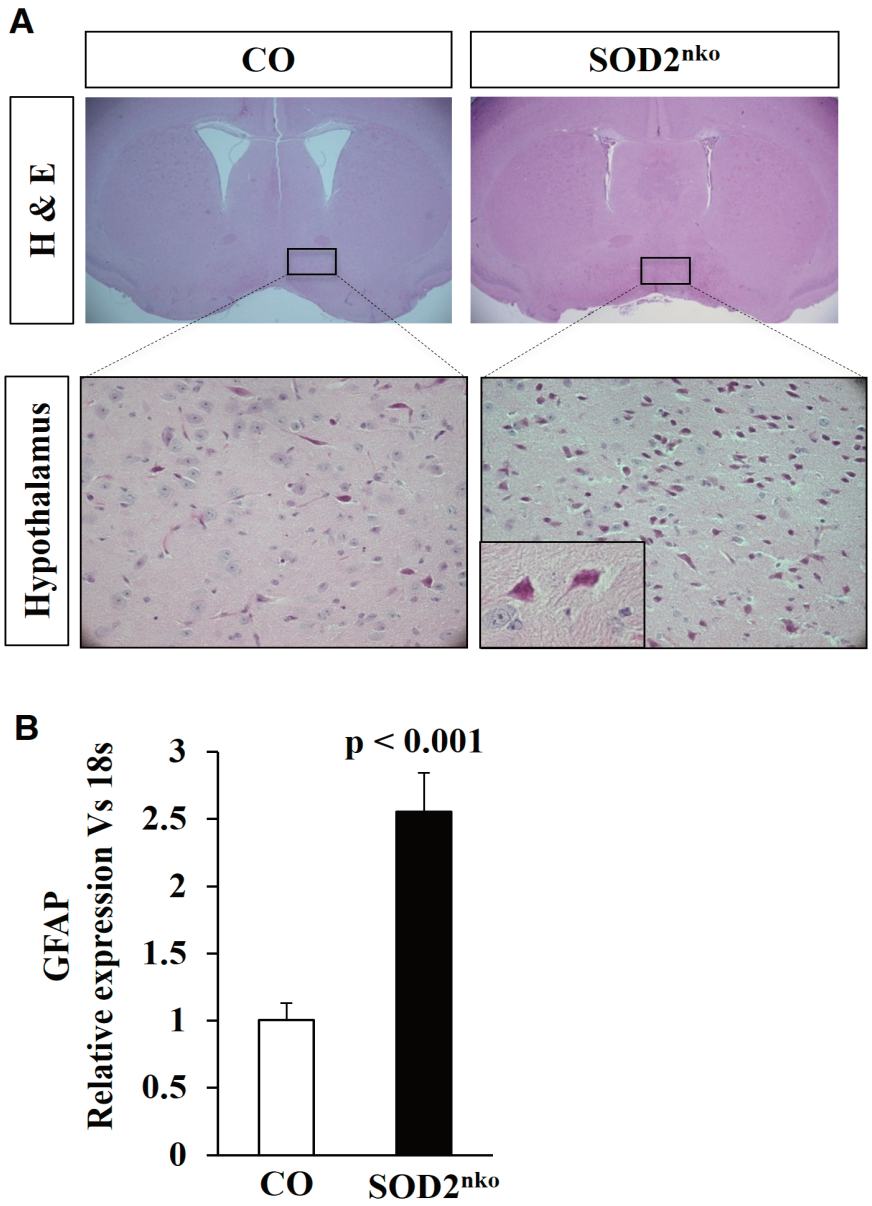

Figure 3.24. Hypothalamic pannecrosis and astrogliosis in SOD2nko mice

A. Detailed histological analysis of coronal brain sections of SOD2^{nko} as well as of control mice by were performed by H&E staining (2.5X). Lower panel represents higher magnfication showing severe necrosis of hypothalamic neurons as identified by accumulation of acidophilic red stainings of cytoplasm (40X), spicifically in magnocellular nuclei of hypothalamus of SOD2^{nko} mice (inset picture: necrotic neurons)

B. qRT-PCR analyses of hypothalamic cDNA revealed upregulation of glial fibrillary acidic protein (GFAP), an established marker for astrocytes in SOD2^{nko} mice when compared with control littermates. Hypothalamic cDNA was prepared from P21 days old control and SOD2^{nko} mice (n=5). 18S rRNA was used as a reference gene (housekeeping gene).

Immunofluorescence staining revealed that hypothalamic neuronal necrosis was also associated with upregulation of GFAP positive astrocytes in different hypothalamic nuclei, specifically in the paraventricular nucleus (Figure 3.25A). In additon, an inflammatory re-

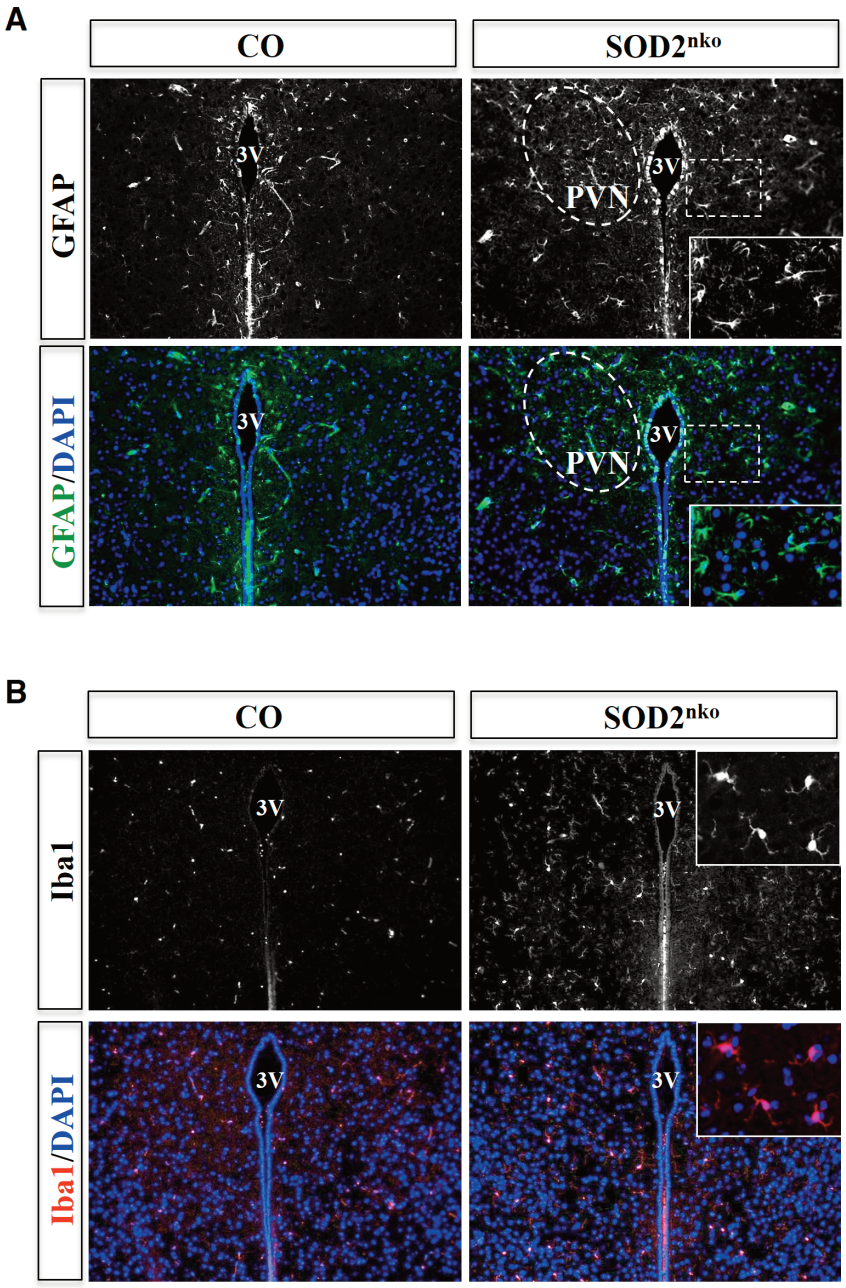

Figure 3.25. Reactive astrogliosis with microglial activation in SOD2^{nko} mice.

A. Upregulation of astrocyte generation found in hypothalamus of SOD2nko mice. Immunostaining against GFAP revealing abnormal astrocytosis (GFAP: green, DAPI: blue, x10) in paraventricular hypothalamic nuclei (PVN) with compared to age-matched controls. Inset picture: asterix shaped GFAP positive astrocytes in higher magnification (20X). P24 days old mice (n=5) were analyzed for immunostainings.

B. Immunofluorescence study using anti-Iba1 antibody (Iba1: Red, DAPI: Blue, x10) marked increased reactive microglia in hypothalamic nuclei, showing specific picture of paraventricular nucleus. Inset picture: higher magnification (20X) of Iba1 positive spider-like microglia; 3V= 3rd ventricle.

sponse was also observed when immunostained with antibodies against Iba1, a marker for reactive microglial cells. A marked increase in Iba1 positive cells was found in different hypothalamic nuclei in a diffused pattern (Figure 3.25B).

3.10 Hypothalamic neuropathology associated impaired counterregulation to hypoglycemia

Under physiological conditions, hypothalamic neurons are known to generate counterregulatory responses to hypoglycemia [Stanley S, 2013]. To investigate the effect of hypoglycemia and the subsequent response in the hypothalamus of SOD2^{nko} mice, expression of different hypothalamic neuropeptides was analyzed. Realtime PCR analyses showed significant downregulation in the expression of two important hypothalamic neuropeptides, namely, corticotropin releasing hormone (CRH) ($p<0.01$) and growth hormone releasing hormone (GHRH) ($p<0.02$) in SOD2^{nko} mice (Figure 3.26A-B). Expression of proopiome-

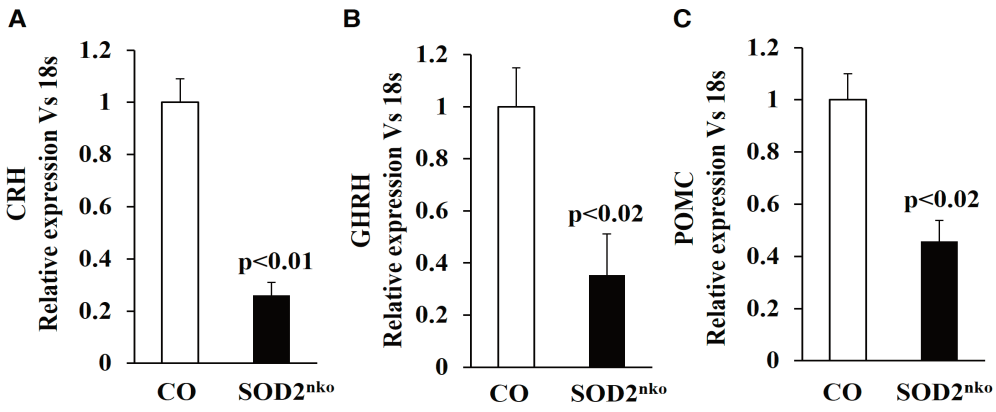

Figure 3.26. Downregulation of essential hypothalamic neuropeptides in SOD2nko mice.
A-C. SYBR green based quantitative RT-PCR analyses revealing strong decrease in expression of three hypothalamic neuropeptides, (A) Corticotropin releasing hormone (CRH) ($p<0.01$, two-tail t-test), (B) Growth hormone releasing hormone (GHRH) ($p<0.02$, two-tail t-test) and (C) Pro-opiomelanocortin (POMC) ($p<0.02$, two-tail t-test) in SOD2^{nko} mice. Hypothalamic cDNA prepared from P21 days old control and SOD2^{nko} mice (n=5). 18S rRNA was used as a reference gene (housekeeping gene).

lanocortin (POMC), the precursor for ACTH and some other hormones was also decreased ($p<0.02$) in hypothalamus of SOD2^{nko} mice (Figure 3.26C). Furthermore, in situ expression of CRH was notably suppressed within the hypothalamus of SOD2^{nko} mice brain compared

with age-matched controls (Figure 3.27A). Immunofluorescence staining with antibodies against CRH-R1, a sub-type of CRH-receptor, revealed a marked reduction of expression specifically in ventromedial hypothalamus (VMH) of SOD2^{nko} mice (Figure 3.27B). Other

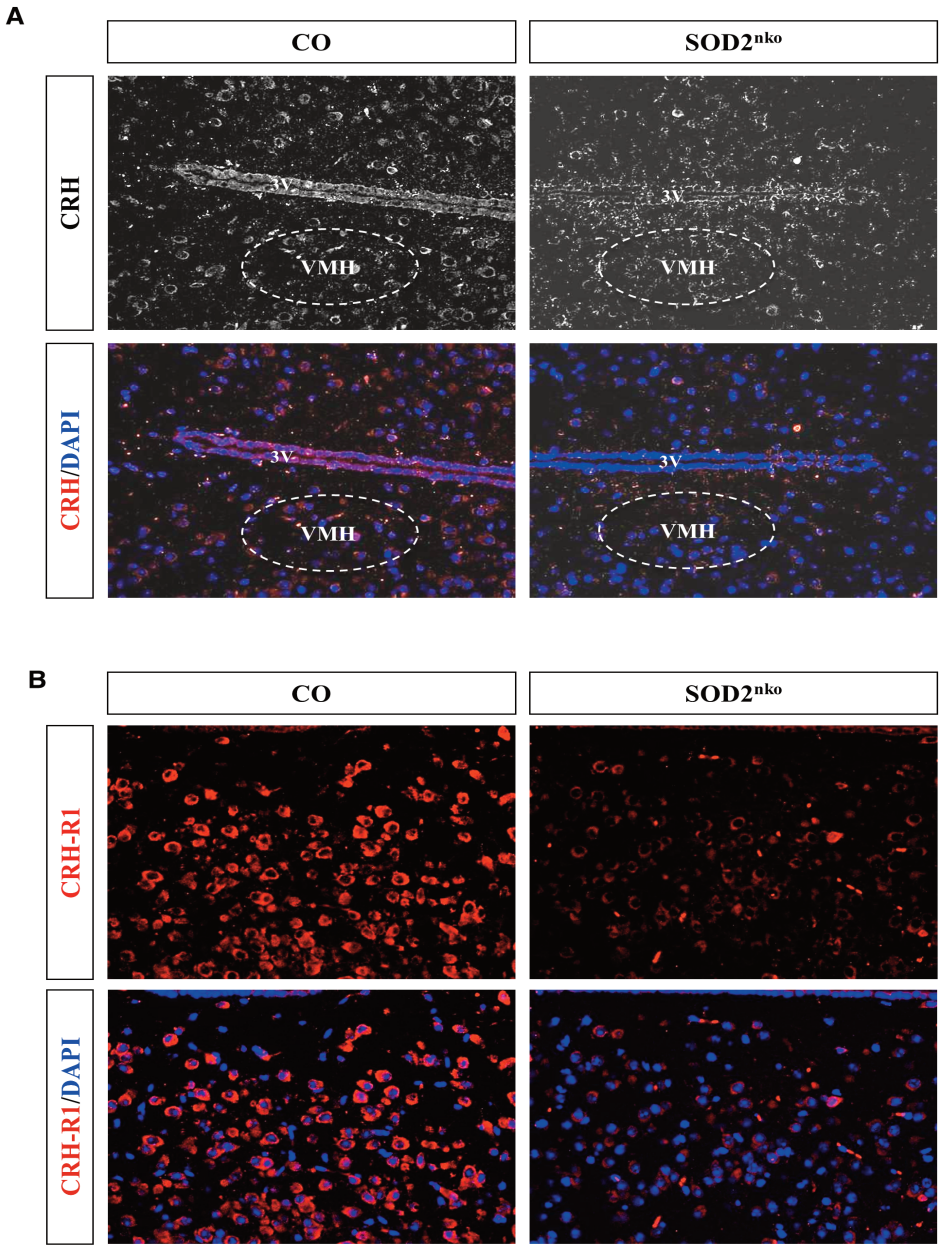

Figure 3.27 Reduced in situ expression of corticotropin-releasing hormone and receptor

A.Immunofluorescence staining (CRH: red, DAPI: blue; x20) showing reduced Corticotropin releasing hormone (CRH) expression within hypothalamus of SOD2^{nko} mice compared with age-matched controls. VMH= Ventromedial hypothalamus; 3V= 3rd ventricle.

B. Diminished expression pattern of CRH-receptor 1 (CRH-R1) specifically in VMH as revealed by immunostaining (CRH-R1: red, DAPI: blue; x20) with antibodies against CRH-R1.

important hypothalamic neuropeptides such as Thyrotropin-Releasing Hormone (TRH), Gonadotropin-Releasing Hormone (GnRH), Neuropeptide Y (NPY), Hypocretin Neuropeptide Precursor (HCRT) and Pro-Melanin-Concentrating Hormone (PMCH) showed unaltered

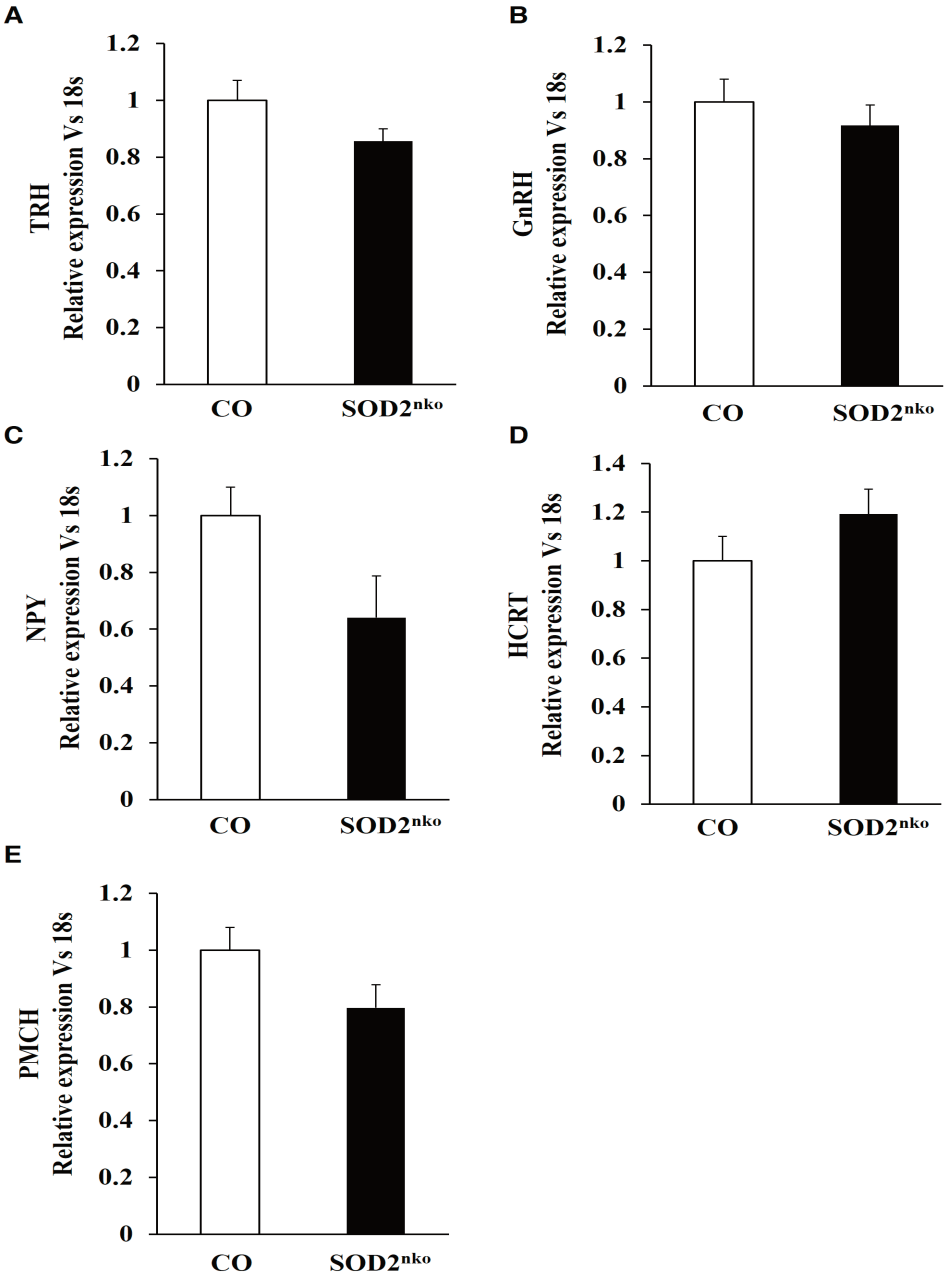

Figure 3.28. Expression analysis of additional hypothalamic neuropeptides

A-E. Quantitative real-time PCR analyses of hypothalamic neuropeptides. Control considered as 1 fold. (A) thyrotropin-releasing hormone (TRH), (B) gonadotropin-releasing hormone (GnRH), (C) Neuropeptide Y (NPY), (D) hypocretin (HCRT) and (E) pro-melanin-concentrating hormone (PMCH) (n=6). Hypothalamic cDNA prepared from P21 days old control and $SOD2^{nko}$ mice (n=5). 18S rRNA was used as a reference gene (housekeeping gene).

expressions (Figure 3.28A-E). Altered expression patterns of CRH, GHRH and POMC suggested a disturbed response of hypothalamic neurons specifically in the central regulation of glucose homeostasis.

We also examined whether the reduced expression of GHRH and CRH would result in reduced secretion of its pituitary target hormones, such as growth hormone (GH) and adrenocorticotropic hormone (ACTH) in SOD2^{nko} mice. Indeed, a significant reduction in serum GH level ($p<0.001$) (Figure 3.29A) and plasma ACTH level ($p<0.001$) (Figure 3.29B) was observed in P21 days old SOD2^{nko} mice further suggesting an impairment in the central counterregulatory cascade to hypoglycemia.

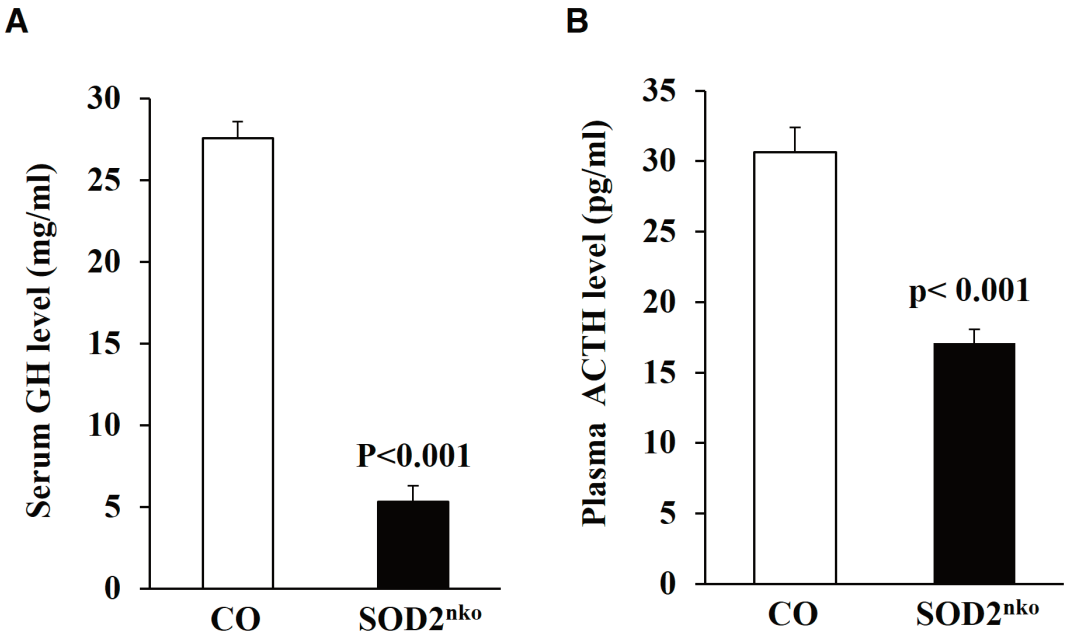

Figure 3.29. Critically impaired hypothalamic regulation of downsrteam pituitary hormones in SOD2^{nko} mice.

ELISA assays were performed to measure A. serum growth hormone (GH) and B. plasma ACTH level. Significant reduction in serum GH level ($p<0.001$, two-tail t-test) and significant downregulation of plasma ACTH level ($p<0.001$, two-tail t-test) found in P21 days old SOD2^{nko} mice with compared to age-matched controls (n=6).

4. DISCUSSION

Although previous studies have reported mitochondrial ROS generation and presence of oxidative damages in several neurodegenerative disorders, there were no direct evidences of redox imbalance dependent generation or progression of the disease. On a related note, mitochondrial abnormality and increased oxidative burdens have been observed in several CNS-regulated metabolic dysfunctions, though lacking the evidences for neuronal redox imbalance regulated metabolic impairments. In all the above-mentioned conditions whether redox imbalance is the consequence or the cause remained poorly understood. Therefore, specific understanding of neuronal redox imbalance and its mode of action are of sheer interests for both basic and applied medical research. The present study characterizes a novel knockout mouse model for the investigation of the consequences of neuronal redox imbalance in neuronal and metabolic homeostasis.

The present study showed that deletion of SOD2 in forebrain neurons resulted in the induction of severe redox imbalance, neuronal death, neuronal pathology, abnormal glucose metabolism, and finally early lethality of the mutant mice within 4 weeks of postnatal life. The $SOD2^{nko}$ mice showed upregulation of Nrf2 and induction of HO-1 in response to oxidative insults. Activation of an oxidative damage-induced apoptotic signaling cascade including activation of JNK, accumulation of p53, induction of PUMA and Bax were observed. The mice develop severe hypoglycemia and central regulation of glucose metabolism was defective resulting in hypoglycemia-induced neuropathology. Together, these findings support a connection between neuronal redox imbalance and impaired central regulation of energy metabolism.

4.1 Crucial role of neuronal SOD2 in overall survival

The significantly shorter life-span of $SOD2^{nko}$ mice indicates the vulnerability of neurons towards oxidative insults and also hints at the exclusive importance of neuronal homeostasis for overall survival. The nervous system with predominantly postmitotic cells is believed to be exquisitely vulnerable to redox imbalance [Halliwell, 2006; Friedman, 2011]. Interestingly, under physiological conditions not only the levels of important anti-oxidant en-

zymes like glutathione peroxidases or catalases, but also the antioxidant vitamin E were found to be reduced in the nervous system with compared to other vital systems [Valko et al., 2007; Asha Devi, 2009]. Under physiological conditions, increased consumption of O_2 produces not only high amounts of energy essential to maintain neuronal activity, but also increased levels of ROS as a byproduct of the respiratory chain [Halliwell, 2006; Friedman, 2011]. Studies with patients having developmental brain disorders revealed increased oxidative stress in both sensory and motor neurons. In childhood onset of ALS disease, oxidative DNA damage and lipid peroxidation lead to motor neuron death [Hayashi et al., 2012]. In our mouse model, significantly increased amount of oxidative DNA damage products were found along with increased oxidative protein damage and lipid damage with loss of proteostasis. Lipid oxidation end products, such as malondialdehyde (MDA) can also react with proteins and nucleic acids and gives rise to cyclic adducts [Zhang et al., 2002; Nair et al., 2007], which unstable the complex. This sort of MDA-DNA adducts are highly mutagenic in nature and can also induce DNA damage [Nair et al., 2007]. Protein-MDA adducts also known to impair the function of proteins [Shao et al., 2010] as well as degradation by ubiquitin-proteosome systems [Negre-Salvayre et al., 2008]. MDA adducts have also been shown to induce inflammation in a variety of tissues [Nair et al., 2007; Uchida, 2013].

SOD2 is an essential component of the cellular antioxidant defense against superoxide anion accumulation [Moreira et al., 2010] and numerous studies tried to investigate the effect of alteration of SOD2 expression in various tissues of different animal models with special emphasis on oxidative stress [Holley et al., 2012]. Earlier studies examining germline inactivation of SOD2 reported that the loss of SOD2 function resulted in perinatal lethality around P10 [Li et al., 1995; Melov et al., 1998]. Brain histology was normal and no neurological phenotype was observed; therefore, the authors concluded that mice died from cardiac myopathy resulting from oxidative stress and abnormal mitochondria within cardiac myocytes [Li et al., 1995]. Since that time, global knock-out of SOD2 has also been examined on various genetic backgrounds [Huang et al., 2006]. While SOD2 deletion in C57Bl/6 mice results in embryonic lethality (E15) due to cardiomyopathy, DBA/2J and B6D2F1 mice survived to 12 days and 3 weeks, respectively, and did not exhibit strong cardiac phenotypes and all these mice most likely died from metabolic acidosis, indicative of overall reduced antioxidant defense [Huang et al., 2006].

In the meantime, several groups have used Cre-loxP technology targeting various tissues in an attempt to circumvent the early lethality of complete SOD2 knockout in mice [Ikegami et al., 2002; Misawa et al., 2006; Nojiri et al., 2006; Lustgarten et al., 2009; Kuwahara et al., 2010; Shimizu et al., 2010; Lustgarten et al., 2011; Parajuli et al., 2011; Treiber et al., 2011]. SOD2 deletion in kidney, skeletal muscle and liver induced oxidative stress in the target organs, but no drastic effects in the specific tissues or lifespan of the mutant mice were observed [Ikegami et al., 2002; Lustgarten et al., 2009; Kuwahara et al., 2010; Lustgarten et al., 2011; Parajuli et al., 2011].

Targeted deletion of SOD2 in postnatal motor neurons has been reported in a model, where Cre expression was driven by the vesicular acetylcholine transporter (VAChT) promoter [Misawa et al., 2006]. These animals exhibiting incomplete SOD2 knockout, did not show any sign of oxidative damage, they have a normal lifespan, and no motor deficits or neuronal losses were observed [Misawa et al., 2006]. Motor neurons within the brain stem and ventral spinal cord, however, did exhibit accelerated Wallerian degeneration following axotomy [Misawa et al., 2006]. A role of oxidative damage and mitochondrial dysfunction in motor neurons has also previously been examined by expressing mutated copper–zinc superoxide dismutase (SOD1) in $SOD2^{+/-}$ mice [Andreassen et al., 2000]. SOD1 mutations are implicated in the pathology of familial amyotrophic lateral sclerosis (ALS). These mutations do not eliminate the dismutase activity of SOD1 and neuronal death is likely due to a toxic gain of function [Ilieva et al., 2009]. Expression of $SOD1^{G93A}$ in $SOD2^{+/-}$ mice resulted in a reduced lifespan and earlier onset of motor neuron death compared to $SOD1^{G93A}$ mice without a SOD2 deficiency [Andreassen et al., 2000].

A conditional strategy was recently applied using nestin promoter-driven Cre expression to delete SOD2 in all cells of the CNS and some cells of the PNS [Shimizu et al., 2010; Oh et al., 2012]. These mice exhibited seizures, failure to gain weight and they died at approximately 3 weeks of age. These mice showed signs of spongiform encephalopathy in the cortex, hippocampus, and in the brain stem [Oh et al., 2012]. Interestingly, in $SOD2^{nko}$ mice no such spongiform pathology was detected, suggesting that the loss of SOD2 in non-neuronal

cells in the brain is critical for this phenotype. The absence of spongiform encephalopathy in fact is consistent with the notion of Oh and colleagues that vacuoles were exclusively observed in non-neuronal cells and neurons were only passively compressed [Oh et al., 2012]. The most likely explanation is therefore that other cells in the CNS like astrocytes or oligodendroglia with a deletion of SOD2 are responsible for the spongiform phenotype. Deletion of SOD2 in astrocytes in addition might explain the lack of astrogliosis in the Nestin-Cre model.

4.2 Consequences of SOD2 deficiency in neuronal homeostasis

There are additional striking differences between the mice bearing the brain-specific deletion of SOD2 and our model of excitatory neuron-specific deletion. We observed neuronal apoptosis via activation of Caspase-3 and cell cycle arrest by upregulation of p21. JNK activation and stabilization of p53 as a result of neuronal oxidative damage are most likely the inducers of apoptosis in $SOD2^{nko}$ mice. Activation of p53 by DNA damage or redox imbalance [Sakaguchi et al., 1998; Lakin and Jackson, 1999; Chen et al., 2003] leads to transcription activation of PUMA gene [Shibue et al., 2006]. PUMA is a proapoptotic protein of BH-3 only group of Bcl-2 family [Nakano and Vousden, 2001]. PUMA with its BH-3 domain binds with antiapoptotic Bcl-2 and therefore displaces Bax from the interaction with Bcl-2. This displacement activates Bax, which then translocates to mitochondria and induces mitochondrial outer membrane permeabilization (MOMP), leading to release of cytochrome c into the cytosol [Nakano and Vousden, 2001; Letai et al., 2002; Shibue et al., 2006]. Once cytochrome c is released into the cytosol, it facilitates the binding of inactive procaspase-9 and apoptotic protease activating factor 1 (apaf-1) [Li et al., 1997; Hu et al., 1998]. This process activates caspase-9, which then through a cascade manner activates caspase-3 [Li et al., 1997]. Induction of apoptosis as well as activation and/or induction of p53, PUMA, Bax and caspase-3 are all observed in the brain of $SOD2^{nko}$ mice. However, such apoptotic phenomena were not observed in the Nestin-Cre model [Oh et al., 2012], suggesting that the neuronal apoptosis that was observed in $SOD2^{nko}$ mice may also not be cell autonomous, but it may rather require the contribution of glial cells.

An irregular distribution pattern in a major neuronal cytoskeletal protein, neurofilament and globular aggregates was observed in SOD2^{nko} mice. This could result in severe alterations in cortical neuronal circuitry. As described earlier, such neurofilamentopathy in forebrain was found in different neurodegenerative disorders such as ALS, Alzheimer's, schizophrenia, Parkinson's disease [Liu et al., 2004]. Decelerated neurite growth and deformed architecture was supported by the presence of mostly bipolar or unipolar hippocampal neurons in the in vitro cultures. In contrast, an excessive proliferation of supportive cells like astrocytes and oligodendrocytes was found suggesting specific inhibition of cell cycle in neuronal compartments. Several neurodegenerative diseases can selectively and differentially trigger multicellular responses as well as reactive astrogliosis. One of such trigger can be neuronal damage or death [Sofroniew, 2014]. In amyotrophic lateral sclerosis (ALS) or Huntington's disease, intrinsic neuronal alterations can perturb cellular function that can act as triggers [Boillee et al., 2006]. Accumulation of abnormal proteins and extracellular toxins, such as amyloid-β in Alzheimer's disease (AD) can also trigger reactive gliosis [Prokop et al., 2013]. Degenerating neurons contribute to alter neurovascular system, which can send signal to recruit nonneural immune cells and thus can propagate an inflammatory response [Zlokovic, 2011]. Indeed, we observed an increase in blood-borne immune and infiltrating cells along with microglial activation in SOD2^{nko} mice brain. Therefore, these findings indicate the development of toxic neuropathy primarily induced by redox imbalance. As a consequence of such neuropathy, abnormal accumulation of ball-like neurofilament-globules within the neuropil in turn induces reactive astrogliosis and inflammatory responses, thus marking the possible importance of neuronal redox imbalance in neurodegenerative diseases.

4.3 Neuronal redox imbalance mediated energetic dysfunction

A significant reduction in cerebral ATP production was found. This represents a depressed energy status in brains of SOD2^{nko} mice. As glucose is the major source of energy for the brain, the blood glucose levels of the SOD2 mutant mice were investigated and found that SOD2^{nko} mice were severely hypoglycemic. There was also impaired mitochondrial respiratory activity, as revealed by reduced SDH enzyme histochemistry staining in SOD2^{nko} brain. COX-SDH activity is a direct measure of mitochondrial respiratory functions [Seligman et al., 1968; Trifunovic et al., 2004; Nojiri et al., 2006; Ross, 2011]. Cells with func-

tional cytochrome oxidase (COX) or complex IV efficiently oxidize DAB to form a brown indamine polymer product, which is formed in saturation in the mitochondria with functional complex IV (COX) [Ross, 2011]. As there is no change in the intensity of COX (oxidized DAB) staining between CO and SOD2^{nko} brain sections, it is possible that complex IV activity remains unaltered. The acitivity of SDH was measured with succinate (susbtrate of SDH) mediated reduction of NBT, forming a blue formazan product, which is easy to visualized under microscope. Brain sections from SOD2^{nko} showed marked reduction in SDH staining, suggestion a loss of SDH (Complex II) activity. Mice with cardiac and skeletal muscles specific SOD2 deficiency also demonstrated a selective loss of Complex II (SDH) enzymatic activity but not Complex IV (COX) activity in the skeletal and cardiac muscles [Nojiri et al., 2006]. In human, although the incidence of respiratory chain deficits involving complex II is rare, there are several reports linking reduction in the expression or activity of SDH with onset of neuromuscular disorders, such as ataxia, encephalomyopathy, hypotonia, loss of postural control [Alston et al., 2012]. Brain uses glucose as main soruce of energy and glucose utilization is directly associated with oxygen supply to the brain. It was estimated that about 20% of total inspired oxygen and 25% of glucose comsumed are directed to brain [Belanger et al., 2011]. Maintenance and restoration of ion gradients across cell membrane during resting and action potentials, uptake and recycling of neurotransmitters, are the main processes contributing to this high energy needs in brain [Attwell and Laughlin, 2001; Alle et al., 2009; Belanger et al., 2011]. If the glucose supply to the brain is limited, brain can not generate ATP, as all the stored energy in the form of NADH has already been utilized by mitochondrial electron transport chain to synthesise ATP. Therefore, when glucose level is limited, energy transfer to NAD to generate NADH through the process of glycolysis and TCA rapidly declines, leading to higher NAD/NADH ratio. This may explain why hypoglycemia often results in higher NAD/NADH ratio and lower ATP levels in brain [Garofalo et al., 1988; Belanger et al., 2011]. Under physiological conditions, a state of oxidation is favored over reduction and cellular redox potential is increased during hypoglycemia [Auer, 2004]. Energy failure up to 25% and decreased oxidative phosphorylation is found in hypoglycemic conditions [Auer, 2004]. In a few recent studies, there are hints of a physiological role of mitochondrial ROS in hypothalamic control of lipid and glucose sensing [Sanchez-Lasheras et al., 2010]. However, there is to date no compelling evi-

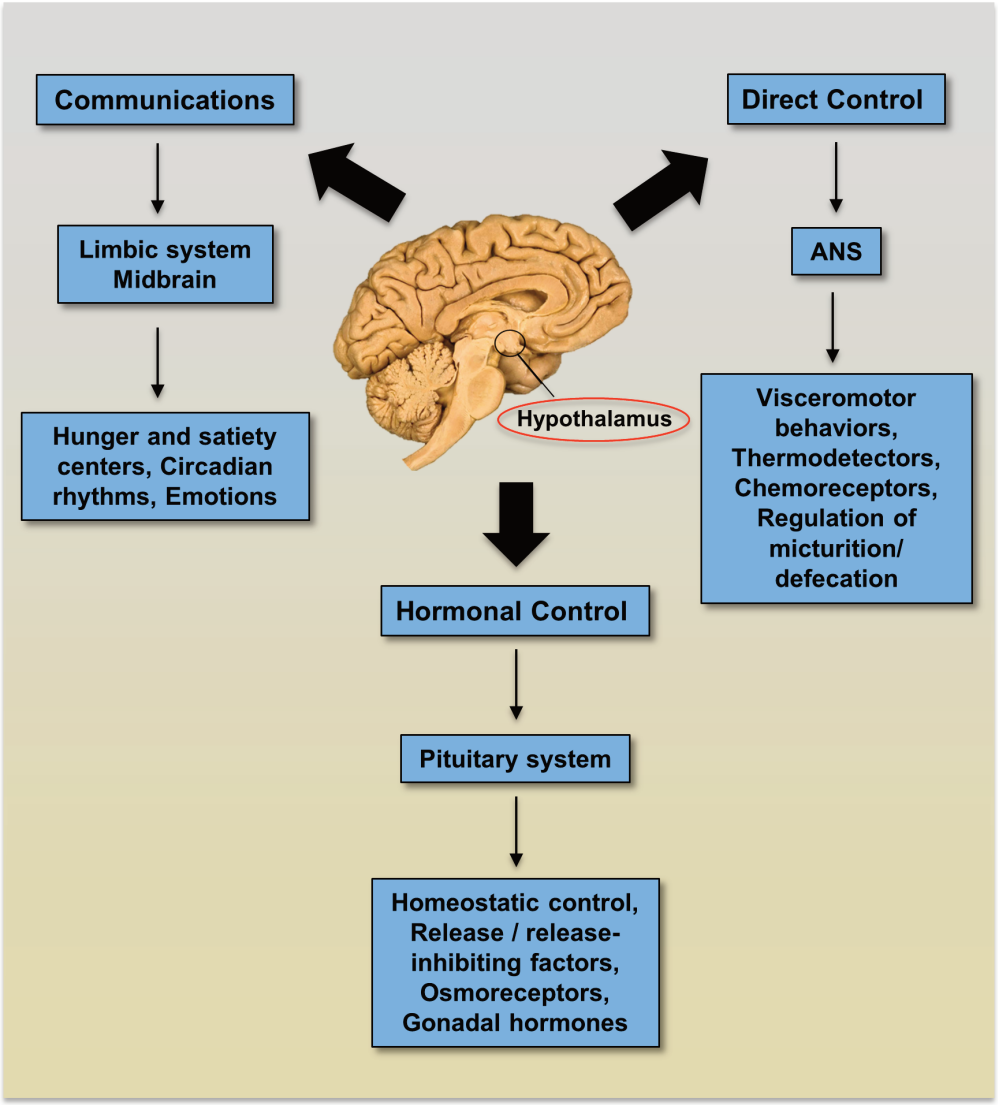

Figure 4.1. Physiological functions of hypothalamus.
Direct control of autonomic nervous system (ANS), Communication with midbrain lymbic systems and hormonal control of pitutary system.

dence of oxidative damage as a result of hypoglycemia or vise versa. None of the previous models studying the loss of SOD2 had revealed alterations in glucose homeostasis.

4.4 Involvement of neuronal SOD2 in CNS-regulated energy homeostasis

Though the direct endocrinal actions on metabolic tissues are necessary for overall metabolic homeostasis, several central nervous system (CNS)-regulated pathways have been identified

to control important aspects of metabolism. One of such important pathways includes hypothalamically regulated hormones (such as glucocorticoids and thyroid hormone) those function in harmony with pancreatic hormones to mediate the crucial counter-regulatory responses [Levin, 2007]. Generally, CNS-regulated pathways modulate metabolism by different cues such as, energy and hormones. These cues act on hypothalamus, which in turn regulates glucose and lipid metabolism, thus maintaining an overall energy balance [Levin and Sherwin, 2011]. Hypothalamus, specifically hypothalamic nuclei have been identified to play a major role in the regulation of several essential physiological functions [Pocai et al., 2005] (Figure 4.1).

Recent studies have shown that specialized neurons located within discrete regions of both the CNS and periphery can detect hypoglycemia. In this context, they may provide an integrated mechanism for whole-body glucose homeostasis [Watts and Donovan, 2010]. Such an integrative glucose-sensing network can be comprised of hypothalamic, hindbrain, and peripheral glucose sensors to form a classical sensory-motor integrative pathway [Watts and Donovan, 2010]. The hindbrain glucose-sensing autonomic reflex loops might be modified by forebrain integrative networks; thus could explain the relation between defective forebrain integrative networks and abnormal counterregulation to hypoglycemia [Watts and Donovan, 2010]. In CNS, specific glucose-sensing neurons were found in different parts of hypothalamus, which respond to hypoglycemic conditions to promote the counter-regulatory responses [Ritter et al., 2011] In addition, hypothalamic glucose sensing also regulates peripheral glucose handling [Pocai et al., 2005]. As blood glucose level declines, central and peripheral glucose sensors transmit this signal to central integrative centers, which in turn coordinates autonomic, behavioral, and neuroendocrine responses to counterregulate hypoglycemia [Tesfaye and Seaquist, 2010]. Ex-vivo electrophysiological studies have identified specific areas in the brain that contain neurons sensitive to local changes in glucose concentration [McCrimmon, 2008]. Within CNS, the specific glucose-sensing neurons have been broadly classified as either glucose-excited (GE), which increases their action potential frequency with an increment in blood glucose; or glucose-inhibited (GI), which increases their action potential frequency with declined blood glucose concentration [Routh, 2002].

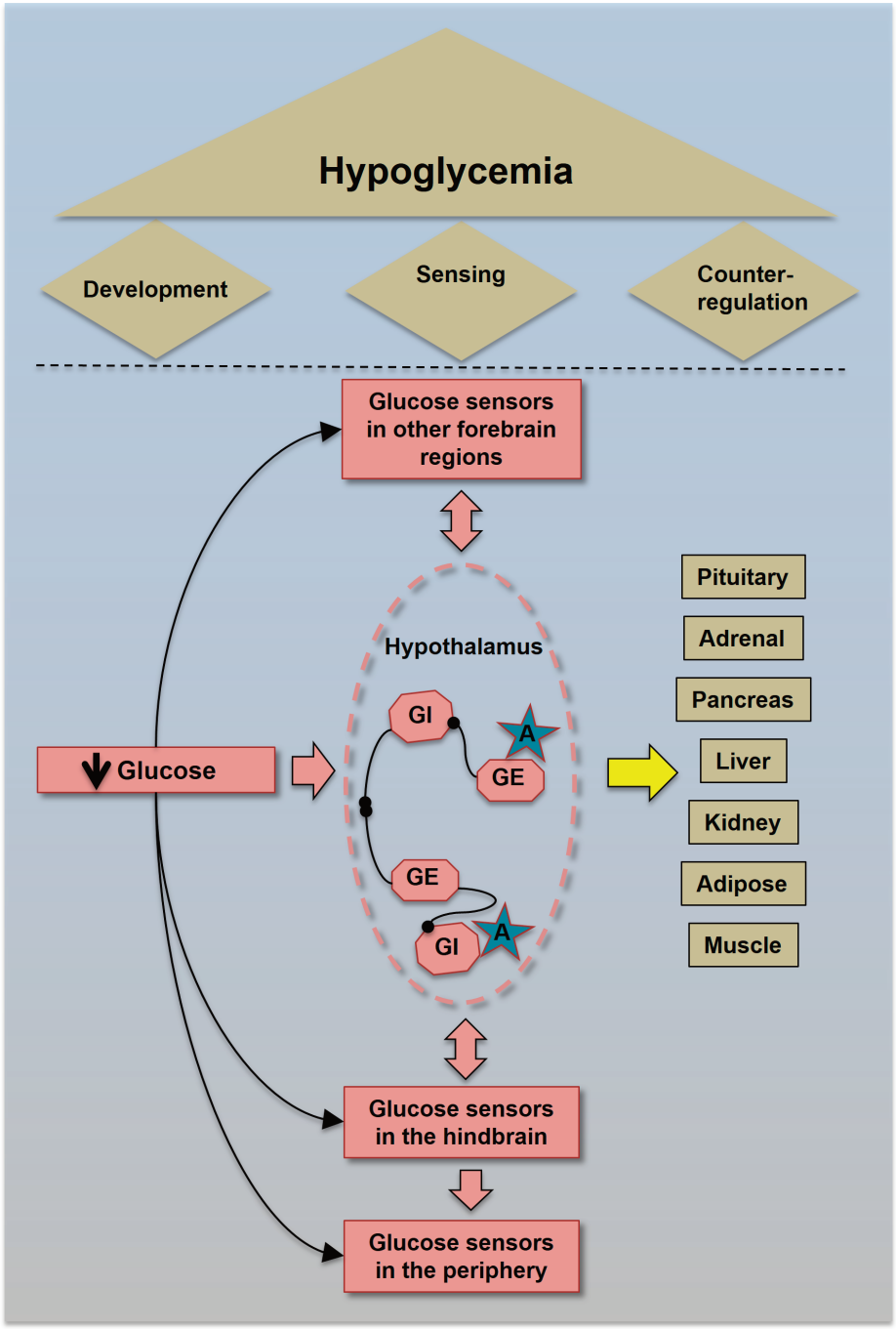

Figure 4.2. Counterregualtion of hypoglycemia

Integrative model of hypoglycemia counterregulation. A falling glucose is detected by central and peripheral glucose-sensing neurons/non-neuronal cells. Within the CNS, astrocytes and neurons work together as functional units. Peripheral glucose sensors signal back to glucose-sensing regions of the hindbrain in turn activating efferent pathways that initiate a counterregulatory response.Glucose sensors in the hypothalamus and other forebrain regions, also activating efferent pathways that initiate a counterregulatory response. Integrative pathways between hindbrain, hypothalamic, and other forebrain regions are reciprocally connected and can modulate responses to the hypoglycemic signal. Glucose-sensing regions in the brain, such as the hypothalamus, contain GE and GI neurons and an astrocytic support structure. A, astrocyte.

Apart from the pancreatic β-cell, peripheral glucose sensors have been observed in the intestine, hepatoportal vein, and carotid body [McCrimmon, 2008]. These neurons are found to function in a coordinated manner in hypoglycemic conditions (Figure 4.2). In addition to the classical pathway of glucose sensing, recent reports have hypothesized that independent of oxidation, glucose might modulate the action potential in glucose-sensing neurons [Burdakov et al., 2005].

Prolonged hypoglycemia induces brain damage, which is often morphologically characterized by the presence of acidophilic necrotic neurons in different brain regions, termed as pannecrosis [Auer, 2004]. We observed such hypoglycemic brain lesions in hippocampus, dentate gyrus, and most evidently in different hypothalamic nuclei of $SOD2^{nko}$ mice. CNS neurons in the hypothalamus play an important role in glucose metabolism and hypothalamic neurocircuitry directly regulates energy homeostasis [Belgardt and Bruning, 2010; Vogt and Bruning, 2013]. CNS-mediated regulation of glucose and energy homeostasis is not limited to anxiogenic stresses; rather, highly responsive to several physiological stresses [McCowen et al., 2001]. Under physiological condition, metabolic cues such as hypoglycemia can trigger this response by directly acting on central regulatory centers to return to normoglycemic conditions [Levin et al., 2004]. As described earlier, acute hypoglycemia could activate a number of pathways involved in the regulation of the neuroendocrine stress response. A potential role for systemic corticotrophin-releasing hormone (CRH) was also described in counterregulatory responses [Flanagan et al., 2003]. Under controlled euglycemic conditions, CRH [Davis et al., 1996] and glucocorticoids [Flanagan et al., 2003] can induce defective counterregulation to next episode of hypoglycemia. Activation of such strictly regulated family of neuropeptides plays an integral role in a number of different forms of stress. We noted that expression of two important hypothalamic neuropeptides, namely CRH and GHRH, was decreased in $SOD2^{nko}$ mice. In human, the role of CRH and related peptides has been characterized in both physiological and disease condition, such as anxiety and depression, sleep disorders, neurological diseases, inflammatory and allergic disorders, addictive behavior, and pre-term labor [Grammatopoulos and Chrousos, 2002]. CRH knockout mice were previously shown to be unresponsive and highly vulnerable to hypoglycemic conditions [Jacobson and Pacak, 2005; Jacobson et al., 2006]. Under physiological condi-

tions, GHRH was also described as a component of the counterregulatory system against hypoglycemia and GHRH deficiency can result in profound hypoglycemia which in turn endangers life expectancy in both humans as well as in rodents [Stanley S, 2013]. Furthermore, reduced expression of CRH-receptor CRH-R1 was observed in the ventromedial hypothalamus (VMH) of SOD2^{nko} mice. Previous studies in transgenic mice have reported that activation of CRH-receptors such as CRH-R1 amplifies, whereas CRH-R2 suppresses the activation of responses towards different physiological stressors [Bale and Vale, 2004]. Taken together, an alteration in the balance between the two CRH-receptors mediated functions, either induced by CRH or glucocorticoids, might lead to suppression of the glucose counterregulatory response during a subsequent exposure to hypoglycemia.

Hypothalamic counterregulatory response is indeed of immense importance, as impairment in such responses increases the frequency and fatality of hypoglycemic events [Myers and Olson, 2012]. Previous studies have showed that repeated hypoglycemia might produce a downregulation of the hormonal counterregulatory response to subsequent hypoglycemia in humans [Heller and Cryer, 1991]. Hypothalamic nuclei contribute to the central regulation of plasma glucose levels via the hypothalamic-pituitary-adrenal axis [O'Connor et al., 2000]. Hypothalamic glucose-sensing neurons can also be regulated by local or peripheral release of neuropeptides [Davis et al., 1996]. As consequence of reduced CRH and GHRH expression, their respective pituitary target hormones ACTH and GH were also significantly downregulated in SOD2^{nko} mice, suggesting an intrinsic failure in blood glucose homeostasis. In acute hypoglycemic condition, vulnerable glucose-sensing neurons (which are activated by hypoglycemia and regulate the stress response) possibly show an enhanced binary effect of metabolic adaptation as well as a feedback inhibition of the stress response caused by persistent hypoglycemia. Persistent hypoglycemia in turn is a likely cause of early lethality.

4.5 Potential mechanism of redox imbalance induced impairment of neuronal and metabolic homeostasis

A potential model is proposed here to explain the pathomechanism of neuronal redox imbalance mediated early lethality preceded by profound hypoglycemia in SOD2^{nko} mice (Figure 4.3). Continuous accumulation of oxidative damaged products with subsequently increased neurofilamentopathy cause acute neuronal loss in the forebrain of SOD2^{nko} mice.

Apoptosis of vulnerable hypothalamic CRH and GHRH neurons results in abnormal secretion of downstream pituitary hormones, such as ACTH and GH. Impaired central regulation of glucose metabolism pathway induces insufficient counterregulatory responses towards transient hypoglycemia finally leading to persistent hypoglycemia. This in turn contributes to severe hypoglycemic brain lesions in a vicious cycle, thus ultimately may result in the death of the $SOD2^{nko}$ mice.

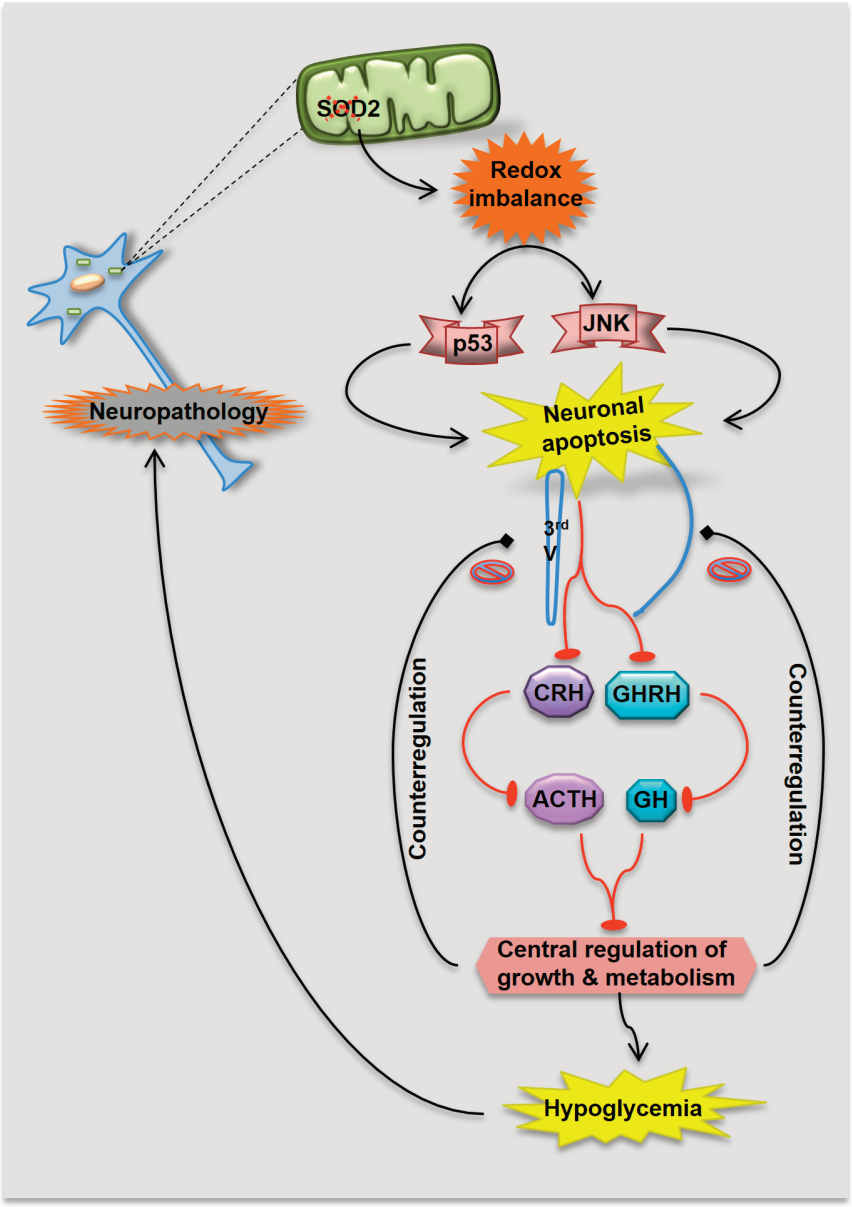

Figure 4.3. Schematic representation of probable pathomechanism

Forebrain specific deletion of SOD2 results in redox imbalance, which induces severe oxidative damage and altered neuronal homeostasis. Activation of JNK and accumulation of p53 probably triggers neuronal apoptosis in vulnerable hypothalamic nuclei. Impaired central regulation of energy metabolism results in persistant hypoglycemia. Profound hypoglycemia induces widespread pannecrosis results in a faliure to survive.

4.6 CONCLUSION

The present study demonstrates that SOD2 is an essential non-redundant enzyme in forebrain neurons. Indeed, SOD2 has been described as an important component of mitochondrial ROS elimination pathway. Deletion of SOD2 in forebrain neurons, leads to accumulation of ROS, development of oxidative stress and neuronal death through apoptosis. Redox imbalance in the forebrain neurons not only induces neuronal death but inhibits the postnatal neurogenesis as well. Neuronal death is however followed by an excessive astrogliosis. Metabolic dysfunction with severe hypoglycemia and regional energetic dysfunction were also observed in the forebrain neuron specific SOD2 deficient mice ($SOD2^{nko}$). The mutant mice die within 4 weeks of age with profound hypoglycemia and severe neuropathology.

Therefore, this present study provides a new insight in the role of SOD2 in neuronal homeostasis. Deficiency of SOD2 in forebrain neurons is sufficient enough for the early postnatal lethality of the mutant mice. As described earlier, prolonged exposure to hypoglycemia enhances morbidity and mortality in human. Hence, understanding of forebrain-mediated pathways, which control counterregulation to hypoglycemia is of immense interest for overall survival. In addition, this study also demonstrates the redox imbalance induced impairment of hypothalamus-mediated sensing and counter-regulation to hypoglycemia.This finding is unique in the sense that normal or physiological level of hypothalamic ROS was shown to be essential for glucose sensing, although overproduction of it may lead to impairment of this sensing mechanism as revealed from this present study.

5. LIST OF ABBREVIATIONS

ACO2	Aconitase 2
ACTH	Adrenocorticotropic hormone
ADP	Adenosine diphosphate
ALS	Amyotrophic lateral sclerosis
ANOVA	Analysis of variance
Apaf-1	Apoptotic protease activating factor 1
ARE	Antioxidant response element
ATP	Adenosine triphosphate
Bax	Bcl-2-associated X protein
Bcl-2	B-cell lymphoma 2
Bcl-xl	B-cell lymphoma-extra large
Bid	BH3 interacting-domain
BSA	Bovine serum albumin
CamKII	Ca2+/calmodulin-dependent protein kinase II
CM-H_2DCFDA	5-(and-6)-chloromethyl-2',7'-dichlorodihydrofluorescein diacetate
CNS	Central nervous system
CO	SOD2 competent control mice
CO_2	Carbon dioxide
COX	Cytochrome C Oxidase
Cre	Cre recombinase
CRH	Corticotropin releasing hormome
CRH-R1	Corticotropin releasing hormome receptor 1
CRH-R2	Corticotropin releasing hormome receptor 2
Ct	Threshold cycle
DAB	3-3' Diaminobenzidine
DAPI	4',6-diamidino-2-phenylindole
DCM	Dilated cardiomyopathy
DCX	Double cortin
DMSO	Dimethyl sulfoxide
DNA	Deoxyribonucleic acid

ECL	Enhanced chemiluminescence
EDTA	Ethylenediaminetetraacetic acid
ELISA	Enzyme-Linked Immunosorbent Assay
ER	Endoplasmic reticulum
FADH	Reduced flavin adenine dinucleotide
FITC	Fluorescein isothiocyanate
FQR	Flavoprotein-ubiquinone oxidoreductase
GE	Glucose-excited neurons
GFAP	Glial fibrillary acidic protein
GH	Growth hormone
GHRH	Growth hormone releasing hormone
GI	Glucose-inhibited neurons
GnRH	Gonadotropin-releasing hormone
GPDH	Glycerol 3-phosphate dehydrogenase
Gpx	Glutathione peroxidase
H&E	Hematoxylin and eosin
H_2O_2	Hydrogen peroxide
HBSS	Hanks' Balanced Salt Solution
HCRT	Hypocretin
HET	Heterozygous (Brain specific SOD2 heterozygous deficient mice)
HO1	Heme Oxygenase 1
HPA	Hypothalamic-Pituitary-Adrenal
HRP	Horseradish peroxidase
Iba1	Ionized calcium-binding adapter molecule 1
iCre	Codon improved Cre recombinase
IgG	Immunoglobin G
JNK	c-Jun N-terminal kinase
MBP	Myelin basic protein
MDA	Malondialdehyde
MnSOD	Manganese superoxide dismutase
NAD	Nicotinamide adenine dinucleotide
NADH	Reduced nicotinamide adenine dinucleotide

NBT	Nitroblue tetrazolium
NeuN	Neuronal Nuclei
NF	Neurofilament
nm	Nanometer
NMEM	Neuronal minimal essential medium
NO	Nitric oxide
NO	Nitric oxide
NOS	Nitric oxide synthatase
NPY	Neuropeptide Y
Nrf2	Nuclear Factor E2-related factor 2
O_2	Oxygen
$O_2^{\cdot -}$	Superoxide anion
$^{\cdot}OH$	Hydroxyl radical
OD	Optical density
OGDH	2-oxoglutarate dehydrogenase
$ONOO^-$	Peroxynitrite
PBS	Phosphate buffer saline
PCR	Polymerase chain reaction
PDH	Pyruvate dehydrogenase
PFA	Paraformaldehyde
PMCH	Pro-melanin-concentrating hormone
PNS	Peripheral nervous system
POMC	Pro-opiomelanocortin
PUFA	Polyunsaturated fatty acids
PUMA	p53 upregulated modulator of apoptosis
RIPA	Radioimmunoprecipitation assay
RNA	Ribonucleic acid
RNS	Reactive nitrogen species
ROS	Reactive oxygen species
RPM	Revolutions per minute
SDH	Succinate Dehydrogenase
SDS–PAGE	Sodium dodecyl sulfate-Polyacrylamide gel electrophoresis

SGZ	Sub-granular zone
SOD	Superoxide dismutase
$SOD2^{nko}$	Brain specific SOD2 deficient mice
TBS	Tris buffer saline
TCA	Tricarboxylic acid cycle
TRH	Thyrotropin-releasing hormone
TUNEL	Terminal deoxynucleotidyl transferase dUTP nick end labeling
VAChT	Vesicular acetylcholine transporter
VMH	Ventromedial hypothalamus

6. REFERENCES

Adibhatla RM, Hatcher JF (2007) Role of Lipids in Brain Injury and Diseases. Future lipidology 2:403-422.

Alam J, Stewart D, Touchard C, Boinapally S, Choi AM, Cook JL (1999) Nrf2, a Cap'n'-Collar transcription factor, regulates induction of the heme oxygenase-1 gene. J Biol Chem 274:26071-26078.

Alle H, Roth A, Geiger JR (2009) Energy-efficient action potentials in hippocampal mossy fibers. Science 325:1405-1408.

Alston CL, Davison JE, Meloni F, van der Westhuizen FH, He L, Hornig-Do HT, Peet AC, Gissen P, Goffrini P, Ferrero I, Wassmer E, McFarland R, Taylor RW (2012) Recessive germline SDHA and SDHB mutations causing leukodystrophy and isolated mitochondrial complex II deficiency. Journal of medical genetics 49:569-577.

Andreassen OA, Ferrante RJ, Klivenyi P, Klein AM, Shinobu LA, Epstein CJ, Beal MF (2000) Partial deficiency of manganese superoxide dismutase exacerbates a transgenic mouse model of amyotrophic lateral sclerosis. Ann Neurol 47:447-455.

Aoki H, Kang PM, Hampe J, Yoshimura K, Noma T, Matsuzaki M, Izumo S (2002) Direct activation of mitochondrial apoptosis machinery by c-Jun N-terminal kinase in adult cardiac myocytes. J Biol Chem 277:10244-10250.

Asha Devi S (2009) Aging brain: prevention of oxidative stress by vitamin E and exercise. ScientificWorldJournal 9:366-372.

Attwell D, Laughlin SB (2001) An energy budget for signaling in the grey matter of the brain. Journal of cerebral blood flow and metabolism : official journal of the International Society of Cerebral Blood Flow and Metabolism 21:1133-1145.

Auer RN (2004) Hypoglycemic brain damage. Forensic science international 146:105-110.

Bale TL, Vale WW (2004) CRF and CRF receptors: role in stress responsivity and other behaviors. Annu Rev Pharmacol Toxicol 44:525-557.

Beckman JS, Koppenol WH (1996) Nitric oxide, superoxide, and peroxynitrite: the good, the bad, and ugly. Am J Physiol 271:C1424-1437.

Belanger M, Allaman I, Magistretti PJ (2011) Brain energy metabolism: focus on astrocyte-neuron metabolic cooperation. Cell Metab 14:724-738.

Belgardt BF, Bruning JC (2010) CNS leptin and insulin action in the control of energy homeostasis. Annals of the New York Academy of Sciences 1212:97-113.

Bell EL, Klimova TA, Eisenbart J, Moraes CT, Murphy MP, Budinger GR, Chandel NS (2007) The Qo site of the mitochondrial complex III is required for the transduction of hypoxic signaling via reactive oxygen species production. The Journal of cell biology 177:1029-1036.

Betteridge DJ (2000) What is oxidative stress? Metabolism: clinical and experimental 49:3-8.

Boillee S, Vande Velde C, Cleveland DW (2006) ALS: a disease of motor neurons and their nonneuronal neighbors. Neuron 52:39-59.

Brand MD (2010) The sites and topology of mitochondrial superoxide production. Experimental gerontology 45:466-472.

Branda CS, Dymecki SM (2004) Talking about a revolution: The impact of site-specific recombinases on genetic analyses in mice. Developmental cell 6:7-28.

Brown GC, Borutaite V (2012) There is no evidence that mitochondria are the main source of reactive oxygen species in mammalian cells. Mitochondrion 12:1-4.

Burdakov D, Luckman SM, Verkhratsky A (2005) Glucose-sensing neurons of the hypothalamus. Philosophical transactions of the Royal Society of London Series B, Biological sciences 360:2227-2235.

Bystron I, Blakemore C, Rakic P (2008) Development of the human cerebral cortex: Boulder Committee revisited. Nature reviews Neuroscience 9:110-122.

Cao Z, Lindsay JG, Isaacs NW (2007) Mitochondrial peroxiredoxins. Sub-cellular biochemistry 44:295-315.

Casanova E, Fehsenfeld S, Mantamadiotis T, Lemberger T, Greiner E, Stewart AF, Schutz G (2001) A CamKIIalpha iCre BAC allows brain-specific gene inactivation. Genesis 31:37-42.

Chen K, Albano A, Ho A, Keaney JF, Jr. (2003) Activation of p53 by oxidative stress involves platelet-derived growth factor-beta receptor-mediated ataxia telangiectasia mutated (ATM) kinase activation. J Biol Chem 278:39527-39533.

Choi AM, Alam J (1996) Heme oxygenase-1: function, regulation, and implication of a novel stress-inducible protein in oxidant-induced lung injury. Am J Respir Cell Mol Biol 15:9-19.

Choi HJ, Kang KS, Fukui M, Zhu BT (2011) Critical role of the JNK-p53-GADD45alpha apoptotic cascade in mediating oxidative cytotoxicity in hippocampal neurons. Br J Pharmacol 162:175-192.

Cohen G, Hochstein P (1963) Glutathione Peroxidase: The Primary Agent for the Elimination of Hydrogen Peroxide in Erythrocytes. Biochemistry 2:1420-1428.

Davis SN, Shavers C, Costa F, Mosqueda-Garcia R (1996) Role of cortisol in the pathogenesis of deficient counterregulation after antecedent hypoglycemia in normal humans. The Journal of clinical investigation 98:680-691.

Demir O, Singh S, Klimaschewski L, Kurnaz IA (2009) From birth till death: neurogenesis, cell cycle, and neurodegeneration. Anatomical record 292:1953-1961.

Dheen ST, Kaur C, Ling EA (2007) Microglial activation and its implications in the brain diseases. Curr Med Chem 14:1189-1197.

Duchen MR (2012) Mitochondria, calcium-dependent neuronal death and neurodegenerative disease. Pflugers Archiv : European journal of physiology 464:111-121.

Emery B (2010) Regulation of oligodendrocyte differentiation and myelination. Science 330:779-782.

Eriksson PS, Perfilieva E, Bjork-Eriksson T, Alborn AM, Nordborg C, Peterson DA, Gage FH (1998) Neurogenesis in the adult human hippocampus. Nature medicine 4:1313-1317.

Finkel T, Holbrook NJ (2000) Oxidants, oxidative stress and the biology of ageing. Nature 408:239-247.

Flanagan DE, Keshavarz T, Evans ML, Flanagan S, Fan X, Jacob RJ, Sherwin RS (2003) Role of corticotrophin-releasing hormone in the impairment of counterregulatory responses to hypoglycemia. Diabetes 52:605-613.

Fridovich I (1997) Superoxide anion radical (O2-.), superoxide dismutases, and related matters. J Biol Chem 272:18515-18517.

Fridovich I (2013) Oxygen: how do we stand it? Med Princ Pract 22:131-137.

Friedlander RM (2003) Apoptosis and caspases in neurodegenerative diseases. The New England journal of medicine 348:1365-1375.

Friedman J (2011) Why Is the Nervous System Vulnerable to Oxidative Stress? In: Oxidative Stress and Free Radical Damage in Neurology, pp 19-28. Heidelberg: Springer

Fuentealba P, Begum R, Capogna M, Jinno S, Marton LF, Csicsvari J, Thomson A, Somogyi P, Klausberger T (2008) Ivy cells: a population of nitric-oxide-producing, slow-spiking GABAergic neurons and their involvement in hippocampal network activity. Neuron 57:917-929.

Gadoth N, Göbel HH (2011) Oxidative stress and free radical damage in neurology: Springer.

Garofalo O, Cox DW, Bachelard HS (1988) Brain levels of NADH and NAD+ under hypoxic and hypoglycaemic conditions in vitro. J Neurochem 51:172-176.

Ghavami S, Shojaei S, Yeganeh B, Ande SR, Jangamreddy JR, Mehrpour M, Christoffersson J, Chaabane W, Moghadam AR, Kashani HH, Hashemi M, Owji AA, Los MJ (2014) Autophagy and apoptosis dysfunction in neurodegenerative disorders. Progress in neurobiology 112:24-49.

Glantz LA, Gilmore JH, Lieberman JA, Jarskog LF (2006) Apoptotic mechanisms and the synaptic pathology of schizophrenia. Schizophrenia research 81:47-63.

Gleeson JG, Lin PT, Flanagan LA, Walsh CA (1999) Doublecortin is a microtubule-associated protein and is expressed widely by migrating neurons. Neuron 23:257-271.

Goetze B, Grunewald B, Kiebler MA, Macchi P (2003) Coupling the iron-responsive element to GFP—an inducible system to study translation in a single living cell. Science's STKE : signal transduction knowledge environment 2003:PL12.

Gotz M, Huttner WB (2005) The cell biology of neurogenesis. Nature reviews Molecular cell biology 6:777-788.

Grammatopoulos DK, Chrousos GP (2002) Functional characteristics of CRH receptors and potential clinical applications of CRH-receptor antagonists. Trends in endocrinology and metabolism: TEM 13:436-444.

Gray B, Carmichael AJ (1992) Kinetics of superoxide scavenging by dismutase enzymes and manganese mimics determined by electron spin resonance. The Biochemical journal 281 (Pt 3):795-802.

Halliwell B (2006) Oxidative stress and neurodegeneration: where are we now? J Neurochem 97:1634-1658.

Halliwell B, Gutteridge J (2007) Free Radicals in Biology and Medicine. New York: Oxford University Press.

Hartl D, Irmler M, Romer I, Mader MT, Mao L, Zabel C, de Angelis MH, Beckers J, Klose J (2008) Transcriptome and proteome analysis of early embryonic mouse brain development. Proteomics 8:1257-1265.

Hayashi M, Miyata R, Tanuma N (2012) OXIDATIVE STRESS IN DEVELOPMENTAL BRAIN DISORDERS. In: Neurodegenerative Diseases (Ahmad SI, ed), pp 278-290. New York: Springer.

Heller SR, Cryer PE (1991) Reduced neuroendocrine and symptomatic responses to subsequent hypoglycemia after 1 episode of hypoglycemia in nondiabetic humans. Diabetes 40:223-226.

Holley AK, Dhar SK, Xu Y, St Clair DK (2012) Manganese superoxide dismutase: beyond life and death. Amino acids 42:139-158.

Holmstrom KM, Finkel T (2014) Cellular mechanisms and physiological consequences of redox-dependent signalling. Nature reviews Molecular cell biology 15:411-421.

Hu Y, Ding L, Spencer DM, Nunez G (1998) WD-40 repeat region regulates Apaf-1 self-association and procaspase-9 activation. J Biol Chem 273:33489-33494.

Huang TT, Naeemuddin M, Elchuri S, Yamaguchi M, Kozy HM, Carlson EJ, Epstein CJ (2006) Genetic modifiers of the phenotype of mice deficient in mitochondrial superoxide dismutase. Human molecular genetics 15:1187-1194.

Ikegami T, Suzuki Y, Shimizu T, Isono K, Koseki H, Shirasawa T (2002) Model mice for tissue-specific deletion of the manganese superoxide dismutase (MnSOD) gene. Biochem Biophys Res Commun 296:729-736.

Ilieva H, Polymenidou M, Cleveland DW (2009) Non-cell autonomous toxicity in neurodegenerative disorders: ALS and beyond. J Cell Biol 187:761-772.

Iwai M, Sato K, Kamada H, Omori N, Nagano I, Shoji M, Abe K (2003) Temporal profile of stem cell division, migration, and differentiation from subventricular zone to olfactory bulb after transient forebrain ischemia in gerbils. Journal of cerebral blood flow and metabolism : official journal of the International Society of Cerebral Blood Flow and Metabolism 23:331-341.

Jacobson L, Pacak K (2005) Combined corticotropin-releasing hormone and glucocorticoid deficiency does not enhance counterregulatory responses after recurrent hypoglycemia in mice. Metabolism: clinical and experimental 54:1259-1265.

Jacobson L, Ansari T, Potts J, McGuinness OP (2006) Glucocorticoid-deficient corti-

cotropin-releasing hormone knockout mice maintain glucose requirements but not autonomic responses during repeated hypoglycemia. American journal of physiology Endocrinology and metabolism 291:E15-22.

Jastroch M, Divakaruni AS, Mookerjee S, Treberg JR, Brand MD (2010) Mitochondrial proton and electron leaks. Essays in biochemistry 47:53-67.

Jourd'heuil D, Jourd'heuil FL, Kutchukian PS, Musah RA, Wink DA, Grisham MB (2001) Reaction of superoxide and nitric oxide with peroxynitrite. Implications for peroxynitrite-mediated oxidation reactions in vivo. J Biol Chem 276:28799-28805.

Keilin D, Hartree EF (1945) Properties of catalase. Catalysis of coupled oxidation of alcohols. The Biochemical journal 39:293-301.

Knoll B, Kretz O, Fiedler C, Alberti S, Schutz G, Frotscher M, Nordheim A (2006) Serum response factor controls neuronal circuit assembly in the hippocampus. Nature neuroscience 9:195-204.

Kos CH (2004) Cre/loxP system for generating tissue-specific knockout mouse models. Nutrition reviews 62:243-246.

Kuwahara H, Horie T, Ishikawa S, Tsuda C, Kawakami S, Noda Y, Kaneko T, Tahara S, Tachibana T, Okabe M, Melki J, Takano R, Toda T, Morikawa D, Nojiri H, Kurosawa H, Shirasawa T, Shimizu T (2010) Oxidative stress in skeletal muscle causes severe disturbance of exercise activity without muscle atrophy. Free Radic Biol Med 48:1252-1262.

Lakin ND, Jackson SP (1999) Regulation of p53 in response to DNA damage. Oncogene 18:7644-7655.

Lebovitz RM, Zhang H, Vogel H, Cartwright J, Jr., Dionne L, Lu N, Huang S, Matzuk MM (1996) Neurodegeneration, myocardial injury, and perinatal death in mitochondrial superoxide dismutase-deficient mice. Proc Natl Acad Sci U S A 93:9782-9787.

Letai A, Bassik MC, Walensky LD, Sorcinelli MD, Weiler S, Korsmeyer SJ (2002) Distinct BH3 domains either sensitize or activate mitochondrial apoptosis, serving as prototype cancer therapeutics. Cancer cell 2:183-192.

Levene MI, Chervenak FA (2009) Fetal and neonatal neurology and neurosurgery: Elsevier Health Sciences.

Levin BE (2007) Neuronal glucose sensing: still a physiological orphan? Cell Metab 6:252-254.

Levin BE, Sherwin RS (2011) Peripheral glucose homeostasis: does brain insulin matter? The Journal of clinical investigation 121:3392-3395.

Levin BE, Routh VH, Kang L, Sanders NM, Dunn-Meynell AA (2004) Neuronal glucosensing: what do we know after 50 years? Diabetes 53:2521-2528.

Li P, Nijhawan D, Budihardjo I, Srinivasula SM, Ahmad M, Alnemri ES, Wang X (1997) Cytochrome c and dATP-dependent formation of Apaf-1/caspase-9 complex initiates an apoptotic protease cascade. Cell 91:479-489.

Li Y, Huang TT, Carlson EJ, Melov S, Ursell PC, Olson JL, Noble LJ, Yoshimura MP, Berger C, Chan PH, Wallace DC, Epstein CJ (1995) Dilated cardiomyopathy and neonatal lethality in mutant mice lacking manganese superoxide dismutase. Nat Genet 11:376-381.

Liu Q, Xie F, Siedlak SL, Nunomura A, Honda K, Moreira PI, Zhua X, Smith MA, Perry G (2004) Neurofilament proteins in neurodegenerative diseases. Cellular and molecular life sciences : CMLS 61:3057-3075.

Lustgarten MS, Jang YC, Liu Y, Qi W, Qin Y, Dahia PL, Shi Y, Bhattacharya A, Muller FL, Shimizu T, Shirasawa T, Richardson A, Van Remmen H (2011) MnSOD deficiency results in elevated oxidative stress and decreased mitochondrial function but does not lead to muscle atrophy during aging. Aging Cell 10:493-505.

Lustgarten MS, Jang YC, Liu Y, Muller FL, Qi W, Steinhelper M, Brooks SV, Larkin L, Shimizu T, Shirasawa T, McManus LM, Bhattacharya A, Richardson A, Van Remmen H (2009) Conditional knockout of Mn-SOD targeted to type IIB skeletal muscle fibers increases oxidative stress and is sufficient to alter aerobic exercise capacity. Am J Physiol Cell Physiol 297:C1520-1532.

Maizels N (2013) Genome engineering with Cre-loxP. Journal of immunology 191:5-6.

Maragakis NJ, Rothstein JD (2006) Mechanisms of Disease: astrocytes in neurodegenerative disease. Nature clinical practice Neurology 2:679-689.

Mariani E, Polidori MC, Cherubini A, Mecocci P (2005) Oxidative stress in brain aging, neurodegenerative and vascular diseases: an overview. Journal of chromatography B, Analytical technologies in the biomedical and life sciences 827:65-75.

Martin LJ (2001) Neuronal cell death in nervous system development, disease, and injury (Review). International journal of molecular medicine 7:455-478.

Mattson MP (2000) Apoptosis in neurodegenerative disorders. Nature reviews Molecular cell biology 1:120-129.

McCowen KC, Malhotra A, Bistrian BR (2001) Stress-induced hyperglycemia. Critical care clinics 17:107-124.

McCrimmon R (2008) The mechanisms that underlie glucose sensing during hypoglycaemia in diabetes. Diabetic medicine : a journal of the British Diabetic Association 25:513-522.

Melov S, Schneider JA, Day BJ, Hinerfeld D, Coskun P, Mirra SS, Crapo JD, Wallace DC (1998) A novel neurological phenotype in mice lacking mitochondrial manganese superoxide dismutase. Nat Genet 18:159-163.

Merkle FT, Alvarez-Buylla A (2006) Neural stem cells in mammalian development. Current opinion in cell biology 18:704-709.

Miao L, St Clair DK (2009) Regulation of superoxide dismutase genes: implications in disease. Free Radic Biol Med 47:344-356.

Migliore L, Fontana I, Colognato R, Coppede F, Siciliano G, Murri L (2005) Searching for the role and the most suitable biomarkers of oxidative stress in Alzheimer's disease and in other neurodegenerative diseases. Neurobiology of aging 26:587-595.

Miranda-Vizuete A, Damdimopoulos AE, Spyrou G (2000) The mitochondrial thioredoxin system. Antioxidants & redox signaling 2:801-810.

Misawa H, Nakata K, Matsuura J, Moriwaki Y, Kawashima K, Shimizu T, Shirasawa T, Takahashi R (2006) Conditional knockout of Mn superoxide dismutase in postnatal motor neurons reveals resistance to mitochondrial generated superoxide radicals. Neurobiol Dis 23:169-177.

Miwa S, Beckman K, Muller F (2008) Oxidative stress in aging: From model systems to human diseases. Totowa, NJ: OBJ Humana press.

Moreira PI, Zhu X, Wang X, Lee HG, Nunomura A, Petersen RB, Perry G, Smith MA (2010) Mitochondria: a therapeutic target in neurodegeneration. Biochim Biophys Acta 1802:212-220.

Mueller S, Riedel HD, Stremmel W (1997) Direct evidence for catalase as the predominant H2O2 -removing enzyme in human erythrocytes. Blood 90:4973-4978.

Murphy MP (2009) How mitochondria produce reactive oxygen species. The Biochemical journal 417:1-13.

Murphy MP, Holmgren A, Larsson NG, Halliwell B, Chang CJ, Kalyanaraman B, Rhee SG, Thornalley PJ, Partridge L, Gems D, Nystrom T, Belousov V, Schumacker PT, Winterbourn CC (2011) Unraveling the biological roles of reactive oxygen species. Cell Metab 13:361-366.

Myers MG, Jr., Olson DP (2012) Central nervous system control of metabolism. Nature 491:357-363.

Nagy A (2000) Cre recombinase: the universal reagent for genome tailoring. Genesis 26:99-109.

Nair U, Bartsch H, Nair J (2007) Lipid peroxidation-induced DNA damage in cancer-prone inflammatory diseases: a review of published adduct types and levels in humans. Free Radic Biol Med 43:1109-1120.

Nakano K, Vousden KH (2001) PUMA, a novel proapoptotic gene, is induced by p53. Molecular cell 7:683-694.

Negre-Salvayre A, Coatrieux C, Ingueneau C, Salvayre R (2008) Advanced lipid peroxidation end products in oxidative damage to proteins. Potential role in diseases and therapeutic prospects for the inhibitors. Br J Pharmacol 153:6-20.

Nijhawan D, Honarpour N, Wang X (2000) Apoptosis in neural development and disease. Annual review of neuroscience 23:73-87.

Nojiri H, Shimizu T, Funakoshi M, Yamaguchi O, Zhou H, Kawakami S, Ohta Y, Sami M, Tachibana T, Ishikawa H, Kurosawa H, Kahn RC, Otsu K, Shirasawa T (2006) Oxidative stress causes heart failure with impaired mitochondrial respiration. J Biol Chem 281:33789-33801.

Nonomura K, Yamaguchi Y, Hamachi M, Koike M, Uchiyama Y, Nakazato K, Mochizuki A, Sakaue-Sawano A, Miyawaki A, Yoshida H, Kuida K, Miura M (2013) Local apoptosis modulates early mammalian brain development through the elimination of morphogen-producing cells. Developmental cell 27:621-634.

O'Connor TM, O'Halloran DJ, Shanahan F (2000) The stress response and the hypothalamic-pituitary-adrenal axis: from molecule to melancholia. QJM : monthly journal of the Association of Physicians 93:323-333.

Oh SS, Sullivan KA, Wilkinson JE, Backus C, Hayes JM, Sakowski SA, Feldman EL (2012) Neurodegeneration and early lethality in superoxide dismutase 2-deficient mice: a

comprehensive analysis of the central and peripheral nervous systems. Neuroscience 212:201-213.

Okouchi M, Ekshyyan O, Maracine M, Aw TY (2007) Neuronal apoptosis in neurodegeneration. Antioxidants & redox signaling 9:1059-1096.

Parajuli N, Marine A, Simmons S, Saba H, Mitchell T, Shimizu T, Shirasawa T, Macmillan-Crow LA (2011) Generation and characterization of a novel kidney-specific manganese superoxide dismutase knockout mouse. Free Radic Biol Med 51:406-416.

Pfaffl MW (2001) A new mathematical model for relative quantification in real-time RT-PCR. Nucleic acids research 29:e45.

Pocai A, Obici S, Schwartz GJ, Rossetti L (2005) A brain-liver circuit regulates glucose homeostasis. Cell Metab 1:53-61.

Prokop S, Miller KR, Heppner FL (2013) Microglia actions in Alzheimer's disease. Acta neuropathologica 126:461-477.

Qureshi GA, Parvez SH (2007) Oxidative stress and neurodegenerative disorders: Elsevier.

Ramilo CA, Leveque V, Guan Y, Lepock JR, Tainer JA, Nick HS, Silverman DN (1999) Interrupting the hydrogen bond network at the active site of human manganese superoxide dismutase. J Biol Chem 274:27711-27716.

Ritter S, Li AJ, Wang Q, Dinh TT (2011) Minireview: The value of looking backward: the essential role of the hindbrain in counterregulatory responses to glucose deficit. Endocrinology 152:4019-4032.

Ross JM (2011) Visualization of mitochondrial respiratory function using cytochrome c oxidase/succinate dehydrogenase (COX/SDH) double-labeling histochemistry. Journal of visualized experiments : JoVE:e3266.

Routh VH (2002) Glucose-sensing neurons: are they physiologically relevant? Physiology & behavior 76:403-413.

Sakaguchi K, Herrera JE, Saito S, Miki T, Bustin M, Vassilev A, Anderson CW, Appella E (1998) DNA damage activates p53 through a phosphorylation-acetylation cascade. Genes & development 12:2831-2841.

Sanchez-Lasheras C, Konner AC, Bruning JC (2010) Integrative neurobiology of energy homeostasis-neurocircuits, signals and mediators. Frontiers in neuroendocrinology 31:4-15.

Sayre LM, Smith MA, Perry G (2001) Chemistry and biochemistry of oxidative stress in neurodegenerative disease. Curr Med Chem 8:721-738.

Scholzen T, Gerdes J (2000) The Ki-67 protein: from the known and the unknown. Journal of cellular physiology 182:311-322.

Seligman AM, Karnovsky MJ, Wasserkrug HL, Hanker JS (1968) Nondroplet ultrastructural demonstration of cytochrome oxidase activity with a polymerizing osmiophilic reagent, diaminobenzidine (DAB). The Journal of cell biology 38:1-14.

Shao B, Pennathur S, Pagani I, Oda MN, Witztum JL, Oram JF, Heinecke JW (2010) Modifying apolipoprotein A-I by malondialdehyde, but not by an array of other reactive carbonyls, blocks cholesterol efflux by the ABCA1 pathway. J Biol Chem 285:18473-18484.

Shibue T, Suzuki S, Okamoto H, Yoshida H, Ohba Y, Takaoka A, Taniguchi T (2006) Differential contribution of Puma and Noxa in dual regulation of p53-mediated apoptotic pathways. The EMBO journal 25:4952-4962.

Shimizu T, Nojiri H, Kawakami S, Uchiyama S, Shirasawa T (2010) Model mice for tissue-specific deletion of the manganese superoxide dismutase gene. Geriatr Gerontol Int 10 Suppl 1:S70-79.

Simonian NA, Coyle JT (1996) Oxidative stress in neurodegenerative diseases. Annu Rev Pharmacol Toxicol 36:83-106.

Soane L, Solenski N, Fiskum G (2007) 6.5 Mitochondrial Mechanisms of Oxidative Stress and Apoptosis. In: Handbook of Neurochemistry and Molecular Neurobiology (Lajtha A, Gibson G, Dienel G, eds), pp 703-734: Springer US.

Sofroniew MV (2014) Multiple roles for astrocytes as effectors of cytokines and inflammatory mediators. The Neuroscientist : a review journal bringing neurobiology, neurology and psychiatry 20:160-172.

Stanley S DA, Kelly L, Garfield A, Damanpour S, Heisler L, Friedman J. (2013) Profiling of Glucose-Sensing Neurons Reveals that GHRH Neurons Are Activated by Hypoglycemia. Cell Metabolism:596-607.

Stewart VC, Heales SJ (2003) Nitric oxide-induced mitochondrial dysfunction: implications for neurodegeneration. Free Radic Biol Med 34:287-303.

Stiles J, Jernigan TL (2010) The basics of brain development. Neuropsychology review 20:327-348.

Strassburger M, Bloch W, Sulyok S, Schuller J, Keist AF, Schmidt A, Wenk J, Peters T, Wlaschek M, Lenart J, Krieg T, Hafner M, Kumin A, Werner S, Muller W, Scharffetter-Kochanek K (2005) Heterozygous deficiency of manganese superoxide dismutase results in severe lipid peroxidation and spontaneous apoptosis in murine myocardium in vivo. Free Radic Biol Med 38:1458-1470.

Tahimic CT, Sakurai K, Aiba K, Nakatsuji N (2013) Cre/loxP, Flp/FRT Systems and Pluripotent Stem Cell Lines. In: Site-directed insertion of transgenes (Renault S, Duchateau P, eds), pp 189-209: Springer Netherlands.

Tesfaye N, Seaquist ER (2010) Neuroendocrine responses to hypoglycemia. Annals of the New York Academy of Sciences 1212:12-28.

Trachootham D, Lu W, Ogasawara MA, Nilsa RD, Huang P (2008) Redox regulation of cell survival. Antioxidants & redox signaling 10:1343-1374.

Treiber N et al. (2011) Accelerated aging phenotype in mice with conditional deficiency for mitochondrial superoxide dismutase in the connective tissue. Aging Cell 10:239-254.

Trifunovic A, Wredenberg A, Falkenberg M, Spelbrink JN, Rovio AT, Bruder CE, Bohlooly YM, Gidlof S, Oldfors A, Wibom R, Tornell J, Jacobs HT, Larsson NG (2004) Premature ageing in mice expressing defective mitochondrial DNA polymerase. Nature 429:417-423.

Uchida K (2013) Redox-derived damage-associated molecular patterns: Ligand function of lipid peroxidation adducts. Redox biology 1:94-96.

Valko M, Leibfritz D, Moncol J, Cronin MT, Mazur M, Telser J (2007) Free radicals and antioxidants in normal physiological functions and human disease. Int J Biochem Cell Biol 39:44-84.

Vasquez-Vivar J, Kalyanaraman B, Kennedy MC (2000) Mitochondrial aconitase is a source of hydroxyl radical. An electron spin resonance investigation. J Biol Chem 275:14064-14069.

Vetrano AM, Heck DE, Mariano TM, Mishin V, Laskin DL, Laskin JD (2005) Characterization of the oxidase activity in mammalian catalase. J Biol Chem 280:35372-35381.

Vogt MC, Bruning JC (2013) CNS insulin signaling in the control of energy homeostasis and glucose metabolism - from embryo to old age. Trends in endocrinology and metabolism: TEM 24:76-84.

Wallace DC (1999) Mitochondrial diseases in man and mouse. Science 283:1482-1488.

Wallace DC (2005) A mitochondrial paradigm of metabolic and degenerative diseases, aging, and cancer: a dawn for evolutionary medicine. Annual review of genetics 39:359-407.

Watts AG, Donovan CM (2010) Sweet talk in the brain: glucosensing, neural networks, and hypoglycemic counterregulation. Frontiers in neuroendocrinology 31:32-43.

Wu S, Ying G, Wu Q, Capecchi MR (2007) Toward simpler and faster genome-wide mutagenesis in mice. Nat Genet 39:922-930.

Yu J, Zhang L (2008) PUMA, a potent killer with or without p53. Oncogene 27 Suppl 1:S71-83.

Zelko IN, Mariani TJ, Folz RJ (2002) Superoxide dismutase multigene family: a comparison of the CuZn-SOD (SOD1), Mn-SOD (SOD2), and EC-SOD (SOD3) gene structures, evolution, and expression. Free Radic Biol Med 33:337-349.

Zhang Y, Chen SY, Hsu T, Santella RM (2002) Immunohistochemical detection of malondialdehyde-DNA adducts in human oral mucosa cells. Carcinogenesis 23:207-211.

Zlokovic BV (2011) Neurovascular pathways to neurodegeneration in Alzheimer's disease and other disorders. Nature reviews Neuroscience 12:723-738.

Declaration

I hereby conform that I have performed the work independently and without using my sources or aids other than those stated. In each individual case, I have clearly identified the source of the passages that are taken word for word or paraphrased from other works.

Ulm, ……....

…….

Gandhari Maity (Kumar)

ACKNOWLEDGEMENTS

First and foremost, I would like to express my sincere gratitude and indebtedness to my Ph.D. supervisor Prof. Dr. Thomas Wirth for providing me the opportunity to work on such an interesting topic in the Institute of Physiological Chemistry. I am highly obliged to him for all his great guidance, help, support, and inspirations. I am also grateful to him for his constant motivation to plan and pursue the work with freedom, and to develop my scientific ideas.

I am deeply grateful to Prof. Dr. Karin Scharffetter-Kochanek for her constant support, helpful discussions, thoughtful suggestions, and friendly encouragements.

Further, I want to thank Prof. Dr. Dietmar R. Thal for sharing his knowledge and kindly helping me to enrich my understandings in the field of neuropathology.

I am extremely thankful to Dr. Bernd Baumann for his valuable suggestions, constructive criticisms and kind involvement with this project.

Moreover, I would like to thank Dr. Henning Beck for his help with primary neuronal culture technique, Ms. Melanie Gerstenlauer and Mrs. Ute Leschik for excellent technical assistance and friendly cooperations inside as well as outside the lab.

It is of immense pleasure to express my heartfelt gratitude to Mrs. Nina Ushmorova and Mrs. Petra Weihrich for all their outstanding support, warm gestures and cordial friendship.

I am highly obliged to Mrs. Olena Sakk for helping me to solve the problems with animal facility. I also thank Mr. Hans-Georg Glöckler for his time and help with computer applications and Frau Beatrix Schwarz for her kind help in official affairs.
Further, I thank all my colleagues and the former and present members of Institute of Physiological Chemistry for the nice working atmosphere.

It is a great privilege to express my deepest sense of gratitude to all my teachers, especially Prof. Dr. Tushar kanti Ghosh and Dr. Dilip kr. Nandi for support and encouragements. I am extremely thankful to Dr. Pallab Maity for his kind support.

No words of gratitude would be enough to express my gratefulness and respect for my beloved mother. Indeed, I am and will forever be greatly indebted to her for unconditional support, unlimited care and endless motivations.

This work would not have been possible without the love and support from my family, friends and well-wishers, who always provided me with great strength and enthusiasm in all those moments of smile, sweat and tears.

CURRICULUM VITAE

I. PERSONAL INFORMATION

Name	:	**Gandhari Maity (Kumar)**
Date of Birth	:	24th December, 1980
Place of Birth	:	Midnapore (West), West Bengal, India
Address	:	University of Ulm Institute of Physiological Chemistry Albert-Einstein-Allee 11 D-89081 Ulm Germany

II. ACADEMIC INFORMATION

2009 - present	Candidate for PhD degree in Biological Sciences (Dr. rer. nat.) Ulm University Institute of Physiological Chemistry (Prof. Dr. Thomas Wirth) Thesis "*Importance of SOD2 in neuronal homeostasis: Study of a novel mouse model* "
2004-2006	Master of Science in Human Physiology with Community Health (M.Sc) Vidyasagar University Department of Human Physiology
Course project	Special paper (Neurophysiology) Project: "*Effect of lesion of Anterior Cerebellar Vermis on some immunological responses in Wister strain albino rats*"
_____	Community health project: "*Evaluation of some common parameters in the high altitude dwellers, to find out beneficial effects of these on the dwellers*" (Supervisor: Prof. Dr. Tushar kanti Ghosh)

Course Seminar	"*Neurophysiological aspects of Dream*" (Course: Neurophysiology)
	"*Clock genes: Regulation of circadian rhythm*" (Course: Advanced Molecular Biology)
	"*Mobile genetic elements*" (Course: Genetic Engineering)
2000-2004	Bachelor of Science in Human Physiology (B.Sc)
	Vidyasagar University
	Department of Physiology
Course project	"*Study on some hematological parameters to find out a difference between alcoholic males and non-alcoholic males of same economic class*" (Course: Hematology)
	"*Evaluation of nutritional status of residences of an area to investi gate any abnormality on them*" (Course: Social physiology)
	(Supervisor: Dr. Dilip kr. Nandi)

III. Publication

Maity-Kumar G, Thal DR, Baumann B, Scharffetter-Kochanek K, Wirth T Neuronal redox imbalance results in altered energy homeostasis and early postnatal lethality. (submitted.)

IV. Seminar Symposium attended

1. 16th Conference of Physiological Society of India – 17th to 19th December, 2004: Delivered seminar on 'Adverse effects of frequent use of mobile phone on nervous system.'

2. Centenary Celebration of 'Physiology as A Basic Science in India' – 3rd to 6th March, 2001: Delivered seminar on 'Hypnotism & its clinical importance.'

3. Prof. N. M. Basu Memorial Lecture: Recent advancement of Physiology in India – 27th July, 2000: Participated in inter-college lecture competition entitled 'Low cost Balanced Diet for people lying under poverty line in India.'